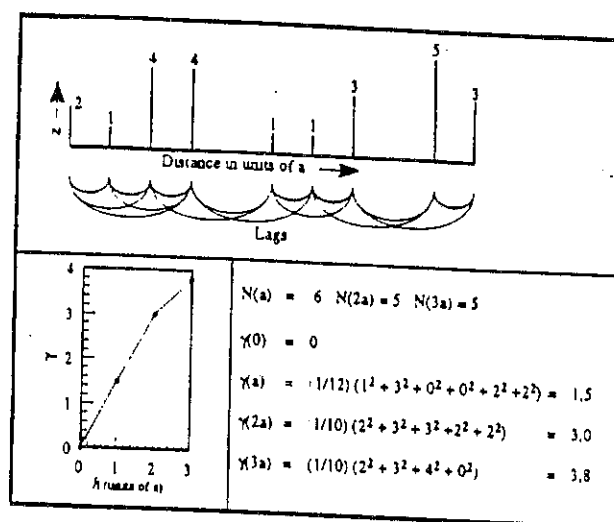


A Comparison of Spatial Bayesian Estimation and Classical Kriging Procedures



by

L. van Sandwyk^(*), G.J. van Tonder^(†), D.J. de Waal^(*) and J.F. Botha^(*)

^(†) Institute for Groundwater Studies

^(*) Department of Mathematical Statistics

Report to the Water Research Commission on the Project:
'A Comparative Study of Two- and Three-Dimensional Groundwater Models'
Project Leader: J.F. Botha

Volume III

WRC Report No 271/3/92

December 1992

Die Instituut vir Grondwater Studies
Universiteit van die Oranje-Vrystaat
Posbus 339 Bloemfontein 9300

The Institute for Groundwater Studies
University of the Orange Free State
P.O. Box 339 Bloemfontein 9300

Obtainable from:

**Water Research Commission
PO Box 824
PRETORIA
0001**

**WRC Report No. 271/3/92
ISBN 1 874858 69 1
Set No. 1 874858 70 5**

ACKNOWLEDGEMENTS

The research in this report emanated from a project funded by the Water Research Commission entitled:

'A Compariative Study of Two- and Three-Dimensional Groundwater Models'

The Steering Committee responsible for the project, whose contributions to the project are hereby gratefully acknowledged, consisted of the following persons:

Mr A G Reynders	Water Research Commission (Chairman)
Mr P W Weideman	Water Research Commission (Secretary)
Dr D.B. Bredenkamp	Department of Water Affairs
Mr R de Vos	Computing Centre for Water Research
Mr H.M. du Plessis	Water Research Commission
Mr J. Herald	Rhodes University
Mr R. Meyer	Ematek, CSIR
Prof J.H. Moolman	University of Stellenbosch
Dr G. Tredoux	Watertek, CSIR
Prof H J Potgieter	University of the Orange Free State
Prof F.D.I. Hodgson	University of the Orange Free State
Prof J.F. Botha	University of the Orange Free State

The authors would like to take this opportunity to express their sincere thanks to the following institutions and people, without whose help the investigation could not have been carried out:

The University of the Orange Free State for the facilities provided in conducting this research.

The Institute for Groundwater Studies, in particular the Director, Prof F.D.I. Hodgson, for his assistance and encouragement during the investigation and Mss M. Botha and C. le Roux, for their contribution in the editing and production of this report.

EXECUTIVE SUMMARY

1 INTRODUCTION

The availability of water in a modern, industrialized country is often taken for granted. South Africa has a particularly acute problem in this regard, because of its arid climate and the rapid increase in its population. The Department of Water Affairs and Forestry projected indeed that all available surface water resources will be fully used by the year 2020. One source of water largely neglected in this country so far is groundwater. Groundwater could therefore make a significant contribution to the demand for water.

One reason, why groundwater has been neglected previously, is because it is invisible and, therefore, difficult to manage and control, especially in the Karoo sediments that underlie a large part of the country. Groundwater is, however, just another physical phenomenon and therefore subjected to well-known physical principles. The question thus arises whether these principles cannot be used to manage and control groundwater resources more efficiently? Judging from the available literature, and previous experience, the answer to this question would seem to be yes. However, groundwater is a natural three-dimensional phenomenon. Large quantities of data are therefore needed, should one wish to investigate the phenomenon in detail. Previous investigations of this nature have consequently concentrated more on a two-dimensional representation of the phenomenon, but this may not be sufficient for aquifers in highly heterogeneous sediments.

2 PURPOSE OF THE PRESENT PROJECT

During an investigation of groundwater pollution in the Atlantis aquifer, it became clear that a groundwater resource cannot always be represented accurately as a two-dimensional phenomenon. The Institute for Groundwater Studies, at the University of the Orange Free State, therefore decided to try to investigate the conditions under which two- and three-dimensional models can be used effectively in the simulation of groundwater phenomena.

Two difficulties, often encountered in the use of large quantities of data, are: (a) how to represent the data in a meaningful and attractive way and (b) how to obtain estimates of unknown data. The present investigation was no exception to this rule. A research proposal 'A Comparative Study of Two- and Three-dimensional Groundwater Models' was therefore put before the Water Research Commission. The purpose of this project, as stated in the final contract with the Commission, was as follows:

An investigation into the use of two- and three-dimensional models in the simulation of groundwater phenomena, with special reference to: (a) the advantages and disadvantages of two- and three-dimensional models, (b) effective estimates for unknown values required by the models and (c) the graphical representation of groundwater data.

The proposal was accepted by the Commission and work on the project began in January 1989. The present report describes the investigations carried out under this project, which ended in December 1991.

3 STRUCTURE OF THE REPORT

The work on this project was divided into three subject areas: (a) the comparative study of two- and three-dimensional models, (b) the graphical representation of groundwater data and (c) the estimation of unknown data values. The Steering Committee thus recommended that the report should be submitted in three separate volumes. These volumes are:

- (1) A Comparative Study of Two- and Three-dimensional Groundwater Models.
- (2) Triangular Irregular Meshes and their Application in the Graphical Representation of Geohydrologic Data.
- (3) A Comparison of Spatial Bayesian Estimation and Classical Kriging Procedures.

The following discussion will, consequently, be based on this division.

4 A COMPARATIVE STUDY OF TWO-AND THREE-DIMENSIONAL GROUNDWATER MODELS

4.1 General

Primitive three-dimensional numerical models for groundwater flow phenomena had already been developed by 1973, but it is only in the last couple of years that these models have been applied extensively in practical investigations. Strangely enough, nowhere in the available literature is there any reference to a comparative study of two- and three-dimensional models that could be used as a criterion in deciding when to use a two-dimensional model, and when would a three-dimensional model be sufficient.

The three-dimensional problems, normally encountered in practice, have no analytical solutions. The computer programs, developed for the present investigation, had therefore to be based on the numerical solution of the flow and mass transport equations. There is no doubt that a finite difference approximation of these equations would be the easiest to implement on a computer. The majority of computer models for three-dimensional groundwater phenomena, available today, are consequently based on this approximation. However, the approximation does not allow the implementation of certain finer physical details, such as mixed or flux boundary conditions, with ease. The models developed in this study were consequently all based on the finite element approximation.

There is very little physical difference between the conceptual models for saturated and unsaturated groundwater flow. The program for variably saturated flow, being the more complex, was therefore developed before the program for saturated flow. There were two main reasons for adopting this philosophy. The first was that it would be easier to adapt the variably saturated flow to saturated flow, than the converse, and the second that the variably saturated flow program would be able to handle saturated flow conditions as well. The possibility thus existed that one program could handle all situations to be covered in this investigation. However, it soon became clear that a separate saturated flow program would execute much faster than the variably saturated flow program. Three programs were, therefore, developed during the investigation.

- Program SAT3 – for the simulation of saturated groundwater flow.
- Program SUF3 – for the simulation of variably saturated groundwater flow.
- Program SUM3 – for the simulation of saturated and variably saturated mass transport.

4.2 Discussion

A good knowledge of the underlying physical principles is of the utmost importance, when a conceptual model is applied to a physical phenomenon. The principles related to the modelling of groundwater flow phenomena have been covered extensively in a previous report: '*Modelling Groundwater Contamination in the Atlantis Aquifer*', to the Water Research Commission. No attempt was therefore made to discuss them again here. The main principles of groundwater flow and contaminant transport, needed to understand the programs, are summarized in Chapters 2 and 3. The finite element approximations used in the three programs are described in Chapter 4.

The generation of a suitable mesh is the most tedious and time consuming aspect in using a finite element approximation to solve a given differential equation. A special three-dimensional mesh generator was therefore adapted as part of the investigation. This generator is discussed in Chapter 5.

It is extremely difficult (many computer scientists will say impossible) to ensure that a computer program, especially those with the size developed for this investigation, is free of errors. However, this does not exempt the developer from his responsibility to ensure that the program is to the best of his knowledge free from serious errors.

There are a number of methods that can be used to 'debug' a computer program. The method almost universally used with programs developed for the simulation of physical phenomena, is to compare the program's output with analytical solutions of simplified conceptual models for the phenomenon. This approach was also followed in this investigation.

Program SAT3 was debugged first. This was done by comparing its output with the two-dimensional analytical solutions of Muskat for a circular homogeneous aquifer with Dirichlet and zero flux boundary conditions, as described in Chapter 6. These solutions were not only useful in the debugging of the program, but they also demonstrated that a two-dimensional model may be considered as equivalent to a three-dimensional model, when working with a confined, homogeneous aquifer. The graphical representation of the piezometric heads in Figure 1, clearly supports this conclusion.

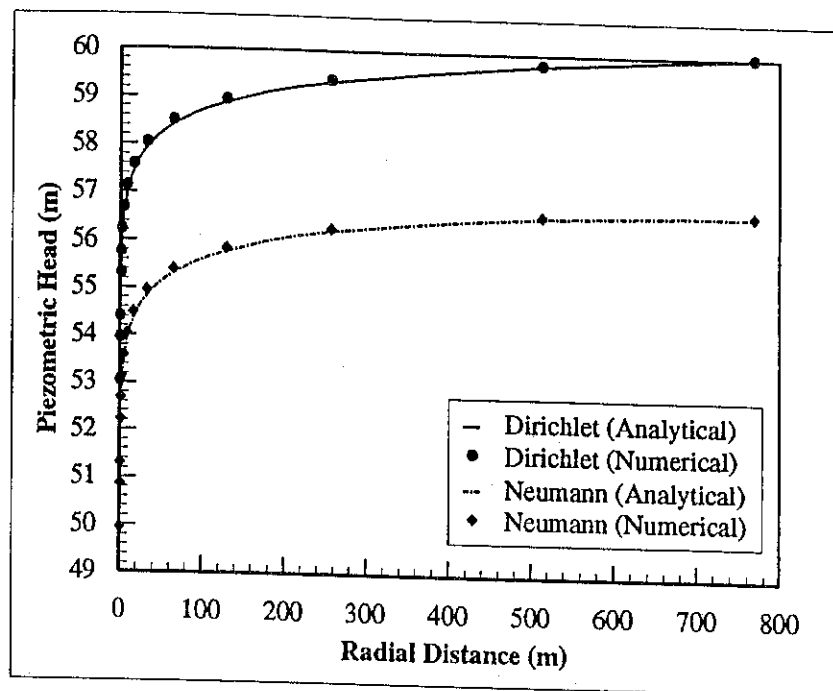


Figure 1 Comparison of the piezometric heads for a homogeneous circular aquifer computed from Muskat's analytical solutions and Program SAT3.

The program MODFLOW, of the United States Geological Survey, is so frequently used in modelling three-dimensional, saturated groundwater flow that it is often considered as the industry standard in many groundwater circles. The program was consequently used as a final check on Program SAT3. This comparison, which was based on a homogeneous, confined aquifer, is described in Chapter 6. As shown in Figure 2, the two programs yielded almost identical piezometric levels in the case of a homogeneous, single layer aquifer.

The debugging of the program for variably saturated flow was considerably simplified by the availability of the saturated flow program. This is illustrated in Chapter 7, where it is shown that Programs SUF3 and SAT3 yielded identical results when applied to the same fully saturated aquifer.

Program SUF3 was also compared with Program UNSAT2 for two-dimensional unsaturated flow, as a further precaution. These results demonstrated that a two-dimensional model is sufficient, even for a variably saturated aquifer, provided that it is homogeneous.

The discussion of the associated three-dimensional mass transport program in Chapter 8, had, unfortunately, to be limited to its debugging phase alone. The reason for this was that no suitable data could be found for a more detailed analysis. Nevertheless, a comparison of the numerical results with an analytical solution, confirmed again, that a two-dimensional model is sufficient for a homogeneous aquifer.

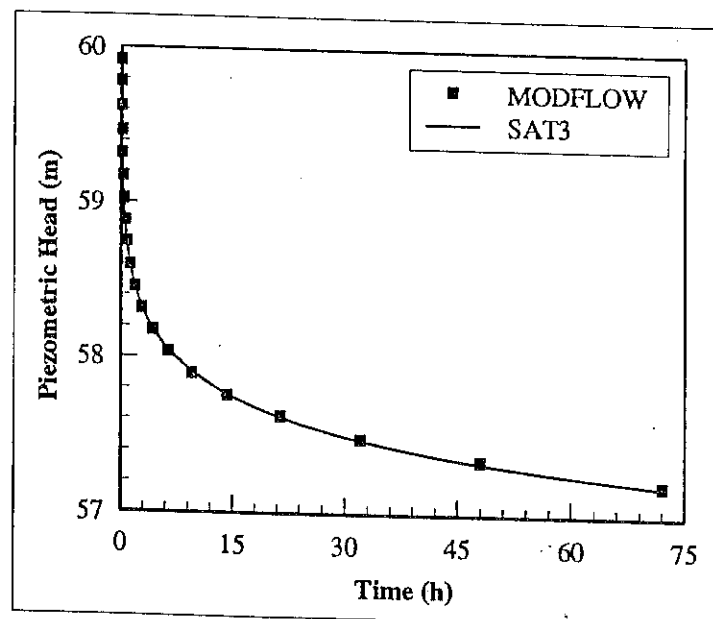


Figure 2 Comparison of the piezometric heads for a circular, homogeneous aquifer, with Dirichlet boundary conditions, computed with the Programs SAT3 and MODFLOW.

The main conclusion, derived from the discussion above, and the results in Chapters 6 to 8, is that there is

absolutely no need to use a three-dimensional model when working with homogeneous aquifers. The question thus arises what the situation will be in the case of heterogeneous aquifers? The answer to this question is taken up in Chapter 9.

In the original proposal to the Water Research Commission, it was anticipated that piezometers would be installed in the Atlantis, Saldanha and Zululand aquifers, and that the piezometric levels could be used in this study. Unfortunately, this expectation never materialized. This meant that the discussion in Chapter 9 had to be restricted to hypothetical aquifers, since the available piezometric levels for these aquifers, are not sufficient for the present purpose. There was, however, one exception in the case of the Atlantis aquifer, where piezometric levels, observed during a previous investigation around the infiltration pan, could be compared with those calculated from the model. The Atlantis aquifer is in this area mainly confined to the Witzand and Duynefontein members of the Bredasdorp Formation, that are in direct hydraulic contact with one another. The Witzand member, which lies on top, is slightly less permeable than Duynefontein. The model used in this study, therefore, consisted of a two-layer aquifer, with slightly different hydraulic conductivities. Since the water levels did not differ considerably at the time of the observations, the same initial piezometric levels were ascribed to both layers.

One would normally expect that the drawdowns in the two layers of such an aquifer will behave very similarly, even if water is pumped only from the lower layer. However, as shown in Figure 3, this is not the case. The piezometric level in the lower layer decreases more rapidly than in the top layer, as the distance from the pumped borehole decreases. It was thus rather satisfactory to find that the numerical model yielded a similar result, be it only qualitatively.

The previous result is clearly of considerable importance for conventional aquifer tests in heterogeneous aquifers, as it means that it is not only important at what depth a pump is installed, but also at what distances observations are taken for the test.

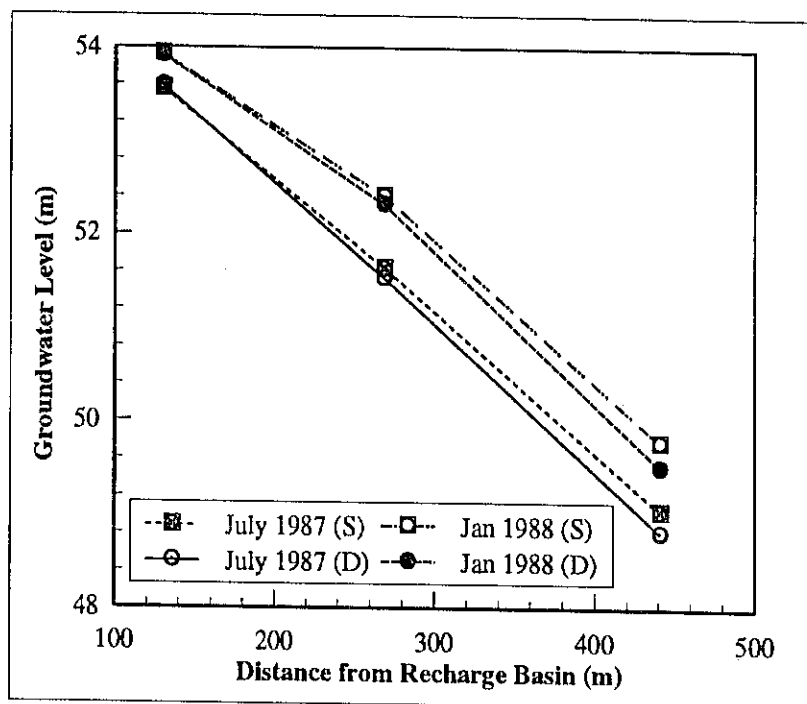


Figure 3 Comparison of the observed water levels in the shallow (S) and deep boreholes in the Atlantis aquifer, when viewed from the infiltration pond towards the Witzand production field.

Another unexpected result that emerged from the study, is that the average drawdown in a layered aquifer may follow the type curve of a completely different kind of aquifer. This is illustrated by the excellent fit between the average drawdown in the same two-layer aquifer, used in the discussion above, and the type curve of a phreatic aquifer in Figure 4. This suggests that it would be foolish to try to analyse drawdowns in a heterogeneous aquifer with a conventional type curve, unless the type curve is confirmed by direct observations on the physical nature of the aquifer.

4.3 Conclusions

The results of the present study can be summarized by saying that a two-dimensional model can be used to analyse the data from a heterogeneous aquifer, provided that the following conditions are satisfied.

- The production and/or observation boreholes must penetrate the aquifer fully.
- Water must be pumped from all layers simultaneously and not from one layer alone.

- (c) Vertical anisotropy in the aquifer is negligible.

It will obviously be extremely difficult to meet these conditions in practical situations. The only conclusion to be reached is that it is well-nigh impossible to derive meaningful results for a heterogeneous aquifer, by analysing the data with a two-dimensional model. This conclusion has far reaching consequences for investigations of multi-layered aquifers, such as those in the Karoo sediments of South Africa. It implies, for example, that the appropriate way, to investigate these aquifers, is to observe and analyse the behaviour of each layer separately. This means that the conventional observation methods will not be very useful in the investigation of heterogeneous aquifers. What needs to be done in this case, is to use more refined observation methods and to analyse the data with a three-dimensional model. For example, one should observe the behaviour of the different water-bearing strata with piezometers, installed in every layer, and not with a partially penetrating borehole as is usually done.

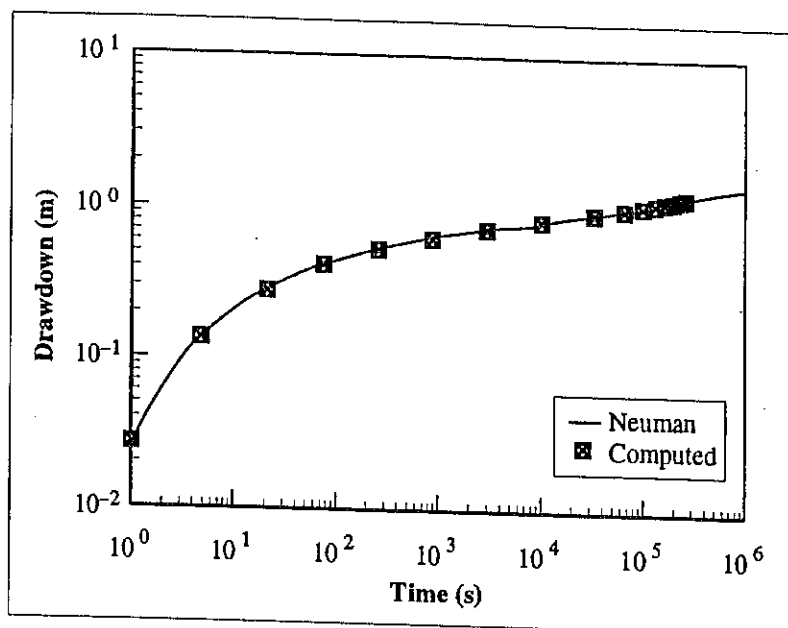


Figure 4 Comparison of the averaged computed drawdown in a two-layer confined aquifer and the Neuman type curve for a phreatic aquifer.

4.4 Recommendations

The most important question to answer at this stage, is whether groundwater researchers (and practitioners) in South Africa, are interested in understanding the behaviour of the heterogeneous aquifers in the country quantitatively, or if a general, qualitative description will do? The indifferent approach, presently in use, will be sufficient for the second alternative, but not for the first. However, it must be kept in mind that both approaches have their own advantages and disadvantages, before selecting a specific approach.

The descriptive approach has two important advantages. (a) It is relatively cheap and easy to implement and (b) can supply a solution in the short term. However, it has been shown, in other countries, that a descriptive solution may sometimes cause more damage to the environment than the problem it was supposed to solve. In addition, the approach cannot provide a reliable framework to management an aquifer efficiently.

The quantitative approach is not without its difficulties either. Two particularly important aspects that must be taken into account in this approach are: (a) how accurately does the conceptual model represent the aquifer, and (b) what is the quality of the data supplied to the model. There is little doubt, that modern conceptual groundwater models can handle very complex phenomena. What is missing, however, is sufficient information on the physical and chemical properties of aquifers and cost-effective methods to determine these properties. This applies in particular to the execution of an aquifer test, which is the only viable method, available now, to study the physical properties and behaviour of an aquifer. These observations suggest that the following procedures be followed in the investigation of a heterogeneous aquifer.

- Obtain a better insight into the physical behaviour of the aquifer. One way to achieve this, is to re-evaluate existing aquifer test data with conventional models and the three-dimensional models developed during this study.
- Supplement the investigations in (a) with more refined field observations, using methods such as ordinary and cross-borehole packer tests and geophysical surveys.
- Give more attention to the development of novel and versatile methods for the observation of the physical properties of an aquifer. A method, that seems to be very promising, is to complement drilling with a seismic survey, using the drill as the source of the seismic waves.

The implementation of the recommendations above, will certainly require more money and suitably trained personnel than the conventional approach. However, the history of science and engineering indicates that the rewards from such an effort usually outweigh the original cost by far.

5 TRIANGULAR IRREGULAR MESHES AND THEIR APPLICATION IN THE GRAPHICAL REPRESENTATION OF GEOHYDROLOGIC DATA

5.1 General

A contour map is without any doubt the method most often used to represent a regionalized variable—a variable that varies in space and or time—graphically. Before the appearance of computers, these maps were usually drawn by hand. Although this is a relatively easy task, it is rather time-consuming. Considerable emphasis has thus been placed on computer graphics to draw contour maps, after computers became commercially available. However, the use of computers for the generation of graphical output raises many mathematical problems. For example it is well-known that classical geometry, which forms the basis for the drawing board and drafting practices, is not algorithmic in nature. In other words, the principles cannot be implemented easily on a computer. Other techniques must therefore be used to derive computer algorithms that exploit the arithmetic power of the computer effectively.

The basic aim of any contouring method is to delineate a regionalized variable through a series of continuous lines that trace prescribed values of the variable on a plane. This suggests that the computerization of a contour map is best achieved with a two-module system. One that discretizes the domain on which the input data is defined and another to represent the contour lines visually. These objectives, unfortunately, are often mutually exclusive. The best one can hope for is a computer package that represents the variable as accurately as possible in an aesthetically acceptable form. Nevertheless, it will be difficult to develop a contouring package that will satisfy all users.

The main aim in developing the package TRICON, was to have a program available that could be used to generate high quality contours of geohydrologic data. However, many of the principles used in the development of TRICON, also apply to other regionalized variables, such as rainfall. The program is thus not restricted to geohydrologic data.

Regionalized variables are usually associated with very large areas. Therefore, it is practically impossible to measure them at all points of interest—least at points where their values may coincide with prescribed contour values. The variable is, consequently, mostly known at a number of points (considerably less than needed to generate smooth contour lines) scattered throughout the domain.

In the days of hand-drawn contours, the deficiency in data points was overcome by using a ruler and pencil to interpolate between the measured values. The same principle can of course also be applied in computer generated contour maps, provided that one can automate the interpolation procedure. Since interpolation is a well-defined mathematical procedure, this would not seem to present serious problems. Unfortunately, the theory is far less developed for two- and higher dimensional domains, than one-dimensional domains. The majority of contouring algorithms, available today, are consequently based on tensor products of one-dimensional interpolation polynomials. This approach is straightforward to apply in cases where the regionalized variable is defined on a square grid, but not when observed at arbitrary spaced points.

There are two methods that can be used to circumvent the discretization of arbitrary spaced point: (a) assign weighted values of the variable to a square grid, overlaid on the observation points, and (b) use an irregular triangular finite element mesh. From a theoretical point of view, one would expect the latter procedure to yield the most accurate results. However, the error, associated with two-dimensional triangular interpolation, is a function of the element shape. The theoretical advantage of a triangular mesh may thus be nullified, if the triangles are not chosen with care.

5.2 Discussion

The characteristics of geological data, more specifically geohydrologic data, presents special problems that need to be taken into account, when devising a contouring package for them. These characteristics and some of the existing methods, for the computation of contour lines, are discussed in Chapter 2.

Chapter 3 is a brief description of work done previously on the computation of triangulations. These methods,

unfortunately, often result in degeneracies, which arise when four or more data points are co-circular. A new method, that avoids degeneracies completely, was consequently developed. This method is also introduced and discussed here. Although the method does not always yield a unique triangulation, in the case of degenerate data, it enables one to handle all types of data—even data defined on a square mesh—without difficulties

The direct triangulation of the data has the advantage that errors, caused by interpolation to rectangular meshes, are eliminated. The contours derived from such a triangulation, therefore, reflect the information in the data, as accurately as the data permit.

The triangulation method was also extended to discontinuous regionalized variables and domains with holes, without any difficulties. This was achieved by using the segmentation of curves to select only those points from a given curve that influence the contour lines significantly. The split-and-merge method used for this purpose is described in Chapter 4.

A new method, referred to as *the method of extra points*, that can be used to approximate discontinuous regionalized variables holes in the domain, is introduced and discussed in Chapter 5. This chapter also contains a complete description of the methods employed to trace and smooth the contour lines. The effectiveness of these methods can be judged from the contour lines in Figure 5.

It is relatively easy to extend the methods in Chapter 3 to include interpolation and the computation of groundwater velocities. These applications are discussed in Chapter 6. Two interpolation methods, that are particularly useful over a triangulated domain, are: triangular and inverse distance weighted gradient interpolation. Both these methods are very accurate and can be quite useful in the interpolation of geohydrologic data, provided that the interpolation points lie within the domain of the data.

Triangular interpolation has another advantage in that it allows one to derive values groundwater velocities, from piezometric heads, which can then be mapped on the domain as shown in Figure 6. This application is particularly useful in investigations of groundwater pollution problems, where it can be used to determine preferential flow directions.

5.3 Conclusions

The package, TRICON is particularly useful for the contouring and interpolation of any set of values, associated with a two-dimensional regionalized variable. The program is also able to draw contours of the difference between two related regionalized variables (e.g., groundwater levels and topography) and to compute groundwater velocities and display them graphically.

The package, which is on-line and menu driven, consists of seven modules. The first module triangulates a given domain. The second and third modules compute the contour lines and groundwater velocities, respectively. The fourth module is the graphical display module, and the fifth module the interpolation module. It may sometimes be necessary to change the input data to such a package and to store intermediate, or final results. This can be achieved by using modules six and seven, respectively. Although the package may not satisfy the needs of all users, experience has shown that it is a very versatile and user friendly package. It also allowed scientists at the Institute for Groundwater Studies and other institutions to solve problems that was previously thought to be intractable. This applies in particular to groundwater pollution studies and phenomena where accurate contours are needed.

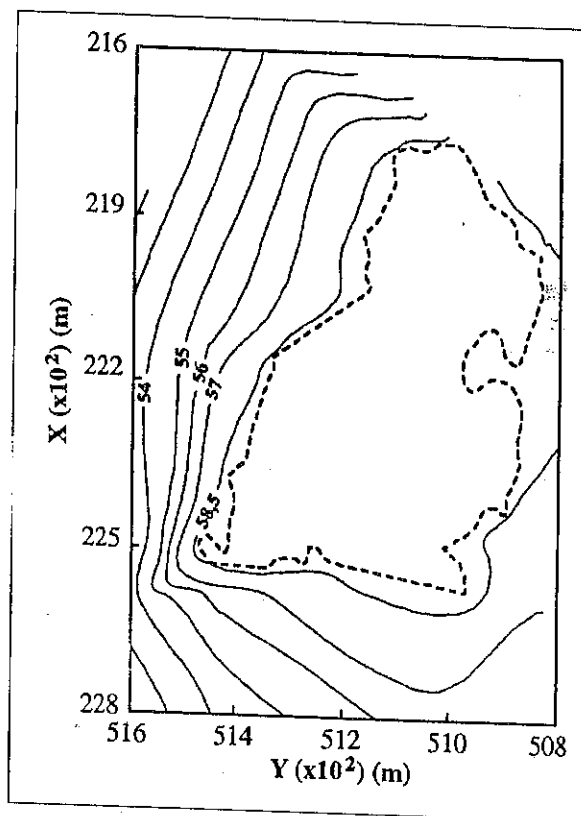


Figure 5 Contours of the piezometric levels in the vicinity of the infiltration pond at Atlantis.

TRICON was developed in the C-language on a personal computer. It is therefore limited to the maximum of 640 KB (kilobytes) addressable memory, generally available on IBM, or IBM-compatible computers. In this format the package can handle up to 800 data points. Another version, TRIBIG, that can handle more than 2 000 data points is available. However, TRIBIG cannot be used to produce graphical output—TRICON must be loaded, after TRIBIG ended, for that purpose.

TRICON was developed on a machine equipped with a numeric co-processor to decrease execution time. Another version, that does not depend on a co-processor, is available, but is significantly slower than the one with the coprocessor. Anyone interested in TRICON should thus to try to have a coprocessor installed in the machine on which the package is implemented.

5.4 Recommendations

There is a tendency today in scientific circles to move from the personal computer to a workstation. This type of computer is not only faster than a personal computer, but can also handle considerably larger sets of data. These machines also use the UNIX operating system, which is much more versatile than the DOS operating system on a personal computer. This factor, and the interest shown by scientists from abroad, for a UNIX version of package, suggest that it may be advantageous to implement the package also on a modern workstation, or 'affordable' supercomputer. Such a conversion will also mean that the package could be implemented on the risc computer of the Computing Centre for Water Research, at the University of Natal in Pietermaritzburg.

6 A COMPARISON OF SPATIAL BAYESIAN ESTIMATION AND CLASSICAL KRIGING PROCEDURES

6.1 General

Environmental variables, such as rainfall, transmissivity of an aquifer and piezometric groundwater levels, vary in space, or time, in ways too complex to represent them with simple deterministic functions. Moreover, it is extremely difficult to measure these variables at all positions of interest. Therefore, it is often necessary either to interpolate or extrapolate the measured values, if values are needed at points where no measurements were taken. The classical interpolation methods are all based on the assumption that the variable of interest can be represented by a smooth function, and are therefore useless for this purpose. What one really need in these circumstances, is a method that not only yields an estimate of the variable, but also the error in the estimate.

The most appropriate way to describe the spatial variability of environmental variables, is to represent them with random functions. This approach has the advantage that it allows one to describe an environmental variable in statistical terms, through the Theory of Regionalized Variables. The best known estimation method, based on this approach, is Ordinary Kriging, or Kriging as it is conventionally known.

Since Kriging is a linear procedure, difficulties are experienced, if the variable to be estimated contains a non-linear trend, or drift as it is called in geostatistical literature. This led to the introduction of what is known today as Universal Kriging. Universal Kriging is, unfortunately, numerically unstable and often singular. Various other approaches, such as the subtraction of trends, have consequently been proposed in the literature. However, the majority of these methods do not satisfy the basic principles associated with a random variable. Their results

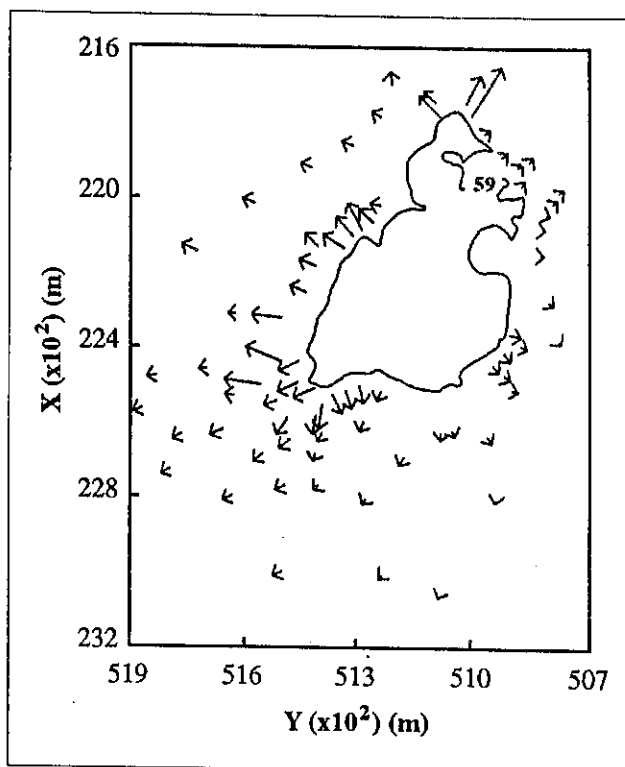


Figure 6 Groundwater velocities around the infiltration pond at Atlantis, computed from the piezometric heads.

cannot therefore always be analysed in a statistical meaningful manner.

There are many situations in the environmental (and exact) sciences where a given variable correlates with another one. For example, groundwater levels often follow the surface topography of the aquifer, see Figure 7. If the latter variable can be sampled more frequently than the first, then one could surely use this information to improve estimates of the first variable.

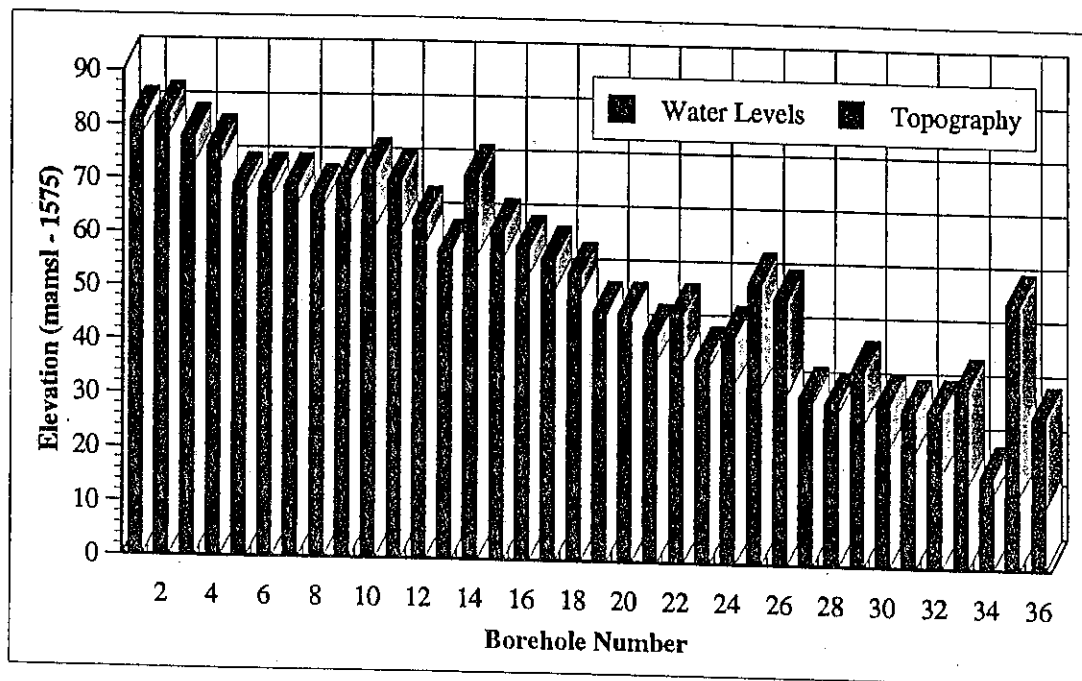


Figure 7 Schematic representation of the correlation between groundwater levels and topography in the Hendrina aquifer.

The first method introduced that used this principle is Cokriging. The method is, from the mathematical point of view, not much more than an extension of Ordinary Kriging to two or more variables. It is thus relatively easy to implement on a computer. However, Cokriging is a very expensive method, as far as computer time and resources are concerned. The method has, therefore, not achieved the same attention as Ordinary or Universal Kriging, until very recently.

Bayesian Kriging is another method that uses this principle. In this approach the classical statistical analysis of Ordinary Kriging is replaced by a Bayesian statistical analysis. The beauty of the Bayesian approach is that it allows one to express prior knowledge of the variable with a 'qualified guess' that can be included in the estimation. The method, unfortunately, still uses the optimization techniques of Ordinary Kriging. It was therefore considered worthwhile to place the technique within a well-formulated Bayesian framework.

Previous work has shown that Ordinary Kriging yields excellent estimates for transmissivities and storage coefficients, but not groundwater levels. The present study was consequently mainly limited to the estimation of groundwater levels.

6.2 Discussion

A review of the available literature revealed that the four methods – Ordinary Kriging, Universal Kriging, Cokriging and the Bayes method – are the only methods able to produce reliable estimates of environmental variables, and their associated errors. The investigation was, therefore, restricted to these four methods.

Terms such as, regionalized variable, semi-variogram and linear estimation, that play an important part in geostatistical estimation theory, are summarized in Chapter 2. This is followed by a discussion of the three Kriging methods, Ordinary, Universal and Cokriging in Chapter 3. However, the purpose of this chapter is only to introduce the reader to the basic terminology and not to describe the theory in depth.

The work done on the Bayes method is described in Chapter 4. Since this work is mostly new, the discussion is fairly complete. Estimation procedures for both univariate and multivariate random functions are discussed. A new semi-variogram for univariate functions, shown in Figure 8, is also introduced there.

The Bayes method is, in mathematical terms, an explicit method, while the Kriging methods are all implicit methods. This is an important advantage that the Bayes method has over the Kriging methods, for it means that the method can be implemented easily on a computer. There are no complex and ill-conditioned sets of linear equations to be solved, as is the case with all three Kriging methods, only the inversion of a single well-behaved correction matrix.

The application and evaluation of the various methods, as to their efficiency in estimating groundwater levels, are discussed in Chapter 5. Water levels from four case studies, the Dewetsdorp aquifer, Zululand coastal aquifer, the 'Pit and Trench' site at Oak Ridge National Laboratory and Hendrina power station site, were used for this purpose. An idea of the accuracy of the method can be obtained from the estimates of water levels for the Dewetsdorp aquifer, in Table 1.

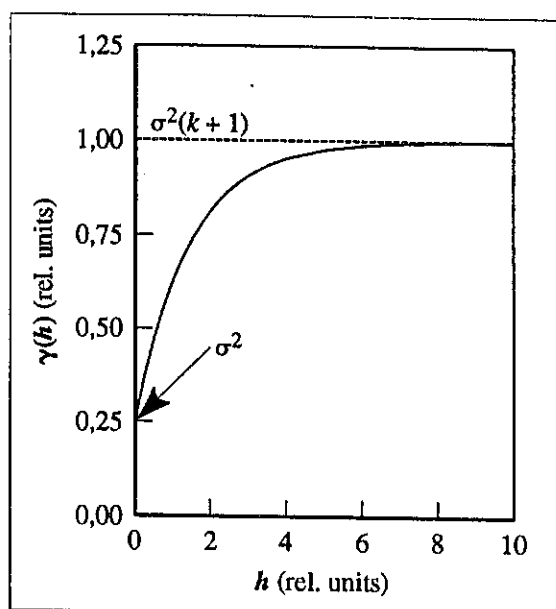


Figure 8 Schematic representation of the semi-variogram, developed for the Bayes method.

Table 1 Estimates of the groundwater levels for 15 boreholes in the Dewetsdorp aquifer, using the four estimation methods described in the report.

Borehole	Topography	Groundwater Levels (mamsl)				
		Observed	Estimated			
			Ordinary Kriging	Universal Kriging	Cokriging	Bayes
1	1500,00	1486,20	1503,80	1507,56	1492,37	1490,62
2	1506,40	1493,60	1493,69	1496,49	1495,08	1495,44
3	1522,30	1518,00	1495,31	1521,48	1507,12	1508,18
4	1539,00	1526,00	1495,50	1531,50	1517,40	1520,64
5	1565,80	1529,80	1522,65	1528,43	1537,94	1540,34
6	1541,00	1533,00	1496,96	1516,84	1517,47	1522,84
7	1555,00	1544,70	1507,50	1515,60	1526,96	1533,27
8	1558,70	1547,00	1498,21	1519,60	1529,66	1536,23
9	1578,00	1571,00	1539,60	1562,08	1551,73	1552,05
10	1623,00	1583,00	1552,02	1574,99	1582,58	1587,83
11	1590,00	1585,90	1529,37	1577,57	1559,61	1562,21
12	1606,30	1595,00	1528,41	1554,94	1566,29	1573,44
13	1615,00	1603,00	1533,06	1614,16	1578,53	1582,18
14	1615,00	1603,60	1533,39	1610,98	1578,36	1582,15
15	1636,30	1610,90	1549,35	1579,15	1591,07	1598,46

6.3 Conclusion

The present investigation has shown that the univariate Bayes method is a versatile estimation procedure for the estimation of groundwater levels. The method also has the advantage that one can use any expert knowledge about a given regionalized variable as a qualified guess. For example, the qualified guesses for groundwater levels near a production field, can be reduced, relative to the water levels further afield. However, difficulties

were experienced to derive a suitable qualified guesses for some regionalized variables. It is therefore recommended that the method be used, whenever the user can establish a suitable qualified guesses, otherwise it may be better to use Ordinary Kriging.

An attempt was also made to expand the method to multivariate variables. However, the method did not yield very satisfactory results, when it was applied to rainfall data from a few rainfall stations in the Orange Free State. The main reason for this was the lack of a suitable, multivariate semi-variogram..

6.4 Recommendations

The program used in this investigation of the Bayes method, is still in the research stage. The method, nevertheless shows considerable promise. It may thus be worthwhile to develop a commercially more viable package, should the need for such a package arise.

7 SUMMARY AND CONCLUSIONS

Insufficient observational data prevented a detailed comparison of two- and three-dimensional models for actual aquifers. Numerical experiments with hypothetical and theoretical aquifers have shown that a two-dimensional model can be used in the study of a homogeneous aquifer, or a single layer, heterogeneous aquifer, provided that the production and observation boreholes penetrate the aquifer fully. A two-dimensional model, however, should never be used to interpret data from a multi-layer aquifer.

The three-dimensional models developed during this investigation were able to handle quite complex situations. However, the results did show that a three-dimensional model is not sufficient to interpret the behaviour of water levels in a heterogeneous aquifer. What is also needed, are observation methods that can be used to delineate the exact nature of a heterogeneous aquifer. This poses a rather severe problem for future investigations of heterogeneous aquifers, since there are very few of these methods available today. More attention should thus be given to the development of sophisticated observational methods, if one wants to understand the behaviour of heterogeneous, especially multi-layer aquifers, better. This may seem to be a formidable and expensive task, but there are quite a number of steps that can already be taken. To quote just one example, it would be foolish to try to analyse data with one of the conventional models, should the borehole lithology indicate that the aquifer is multi-layered.

The Bayes method developed in this investigation proved to be more efficient than either Universal Kriging or Cokriging in the estimation of groundwater levels, and in tracing the movement of contaminated water near an abandoned coal field.. Although the lack of sufficient data prevented its application to three-dimensional water levels, the method could be very useful in the estimation of water levels for three-dimensional models.

The original idea behind the third objective of the study was to have an efficient contouring package for arbitrarily spaced data. As the package developed, it became clear that the algorithms used could be easily adapted for other purposes as well. Two such applications that were included in the present package are: an interpolation technique and the computation of groundwater velocities. Although the contouring section of the package and groundwater velocity calculations are restricted to two-dimensions, the package has already been used with success in investigations of multi-layer aquifers. Preliminary calculations have also shown that the interpolation technique could be extremely useful in the processing of data for three-dimensional models. This applies especially in situations where one does not have a suitable variable to use as qualified guess or covariate for the Bayes and Cokriging methods, respectively.

CONTENTS

Acknowledgements	(i)
Executive Summary	(iii)
Table of contents	(xv)
List of Figures	(xix)
List of Tables	(xxiii)
List of Symbols	(xxv)

Chapter 1 Introduction 1

1.1 General	1
1.2 Conceptual Models for Groundwater Phenomena	1
1.3 Purpose and Scope of the Present Study	3

Chapter 2 The Conceptual Model for Groundwater Motion 7

2.1 General	7
2.2 Fluid Pressure in a Porous Medium	7
.1 The Piezometric Head	7
.2 Hydraulic Conductivity	8
2.3 The Porous Continuum	8
.1 Porosity	8
.2 Water Contents and Saturation	9
.3 Density	9
.4 The Moisture Retention Curve	10
.5 Specific Storativity	11
2.4 The Conceptual Model for Groundwater Motion	12
.1 Mathematical Formulation	12
.2 Initial and Boundary Conditions	13
.3 Precipitation/Evaporation Boundary Conditions.	15
.4 Seepage Boundary Condiions	17
2.5 Sources and Sinks	18

Chapter 3 The Conceptual Model for Groundwater Contamination 21

3.1 General	21
3.2 Basic Transport Processes in Groundwater	22

.1	Introduction	22
.2	Basic Principles	22
.3	The Dispersion Coefficient	23
3.3	The Hydrodynamic Dispersion Equation	25
.1	General	25
.2	Initial and Boundary Conditions	25
.3	Sources and Sinks in Hydrodynamic Dispersion	27

Chapter 4 Numerical Approximations 29

4.1	General	29
4.2	Discretization of the flow equation	30
.1	Variably Saturated Flow	30
.2	Fully Saturated Flow	33
4.3	The Hydrodynamic Dispersion Equation	33

Chapter 5 The Grid Generator 37

5.1	General	37
5.2	Structure of the Generator	37
5.3	Practical Application of Program QBIK	38

Chapter 6 The Saturated Flow Program 41

6.1	Introduction	41
6.2	Comparison of the Numerical Saturated Flow Model with Analytical Models ...	42
6.3	Convergence of the Numerical Solution	45
.1	General	45
.2	Convergence in Time	46
.3	Convergence in Space	46
6.4	Comparison of SAT3 with Modflow	49
6.5	Discussion	52

Chapter 7 The Unsaturated Flow Program 53

7.1	Introduction	53
7.2	The Drainage Problem	53
.1	Description of the Problem	53
.2	Comparison of Program SUF3 with Program UNSAT2	53
7.3	Convergence of the Numerical Model	57
.1	Iteration Convergence	57
.2	Convergence in Time and Space	59

7.4	Conclusions	61
Chapter 8 The Mass Transport Program 63		
8.1	Introduction	63
8.2	Debugging of the Program	64
.1	The Model Problem	64
.2	Finite Element Approximation of The Model Problem	65
8.3	Convergence of The Numerical Model	67
.1	Convergence in Time	67
.2	Convergence in Space	68
8.4	Discussion	68
Chapter 9 Application of the Three-Dimensional Saturated Flow Program 69		
9.1	General	69
9.2	The Single-Layer Aquifer	70
.1	The Homogeneous Uniform Aquifer	70
.2	An Aquifer with Quadratically Distributed Parameters	71
.3	An Aquifer with Gaussian Distribute Parameters	72
9.3	Multi-layer Aquifers	75
.1	General	75
.2	The Two-layer Aquifer	77
.3	The Three-Layer Aquifer	80
9.4	Summary and Conclusions	82
Chapter 10 Conclusions and Recommendations 83		
10.1	Conclusions	83
10.2	Recommendations	85
Appendix A The Three-Dimensional Isoparametric Transformation 87		
A.1	Definition	87
A.2	Transformation of Derivatives	88
A.2	Transformation of Integrals	89
.1	General	89
.2	The Volume Integral	90
.3	The Surface Integral	92
References		95

LIST OF FIGURES

Chapter 1 Introduction 1

- Figure 1-1 Graphical representation of the different aquifers, and thus flow patterns, in a typical multi-layer aquifer. 2

Chapter 2 The Conceptual Model for Groundwater Motion 7

- Figure 2-1 Schematic illustration of a soil moisture retention curve. 10
- Figure 2-2 Schematic representation of the domain, W , of a differential equation and its associated boundary, ∂W 13
- Figure 2-3 Definition of the various symbols used in describing the distribution of water on and in the earth's subsurface. 16
- Figure 2-4 Schematic representation of the different domains in a phreatic aquifer. 17
- Figure 2-5 Distribution of the piezometric head near a borehole, before and after pumping was initiated. 18
- Figure 2-6 Illustration of the different saturation zones near a borehole drilled into a single layer aquifer. 19
- Figure 2-7 Graphical idealization of a multi-layer aquifer. 19

Chapter 3 The Conceptual Model for Groundwater Contamination 21

- Figure 3-1 Dispersion of a slug of pollution introduced into an aquifer with flow restricted to the x -direction as a function of time. 23
- Figure 3-2 Vertical cross-sections through (a) a clean aquifer with a pollution source and (b) a polluted aquifer with a sink. 27

Chapter 5 The Grid Generator 37

- Figure 5-1 Example of a hexahedral element in three-space and the numbering convention used by KUBIK. 38
- Figure 5-2 Schematic representation of the domain used in the discussion of Program QBIK. Dark grey area represent subdomains that require more refined finite element grids. 39
- Figure 5-3 The finite element grid generated for the global domain in Figure 5-2, with Program QBIK. The different shades of grey denote the subdomains into which the domain was divided. 40

Chapter 6 The Saturated Flow Program 41

Figure 6-1	Schematic representation of the hypothetical aquifer used in debugging Program SAT3.	43
Figure 6-2	Comparison of the analytical and numerical solutions of the Muskat aquifer as a function of the distance from the borehole ($t = 72$ h).	44
Figure 6-3	Convergence of the numerical solution for the saturated flow equation, as a function of time at different distances from the borehole.	46
Figure 6-4	Hypothetical aquifer used in studying the convergence rate of Program SAT3 in space.	47
Figure 6-5	The radial finite element grid used with the hypothetical aquifer of Figure 6-4 in studying the spatial convergence of program SAT3.	48
Figure 6-6	Schematic representation of a radial finite element in the horizontal plane of Figure 6-4.	49
Figure 6-7	Radial spacings of the finite element grid, used in studying the spatial convergence of program SAT3, for the hypothetical aquifer in Figure 6-4.	49
Figure 6-8	Spatial convergence of the program SAT3, for the hypothetical aquifer in Figure 6-4 and three of the grids in Table 6-3. ($Dt = 1$ h.)	50
Figure 6-9	Convergence of the numerical solution of Equation 6-1, for three distances from the centre of the borehole.	50
Figure 6-10	The hypothetical homogeneous aquifer used in comparing Programs SAT3 and MODFLOW.	51

Chapter 7 The Unsaturated Flow Program 53

Figure 7-1	Schematic representation of the flume used by Duke (1973) and Hedstrom et al. (1971) in studying the drainage problem.	54
Figure 7-2	Graphs of the experimentally determined moisture retention curve and associated Van Genuchten approximation for Poudre Sand.	54
Figure 7-3	The physical dimensions and boundary conditions used with the drainage problem in the comparison of Programs UNSAT2 and SUF3.	55
Figure 7-4	Vertical cross-section of the three-dimensional grid used with Program SUF3 in comparing it with Program UNSAT2.	55
Figure 7-5	Comparison of the phreatic surfaces, $z(0)$, in the flume simulated with Programs SUF3 and UNSAT2 after 1 and 8 days.	56
Figure 7-6	Convergence properties of the iteration algorithm in Program SUF3.	57
Figure 7-7	Vertical cross-section of the three-dimensional grid used to investigate the convergence of Program SUF3 as a function of the time step.	59
Figure 7-8	Convergence of Program SUF3 for the drainage problem as a function of the	

time step.	60
Figure 7-9 Vertical cross-sections of the three-dimensional grids used to investigate the convergence of Program SUF3 as a function of the element size.	60
Figure 7-10 Graphical representation of the spatial convergence of Program SUF3.	61

Chapter 8 The Mass Transport Program 63

Figure 8-1 Graphical representation of the Cleary-Ungs two-dimensional strip source problem.	64
Figure 8-2 Graphical representation of the three-dimensional aquifer, and associated parameters, used in debugging program SUM3.	65
Figure 8-3 Plan view of the finite element grid, used with the aquifer of Figure 8-3, in debugging Program SUM3.	66
Figure 8-4 Comparison of the numerical and analytical solutions for the aquifer in Figure 8-2, along the lines $(x, 4, 1)$ and $(4, y, 1)$, at the times indicated.	66
Figure 8-5 Convergence of the numerical solution obtained for the model equation with Program SUM3, as a function of the time step at the two points $(1,4,1)$ and $(4,4,1)$	67
Figure 8-6 Convergence of Program SUM3 for the model aquifer as a function of the element size, at the time $t = 0,25$ d.	68

Chapter 9 Application of the Three-Dimensional Saturated Flow Program 69

Figure 9-1 Comparison of the Muskat solution in Equation (6.1) and the piezometric levels computed with SAT3 for the hydraulic parameters in Table 9-1.	70
Figure 9-2 Computed piezometric heads in the model aquifer for the average hydraulic parameters at all elevations, as a function of the time.	72
Figure 9-3 Graphs of the of S_0 and K as functions of elevation above the bottom of the aquifer.	73
Figure 9-4 Graphs of the piezometric heads at three elevations in an observation borehole, 11m from the pumped borehole, computed with the Gaussian distributed hydraulic parameters. The piezometric heads for the average parameters are also shown for comparison.	74
Figure 9-5 Profiles of the piezometric levels in an aquifer with Gaussian distributed hydraulic parameters, and of an aquifer with parameters equal to the average (constant) values of the Gaussian parameters.	74
Figure 9-6 Graphs of the piezometric heads for various elevations in the aquifer, with a partially penetrating borehole, at a distance of 11 m from the pumped borehole and 72 hours of pumping.	75
Figure 9-7 Graphical representation of the model aquifers used in the study of multi-layer	

aquifers.	76
Figure 9-8 Computed piezometric heads at the centre of each layer in the two-layer aquifer and the vertically averaged piezometric head, when the pumped borehole penetrates both aquifers. (Distance from the pumped borehole = 11m.)	78
Figure 9-9 Comparison of the average piezometric heads computed for the two-layer confined aquifer and the Neumann type curve for a phreatic aquifer.	79
Figure 9-10 Computed piezometric heads at the centre of each layer in the two-layer aquifer and the vertically averaged piezometric head, if the upper aquifer was cased off. (Distance from the pumped borehole = 11 m.)	79
Figure 9-11 Piezometric heads in the hypothetical, two-layer aquifer as a function of the radial distance, after three days of pumping in the lower aquifer.	80
Figure 9-12 Piezometric levels observed in the well points WP02, 03, 09 and WP 01, 04, 10 at Atlantis in July 1987 and January 1988.	80
Figure 9-13 Computed piezometric heads in the three-layer aquifer as a function of the time; (a) when water is withdrawn from the full thickness of the aquifer and (b) only from the bottom layer.	81
Figure 9-14 Vertical profiles of the piezometric heads in Figure 9-13.	81
 Appendix A The Three-Dimensional Isoparametric Transformation 87	
Figure A-1 Schematic representation of a three-dimensional finite element (a) in local and (b) in global coordinates.	88
Figure A-2 Graphical representation of the tangent vector to a space curve.	90
Figure A-3 Illustration of the two coordinate systems used in deriving an expression for the transformation of the volume integral.	91
Figure A-4 Illustration of the elementary volume element in the transformed space.	91
Figure A-6 Schematic representation of the tangent plane to the three-dimensional surface $\phi(x, y, z)$	92



LIST OF TABLES

Chapter 5 The Grid Generator 37

Table 5-1	Local and global coordinates used to generate the finite element grid in Figure 5-3 for subdomain A in Figure 5-2.....	39
-----------	------------------------------------------------------------------------------------------------------------------------	----

Chapter 6 The Saturated Flow Program 41

Table 6-1	Dimensions and hydraulic parameters of the aquifer used with the Muskat aquifer in debugging Program SAT3.	44
Table 6-2	Comparison of the analytic and computed piezometric heads in the aquifer of Figure 6-1 for the parameters in Table 6-1, with different values of r_0 . [$t = \Delta t = 0,5$ (h)]	45
Table 6-3	Maximum sizes of elements used in studying the spatial convergence of program SAT3, for the hypothetical aquifer in Figure 6-4.	48
Table 6-4	Computed piezometric heads for the aquifer in Figure 6-9 at diagonal distances of r (m) from the borehole as a function of time.....	51

Chapter 7 The Unsaturated Flow Program 53

Table 7-1	Comparison of the matric heads, at $t = 480$ (s), computed with Program SUF3 for the same time steps used in Figure 7-6.	58
-----------	-------------------------------------------------------------------------------------------------------------------------------	----

Chapter 8 The Mass Transport Program 63

Table 8-1	Absolute errors in the numerical solution of the model problem, along the lines (1, y, 1) and (4, y, 1), for different time steps. ($t = 1$ d)	67
Table 8-2	Absolute errors in the concentrations, computed with SUM3, for three grids in Figure 8-3, with a constant time step of 0,25 (d), at the nodes (1,4,1) and (4,4,1).	68

Chapter 9 Application of the Three-Dimensional Saturated Flow Program 69

Table 9-1	Hydraulic conductivity (K) and specific storativity (S_0) values, determined from fits of the Muskat and Theis type curves to the piezometric levels of Figure 9-1.	70
Table 9-2	Comparison of the quadratically distributed hydraulic conductivity, specific storativity and pumping rates at a few depths in a hypothetical aquifer with their	

	average values.	71
Table 9-3	Values of S_0 , K and Q at a few elevations above the bottom of the aquifer and their average values computed from Equations (7.1) and (7.2).	73
Table 9-4	Average piezometric heads, observed in a heterogeneous aquifer, with (a) a fully and (b) a partially penetrating pumped borehole.	75
Table 9-5	Vertical spacing of the elements in the finite element grid used with the aquifer in Figure 9-7(b).	77
Table 9-6	Comparison of the prescribed hydraulic parameters and those derived from fitting a Theis type curve to the average drawdowns in Figure 9-8.	78
Table 9-7	Aquifer parameters obtained by fitting the average piezometric heads in Figure 9-9 to the Neumann type curve for a phreatic aquifer.	78

LIST OF SYMBOLS

1 LATIN SYMBOLS

c	= Volumetric concentration of a dissolved solid	[M.L. ⁻³]
c_0	= Concentration of dissolved solids in the boundary flux	[M.L. ⁻³]
c_s	= Concentration of the source term	[M.L. ⁻³]
d	= Thickness of an aquifer at x	[L]
$f(x, t)$	= Strength of a source	[T ⁻¹]
g	= Acceleration of gravity	[M.L.T ⁻²]
h	= Magnitude of tangent vector	[L]
$h(x, t)$	= Pressure head	[L]
$l(x)$	= Thickness of an aquifer at x	[L]
$l_k(t)$	= Lagrange interpolation polynomial	[L]
m	= The total mass of fluid and solids in a volume of fluid	[M]
m_a	= The mass of solids absorbed on a volume of porous matrix	[M]
m_b	= The total mass of solids in a volume of porous material	[M]
m_f	= The mass of fluid in a volume of fluid	[M]
m_s	= The mass of solids dissolved in a volume of fluid	[M]
m, n	= Parameters in Van Genuchten's expression for the moisture retention curve	[L]
n	= Outward directed unit normal vector to a surface	[L]
p	= Fluid pressure	[M.L. ⁻¹ .T ⁻²]
$q(x, t)$	= Magnitude of the Darcy velocity $q(x, t)$	[L.T ⁻¹]
q_n	= Normal Darcy flux over a boundary surface	[L.T ⁻¹]
q_0, q_0	= Boundary flux, magnitude and vector form	[L.T ⁻¹]
$q(x, t)$	= Darcy velocity of a fluid in a porous medium	[L.T ⁻¹]
q_m	= Diffusive flux	[L.T ⁻¹]
q_0	= Deviations from the seepage velocity	[L.T ⁻¹]
r_0	= Radius of a borehole	[L]
r	= Distance	[L]
r	= Radius vector	[L]
s	= Mass fraction of dissolved solids	[M.M ⁻¹]
s	= Drawdown in an aquifer	[L]
t	= Time	[T]
u	= A general function	[T]

v	= Volume of a fluid	[L ⁻³]
\mathbf{v}^*	= Microscopic groundwater velocity	[L.T ⁻¹]
$w(z,t)$	= Pressure head along the inside of a borehole	[L]
\mathbf{x}	= x, y, z = Cartesian coordinates of a point	[L]
z	= Elevation above a reference level	[L]
\mathcal{A}	= Surface integral	[L ²]
A	= Surface	[L ²]
$C(h)$	= Moisture capacity	
\mathcal{C}	= Space curve	
C	= Mass fractional concentration of a dissolved solid	[M.M ⁻¹]
\mathcal{D}	= Diffusion coefficient	
$\underline{\mathbf{D}}_d$	= The dispersion tensor	[L ² .T ⁻¹]
$\underline{\mathbf{D}}_h$	= The coefficient of the hydrodynamic dispersion, $\underline{\mathbf{D}}_h = \underline{\mathbf{D}}_m + \underline{\mathbf{D}}_d$	[L ² .T ⁻¹]
$\underline{\mathbf{D}}_m$	= The molecular diffusion tensor	[L ² .T ⁻¹]
D_{ij}	= The ij -th component of the hydrodynamic dispersion tensor	[L ² .T ⁻¹]
D_m	= Molecular diffusion coefficient of mass in a free fluid	[L ² .T ⁻¹]
$\underline{\mathbf{D}}_m$	= Molecular diffusion tensor in a porous medium	[L ² .T ⁻¹]
$Df(t)$	= Derivative of f with respect to t	
D_t	= Partial derivative with respect to t	
E	= Rate of evapotranspiration	[L.T ⁻¹]
E	= Magnitude of E	[L.T ⁻¹]
$E(\tau)$	= Error associated with the Lagrange interpolation polynomial	
J	= $\det(\mathbf{J})$, the Jacobian of the transformation	[L ³]
\mathbf{J}	= Jacobi matrix	[L]
\mathbf{J}	= Total mass flux	[M.L ²]
\mathbf{J}_a	= Advective mass flux	[M.L ²]
\mathbf{J}_d	= Dispersive mass flux	[M.L ²]
J_0, J_1	= Zeroth and first order Bessel functions of the first kind	
K	= Magnitude of hydraulic conductivity	[L.T ⁻¹]
K_0	= Vertical hydraulic conductivity of a semi-permeable layer	[L.T ⁻¹]
$\underline{\mathbf{K}}(\mathbf{x})$	= Hydraulic conductivity tensor	[L.T ⁻¹]
$\underline{\mathbf{K}}_o(\mathbf{x})$	= Unsaturated hydraulic conductivity	[L.T ⁻¹]
$\underline{\mathbf{K}}_r(\mathbf{x})$	= Residual hydraulic conductivity	[L.T ⁻¹]
$\underline{\mathbf{K}}_s(\mathbf{x})$	= Saturated hydraulic conductivity	[L.T ⁻¹]
K_d	= Volumetric distribution coefficient	[L ³ .M ⁻¹]
K_r	= Horizontal hydraulic conductivity	[L.T ⁻¹]
K_z	= Vertical hydraulic conductivity	[L.T ⁻¹]
L	= Symbolic operator	

M	= Mass of a body	[M]
M_a	= Mass of air	[M]
M_s	= Mass of solids	[M]
M_w	= Mass of water	[M]
N_r	= Maximum rate of evapotranspiration through the soil	[L.T ⁻¹]
N_s	= Maximum rate at which the soil can absorb rain	[L.T ⁻¹]
Q_a	= The rate of discharge from the aquifer to the borehole	[L ³ .T ⁻¹]
$Q(x,t)$	= Rate of water injection (+) or withdrawal (-) from a borehole	[L ³ .T ⁻¹]
R	= Radius of an aquifer	[L]
R	= Rainfall intensity	[L.T ⁻¹]
R	= Magnitude of the rainfall intensity	[L.T ⁻¹]
$S(x)$	= $S_0(x)/l(x)$, the storage coefficient of a confined aquifer	[1]
$S_0(x)$	= Specific storativity of an aquifer	[L ⁻¹]
S_w	= Water saturation	[1]
$S_y(x)$	= Specific yield of an unconfined aquifer	[1]
\mathcal{S}	= Surface in three-dimensional space	
T	= Magnitude of transmissivity tensor	[L ² .T ⁻¹]
\mathbf{T}	= Tangent vector	[L]
\mathbf{T}	= Tortuosity tensor of a porous medium	[1]
$\mathbf{T}(x)$	= $\mathbf{K}(x)/l(x)$, the transmissivity tensor	[L ² .T ⁻¹]
\mathcal{V}	= Volume integral	[L ³]
V	= Volume of a fluid	[L ³]
V	= Total volume of porous material	[L ³]
V_a	= Volume of air	[L ³]
V_b	= Volume of porous medium	[L ³]
V_s	= Volume of solids	[L ³]
V_w	= Volume of water	[L ³]
V_0	= Proper volume element	[L ³]

2 GREEK SYMBOLS

α	= Parameter in Van Genuchten's moisture retention curve	
α	= The compressibility of a porous medium	[L.T ² .M ⁻¹]
α	= Roots of the Bessel function	
α_L	= Longitudinal dispersivity	[L]
α_T	= Transverse dispersivity	[L]
β	= Isothermal compressibility of a fluid	[L.T ² .M ⁻¹]
$\delta(x-x_0)$	= Dirac delta function	

δ_{ij}	= Kronecker delta	
ε	= Porosity of a porous medium	
$\phi(\mathbf{x}, t)$	= Piezometric head	[L]
$\phi_b(\mathbf{x}, t)$	= Piezometric head on the boundary	[L]
$\phi_0(\mathbf{x}, t)$	= Piezometric head in a semi-permeable layer	[L]
φ	= Three-dimensional finite element basis function	
λ	= Radioactive decay constant	[T ⁻¹]
γ	= Function describing boundary conditions	[L]
θ	= Angle	
θ	= Volumetric water contents	
θ_r	= Residual water contents	
θ_s	= Saturated water contents	
ρ	= Dimension of an element	[L]
ρ	= Density of a fluid	[M.L ⁻³]
ρ_b	= Dry bulk density	[M.L ⁻³]
ρ_s	= Density of the solids	[M.L ⁻³]
ρ_w	= Wet bulk density	[M.L ⁻³]
ψ	= Soil matric pressure head	[L]
(ξ, η, ζ)	= Coordinates of the local domain Γ	[L]
Δ	= Small increment	
Θ	= Reduced water content	[1]
Γ	= Local domain	
∇	= Gradient operator	[L ⁻¹]
Ω	= Global domain	[L ³]
Ω	= Boundary of the global domain Ω	[L ²]

CHAPTER 1

INTRODUCTION

1.1 GENERAL

There can be no doubt that the availability of clean water is of utmost importance in any country, and yet is often taken for granted. South Africa has a particularly acute problem in this regard, because of the semi-arid climate and rapid increase in its population. The Department of Water Affairs and Forestry indeed already has projected that all available surface water resources will be used fully, by the year 2020. However, there is one source of water that has been largely neglected this far in the country, and that is groundwater.

One reason for this negligence is that groundwater is invisible, and therefore difficult to manage and control. This is especially true in those parts of the country underlain by the highly heterogeneous Karoo sediments. Groundwater is, however, just another physical phenomenon and therefore subjected to well-known physical principles. The question thus arises whether these principles cannot be used to manage and control groundwater resources more efficiently? Judging from the available literature, and previous experience, the answer to this question would seem to be yes, provided that these principles are fully understood. Groundwater could thus become a valuable, additional source of water, if managed correctly.

Another reason why it is necessary to understand the behaviour of groundwater better, is the worldwide problem of groundwater pollution. This problem has already received some attention in South Africa (Botha *et al.*, 1990; Cogho *et al.*, 1990; Levin, 1988). However, more work needs to be done, before the pollution of the country's groundwater supplies can be combated effectively on a national scale. The evaluation of the impact that new and existing waste disposal sites have on the groundwater and environment, as required by the Environment Conservation Act of 1983, could contribute significantly towards this goal, if conducted in a scientific manner.

There is no doubt that the most efficient method to solve the problem of groundwater pollution, is through a better understanding of the underlying physical and chemical principles (Cherry, 1989; Schäfer and Kobus, 1989). This implies that attention should be given, not only to observations of the pollution, but also to the causes of the pollution and the effects it may have on the environment.

1.2 CONCEPTUAL MODELS FOR GROUNDWATER PHENOMENA

The motion of groundwater is largely controlled by two fundamental forces in nature—gravity and fluid pressure. It is thus not too difficult to develop a suitable *conceptual model*

for groundwater flow (Botha *et al.*, 1990). The advantages of such a model are twofold: it combines the basic physical principles into a logical structure and provides a relatively cheap method with which to study the general behaviour of groundwater flow (Mercer and Faust, 1980).

Groundwater is by its very nature a *three-dimensional phenomenon*; in other words, it depends on all three dimensions of space and time. Since a conceptual model is worthless without the support of sufficient observational (experimental) evidence, a large volume of data will be needed, if groundwater phenomena are to be investigated with a three-dimensional model. This poses a major difficulty for the use of conceptual models in groundwater studies, because an aquifer cannot be studied under laboratory conditions. Previous applications of conceptual models in groundwater investigations have consequently been restricted to two-dimensional versions of the conceptual models. Although a simplified model can be quite useful, there are situations where this is not the case (Bear, 1979). Consider for example the multi-layered aquifer of which a schematic view is shown in Figure 1-1. It is not difficult to see that a two-dimensional model will never be able to describe the horizontal and vertical movements of water in this aquifer. There is thus a definite demand for three-dimensional models in groundwater investigations, and this demand will increase as more complex groundwater resources are tapped.

Man's ability, to define conceptual models for groundwater phenomena, has vastly outpaced the methodology for measuring the relational parameters in these models. The measurement of the physical properties of heterogeneous subsurface materials must therefore be considered as *the* central challenge to modern subsurface hydrology (Dane and Moltz, 1991). However, the new 'affordable' supercomputers, with their parallel and multiprocessor options, also place new demands on the computational methods used with these models. It is thus of considerable importance that efforts should be made to develop methods that allow a more efficient implementation of existing (and future) conceptual models.

There are essentially five ways in which conceptual models can be applied more efficiently in practice.

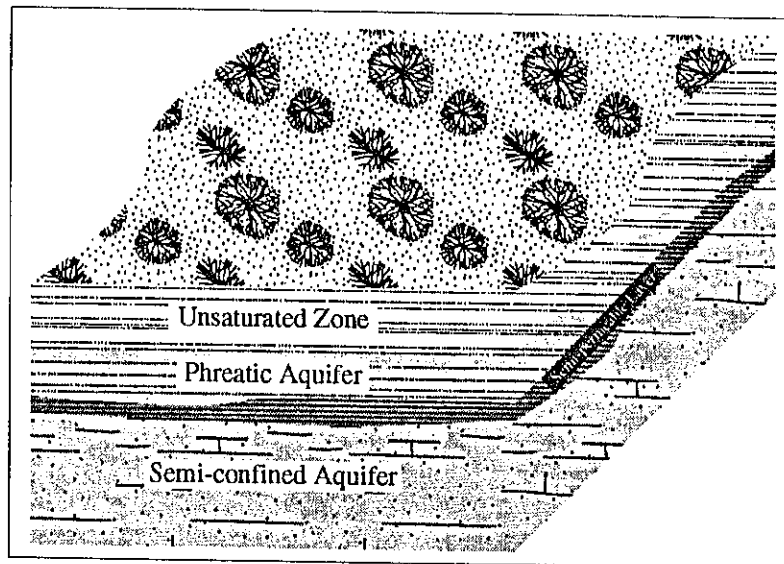


Figure 1-1 Graphical representation of the different aquifers, and thus flow patterns, in a typical multi-layer aquifer.

- Select the conceptual model carefully.
- Use more efficient computational techniques in the implementation of the models.
- Develop more accurate and visually attractive graphical displays for the observational data and computational results.
- Develop more efficient estimation procedures for observational data.
- Develop new and better observational methods.

The first two of these alternatives is addressed in this first volume of the report, while more efficient graphical techniques to compute and display contours, are discussed in Volume II, entitled:

Triangular irregular meshes and their application in the graphical representation of geohydrological data.

It is, and always will be, difficult to have enough information on water levels when using a conceptual model in investigations of groundwater phenomena. A new Bayesian estimation procedure, developed as part of this investigation, is introduced and discussed in Volume III of this report:

A comparison of spatial Bayesian estimation and classical Kriging procedures.

The development of better observational methods is too vast a subject to do justice to it in a project with a limited objective, such as the present one. No attempt will therefore be made to discuss it any further here.

1.3 PURPOSE AND SCOPE OF THE PRESENT STUDY

Investigations conducted during the Atlantis project (Botha *et al.*, 1990), made it clear that two-dimensional conceptual models are not always able to simulate groundwater phenomena accurately. However, three-dimensional models require such vast quantities of data and are so much more complex computationally, that they should only be applied when really necessary. This raises the problem of finding suitable criteria that can be used in deciding when to use a two-dimensional and when a three-dimensional model. Since such criteria could not be found in the available literature, or from other colleagues, the Institute for Groundwater Studies put a research proposal before the Water Research Commission, entitled: 'A Comparative Study of Two- and Three-dimensional Groundwater Models'. The objectives of this study were as follows:

An investigation of two- and three-dimensional models in the simulation of groundwater phenomena, with special reference to: (a) the advantages and disadvantages of two- and three-dimensional models, (b) effective estimates for unknown values required by the models and (c) the graphical representation of groundwater data.

The Commission accepted this proposal and work on the project began in January 1989. The present volume is a report of the work done under objective (a) of the proposal.

A search for computer programs that implements the three-dimensional flow and mass transport conceptual models efficiently, was met without success. The only alternative was thus to develop the programs almost from scratch.

The physical background, needed for the practical implementation of these programs, is discussed at length in the report of the Atlantis project. No attempt will therefore be made to repeat them in any detail. However, the basic principles, needed to understand the new flow and mass transport programs, are discussed briefly in Chapters 2 and 3. Since the programs were developed anew, the opportunity was taken to devise new and more efficient algorithms for them. These algorithms and the numerical approximations used in them are discussed in Chapter 4.


A problem, associated with all computer implementations of conceptual models, is the generation of a suitable spatial grid, needed in the discretization of the governing equations (Botha and Pinder, 1983). As can be expected, this problem is more acute for three- than two-dimensional models. Fortunately, it was not necessary to develop a new grid generator, since a suitable one was found in the Computer Physics Communications Library (Pissanetzky, 1984). This generator and some minor modifications, required to run it on the available computer facilities, are discussed in Chapter 5.

Two separate programs were developed for the conceptual three-dimensional ground-water flow model. The first, developed specifically for *saturated flow*, is discussed in Chapter 6 and the second, for *variably saturated flow*, in Chapter 7, while the program for mass transport is discussed in Chapter 8.

The original project proposal envisaged an evaluation of the newly developed numerical models with data from the Atlantis, Saldanha and Zululand aquifers. Unfortunately, the required data for the latter two aquifers did not realize by the time the project had to be completed, while the data from the Atlantis aquifer were insufficient. The evaluation, therefore, had to be limited to hypothetical, saturated aquifers. This approach has the advantage that it was possible to prescribe exact relational parameters for the models. A number of these investigations, which have a considerable bearing on the Karoo aquifers in South Africa, are described in Chapter 9. However, this meant that it was unnecessary to apply the Bayesian method in Volume III in conjunction with the numerical models. The contouring technique, described in Volume II, proved to be very useful on the other hand, especially in delineating the position of different piezometric levels. Indeed, it is extremely difficult to interpret the results of the three-dimensional models without the use of a contouring package such as TRICON (Buys *et al.*, 1992).

In conclusion, it should be mentioned that this investigation gained considerably from the installation of a Convex 120 'affordable' supercomputer by the University of the Orange Free State in 1991. Indeed, some of the simulations would not have been possible without this computer. A copy of these programs will be supplied to the Computer Centre For Water

Research, on the Campus of Natal University at Pietermaritzburg, where a similar machine has been installed recently. Researchers who want to use these models, but lack the computational power, can therefore approach this Centre.



CHAPTER 2

THE CONCEPTUAL MODEL FOR GROUNDWATER MOTION

2.1 GENERAL

The conceptual model used in this study of groundwater flow, is the porous medium model. A complete description of the model can be found in Bear and Bachmat (1990), Botha *et al.* (1990) and Bear (1979, 1972). The present discussion is therefore limited to those principles that play an important role in the implementation of the model on a computer and its practical application.

A conceptual model is build around two basic quantities—*variables* and *relational parameters* (Botha *et al.*, 1990). The porous medium model for groundwater flow contains one dependent variable and two relational parameters besides the spatial coordinates and time. These are: the piezometric head, hydraulic conductivity and specific storativity (Botha *et al.*, 1990). The piezometric head and hydraulic conductivity are discussed in Section 2.2. This is followed by a discussion of the porous continuum and its associated parameters in Section 2.3. The conceptual model, its associated initial and boundary conditions and the forcing function, for boreholes, are discussed in Section 2.5.

2.2 FLUID PRESSURE IN A POROUS MEDIUM

2.2.1 The Piezometric Head

The motion of all fluids on earth, not subjected to artificially applied forces, are governed by two fundamental forces—the fluid pressure, $p(x, t)$, and gravity. The effect of these two forces are conventionally combined into a single variable, known as *Hubert's potential* or the *piezometric head*, defined by the equation

$$\phi(x, t) = h + z \quad (2.1)$$

where z is the elevation of the fluid above a suitable reference datum, and

$$h(x, t) = \int_{p_0}^p dp/\rho g \quad (2.2)$$

the pressure head. The compressibility of water is so small that the pressure head is often simply taken as

$$h(x, t) = p/\rho g \quad (2.3)$$

although this is strictly only valid for incompressible fluids.

2.2.2 Hydraulic Conductivity

The *flux* of water through a porous medium—the volume of water flowing through a unit area, per unit of time, normal to the direction of flow—is a very important quantity in the flow of groundwater. Based on the pioneering work of the French engineer Henri Darcy, this flux is conventionally expressed in the form

$$\mathbf{q} = -\mathbf{K}(\mathbf{x}, t) \nabla \phi(\mathbf{x}, t) \quad (2.4)$$

where $\nabla \phi(\mathbf{x}, t)$ is the gradient of the piezometric head and $\mathbf{K}(\mathbf{x}, t)$ the *hydraulic conductivity*, of the medium. The dimension of \mathbf{q} is $[L \cdot T^{-1}]$. It has consequently become a common practice to refer to \mathbf{q} as the *Darcy velocity*, although it is not really a velocity.

The hydraulic conductivity, $\mathbf{K}(\mathbf{x}, t)$, which describes the ease with which water can flow through the porous medium, is in general a *symmetric second rank tensor*. In other words, the value of \mathbf{K} depends on the direction in which it is measured (Botha *et. al.*, 1990). Such a medium is called *anisotropic*. If \mathbf{K} is not a function of \mathbf{x} , the medium is said to be *homogeneous*, otherwise it is *heterogeneous*. The porous media, associated with groundwater flow phenomena, vary from *uniform*, or *homogeneous isotropic* ($\mathbf{K} = \text{a constant}$ throughout the medium), to *heterogeneous anisotropic* [$\mathbf{K} = \mathbf{K}(\mathbf{x}, t)$].

Groundwater levels tend to follow the topography of the terrain closely (Van Sandwyk *et al.*, 1992). It is thus often assumed that groundwater flow is parallel to the earth's surface. This can only be true, according to Equation (2.4), if

$$D_z \phi(\mathbf{x}, t) = 0$$

The piezometric head in such an aquifer, will thus always remain constant, in the vertical direction. In other words the piezometric head in such an aquifer must satisfy the hydrostatic equation

$$\phi(\mathbf{x}, t) = h + z = \text{constant}$$

in the vertical direction.

2.3 THE POROUS CONTINUUM

2.3.1 Porosity

The volume of fluid that a porous medium can hold, is determined completely by the volume of its pores. One can thus expect that this quantity will play an important role in the study of fluid flow through a porous medium. The volume of pores will obviously depend on the volume of porous material considered, and is thus not a particularly useful concept. Most

descriptions of a porous medium are consequently based on the concept of *porosity*, defined by the equation

$$\varepsilon = \lim_{\Delta V \rightarrow \Delta V_0} \frac{\Delta V_w + \Delta V_a}{\Delta V} \quad (2.5)$$

where

$$\Delta V = \Delta V_w + \Delta V_s + \Delta V_a$$

is the total volume of porous material, and ΔV_w , ΔV_s and ΔV_a the volume of water, solids and air in ΔV , respectively (Botha *et al.*, 1990).

The *proper volume element*, ΔV_0 , was introduced in Equation (2.5) to account for the experimental fact that the ratio

$$e = \frac{\Delta V_w + \Delta V_a}{\Delta V}$$

is not a constant in natural porous materials, as one might expect intuitively, but a function of ΔV . From the mathematical point of view, this element should be large enough to hide any microscopic properties of the medium, but also small enough to allow ε (and other quantities derived from it) to be differentiable.

2.3.2 Water Contents and Saturation

The porosity is a very convenient measure for the volume of voids in a porous medium. However, it is often as important to know how much fluid the medium contains in the study of flow through an unsaturated, or variably saturated, porous medium. This quantity is conventionally measured in terms of either the *water contents* of the medium defined as,

$$\theta = \lim_{\Delta V \rightarrow \Delta V_0} \frac{\Delta V_w}{\Delta V} \quad (2.6)$$

or the *water saturation*

$$S_w = \theta / \varepsilon$$

The advantage of the latter quantity is that it allows one to express the water contents of a porous medium directly in terms of its porosity.

2.3.3 Density

Another quantity that plays a particular important role in the flow of subsurface fluids is *density*. Because a porous material does not consist of a single component, density is a rather ambiguous term to use in the case of a porous medium. This ambiguity is usually circumvented by introducing not one, but three densities. These densities, defined in terms of the

proper sample volume, introduced in Equation (2.5), and the mass fractions

$$\Delta M = \Delta M_w + \Delta M_s + \Delta M_a$$

are:

- (a) Density of solids $\rho_s = \Delta M_s / \Delta V_s$
- (b) Dry bulk density $\rho_b = (\Delta M_s + \Delta M_a) / \Delta V$
- (c) Wet bulk density $\rho_w = \Delta M / \Delta V$

2.3.4 The Moisture Retention Curve

It has been observed experimentally that the curvature of the menisci, formed by the remaining capillary water with the matrix grains, decreases, if capillary water is removed from an unsaturated porous medium. However, Laplace's equation for capillary pressure requires that a decrease in radius must be accompanied by a decrease in the pressure of the water. The pressure in an unsaturated porous medium is thus closely related to the volume of water contained by the medium. This relation, known as the *moisture retention curve*, can be conveniently expressed mathematically in terms of the volumetric water contents θ , defined in Equation (2.6), as

$$\psi = \psi(\theta) \quad (2.7)$$

where $\psi = -h$ is known as the *matric pressure head* of the fluid.

The moisture retention curve, of which an example is shown in Figure 2-1, cannot be expressed in simple mathematical terms. It is not only highly non-linear, but also shows a *hysteresis effect*. This means that the curve is double legged, with one leg valid during the drying cycle (desorption) and the other one during the wetting cycle (sorption). This behaviour of the retention curve and the fact that it is difficult to withdraw water from the unsaturated zone, are probably the reasons why geohydrologists have not paid much attention to the unsaturated zone in the past.

It is interesting that the moisture retention curve generally does not approach infinity along the matric pressure axis as the moisture contents decreases, but along a line through a small positive value of θ . This quantity, known as the *residual water contents*, is usually denoted by the symbol θ_r . The water contents of a soil are consequently often expressed in terms of its *reduced water contents*

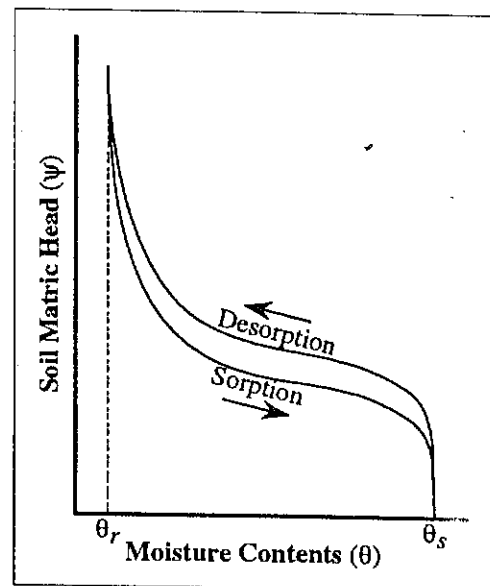


Figure 2-1 Schematic illustration of a soil moisture retention curve.

$$\Theta = (\theta - \theta_r) / (\theta_s - \theta_r) \quad (2.8)$$

where $\theta_s (= \epsilon)$ is the *saturated water contents* of the medium.

Viewed from a mathematical point of view, one should be able to represent the moisture retention curve by a smooth and continuous relation. However, since the curve can only be determined experimentally, this is not possible. The curve is consequently often approximated in practice by a smooth function. One function used for this purpose is the function

$$\Theta = [1 + (\alpha\psi)^n]^{-m} \quad (2.9)$$

originally proposed by Van Genuchten (1980), where the parameters α and n may be considered as characteristic constants for a particular soil. Van Genuchten suggested in his original paper that m should be taken as $(1 - 1/n)$, but in a later paper (Van Genuchten and Nielsen, 1985) that it should be considered as an independent third characteristic constant. However, a detailed study has shown that his original proposal fits the experimental data of South African soils better. The variably saturated flow model, discussed in Chapter 7, was consequently based on Van Genuchten's original proposal.

A particular advantage of the Van Genuchten approximation in Equation (2.9) is that it allows one to express the unsaturated hydraulic conductivity in the very simple form

$$\underline{K}(\Theta) = \underline{K}_s \Theta^{1/2} [1 - (1 - \Theta^{1/m})^m]^2 \quad (2.10)$$

where \underline{K}_s is the saturated hydraulic conductivity. Since θ is a function of ψ , $\underline{K}(\Theta)$ will also be a function of ψ and thus the pressure head h (Botha *et al.*, 1990).

2.3.5 Specific Storativity

The volume of fluid that can be stored in (or retrieved from) a porous medium, is a very important quantity in the management of groundwater resources. The water contents, θ , would obviously be an ideal measure to use for this purpose. However, since both the subsurface of the earth and water are compressible materials, θ depends on the forces acting on the medium. It is thus not a very useful measure for saturated flow.

The quantity universally used to measure the volume of fluid in the saturated zone is the *specific storativity*, or simply *storativity*, which is related to the *compressibility of the medium*, α , and the *compressibility of water*, β , through the equation (Bear, 1979; Bear and Bachmat, 1990)

$$S_0 = \rho g [\alpha(1 - \epsilon) + \epsilon\beta] \quad (2.11)$$

where ρ is the density of water and g the *acceleration of gravity*.

If the dependence of ρ on the fluid pressure is neglected, Equation (2.11) can also be expressed in the form (Botha *et al.*, 1990),

$$S_0 = \frac{1}{\Delta V_b} \frac{\Delta V_w}{\Delta \phi}$$

where ΔV_w is the volume of water added to (or withdrawn) from a porous medium with volume ΔV_b , and $\Delta \phi$ is the resulting change in piezometric head. This equation is the basis for the common interpretation of storativity as the volume of water released from a unit volume of aquifer, per unit decline in piezometric head.

2.4 THE CONCEPTUAL MODEL FOR GROUNDWATER MOTION

2.4.1 Mathematical Formulation

Groundwater flow is a physical phenomenon and thus subject to the law of mass conservation. The easiest way to derive a conceptual model for groundwater flow is thus to combine the law of mass conservation with Darcy's law in Equation (2.4). By following this procedure, it can be shown (Botha *et al.*, 1990; Huyakorn *et al.*, 1986b; Huyakorn and Pinder, 1983) that the most general conceptual model for groundwater flow is described by the equation

$$D_t[\rho\theta(\mathbf{x},t)] = \nabla \cdot [\rho \underline{\mathbf{K}}(\mathbf{x},t) \nabla \phi(\mathbf{x},t)] + \rho f(\mathbf{x},t) \quad (2.12)$$

where

$$f(\mathbf{x},t) = \frac{\text{Volume of fluid entering a volume of porous material per unit time}}{\text{Volume of porous material}} \quad (2.13)$$

is known as the *strength* of any sources or sinks that may be present in the medium.

Although density-dependent flow phenomena are often encountered in groundwater investigations (e.g., the problem of sea-water intrusion), the present investigation will be restricted to density-independent flow problems. This means that one can divide Equation (2.12) throughout with ρ to obtain the somewhat simpler equation

$$D_t[\theta(\mathbf{x},t)] = \nabla \cdot [\underline{\mathbf{K}}(\mathbf{x},t) \nabla \phi(\mathbf{x},t)] + f(\mathbf{x},t) \quad (2.14)$$

Equation (2.14) is a three-dimensional partial differential equation, which contains different dependent variables on its left- and right-hand sides. Such a formulation is not very useful when a differential equation has to be solved analytically. Equation (2.14) is consequently usually transformed into an equation with one dependent variable. This can be achieved by using the water retention curve, defined in Equation (2.7), to replace θ with ϕ . However, Allen (1985) has shown that it is easier to satisfy the law of mass conservation in a numerical approximation based on Equation (2.14), than in one that is based on the transformed equation. The two numerical flow models, developed in this investigation, were consequently based on Equation (2.14).

Equation (2.14) may be somewhat perplexing to someone not acquainted with unsaturated flow. However, it is not too difficult to show (Botha *et al.*, 1990) that Equation (2.14) reduces indeed to the better known equation

$$S_0 D_t \phi(\mathbf{x}, t) = \nabla \cdot [\mathbf{K}(\mathbf{x}, t) \nabla \phi(\mathbf{x}, t)] + f(\mathbf{x}, t) \quad (2.15)$$

where S_0 is the storativity, defined in Equation (2.11), for saturated flow.

Equation (2.15) is a much simpler equation than Equation (2.14), from the mathematical point of view. However, the superior numerical properties suggest that it still would be more advantageous to use Equation (2.14) in developing a computer model for saturated flow. As will be shown in Chapter 6, this is indeed the case.

2.4.2 Initial and Boundary Conditions

The solution of any partial differential equation always contains a number of integration constants, that have to be determined in one way or another. The method, universally used for this purpose, is to associate the equation with an *interior domain* (Ω say) and a *boundary* ($\partial\Omega$ say), as shown in Figure 2-2. The integration constants can then be determined by prescribing suitable *initial* and *boundary conditions* (Botha and Pinder, 1983).

It is usually not very difficult to choose a suitable initial condition for a given equation. All that is needed, is to know how the dependent variable varies over Ω at a certain moment, usually taken as $t_0 = 0$. An initial condition for Equation (2.14) can, for example, be expressed in the form

$$\phi(\mathbf{x}, t_0) = \phi_0(\mathbf{x}) \quad (\mathbf{x} \in \Omega) \quad (2.16)$$

where $\phi_0(\mathbf{x})$ is the piezometric head at the time $t = 0$.

In contrast to what one may expect, the theory of differential equations allows only three types of boundary conditions to be associated with the differential equation

$$\mathbf{L}u(\mathbf{x}, t) = f(\mathbf{x}, t)$$

These are (Hildebrand, 1976):

- (a) *Dirichlet* conditions (or boundary conditions of the *first* type)

$$\alpha(\mathbf{x}, t)u(\mathbf{x}, t) = \gamma(\mathbf{x}, t)$$

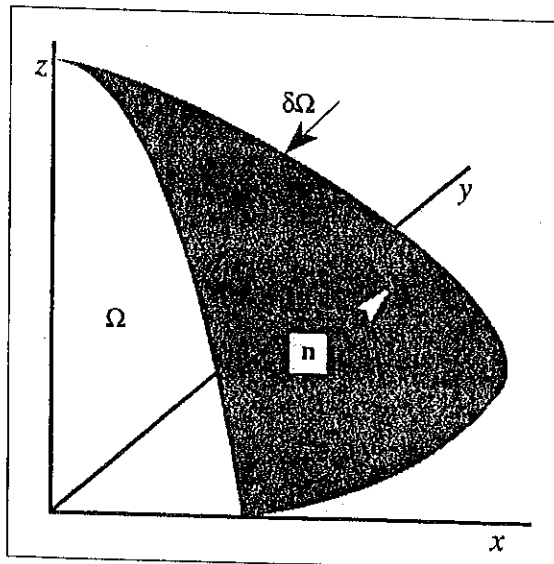


Figure 2-2 Schematic representation of the domain, Ω , of a differential equation and its associated boundary, $\partial\Omega$.

(b) *Neumann* conditions (or boundary conditions of the *second* type)

$$\beta(\mathbf{x}, t) \nabla u(\mathbf{x}, t) = \gamma(\mathbf{x}, t)$$

(c) *Cauchy* conditions (or boundary conditions of the *third* type)

$$\alpha(\mathbf{x}, t) u(\mathbf{x}, t) + \beta(\mathbf{x}, t) \nabla u(\mathbf{x}, t) = \gamma(\mathbf{x}, t)$$

where $\alpha(\mathbf{x}, t)$, $\beta(\mathbf{x}, t)$ and $\gamma(\mathbf{x}, t)$ are known functions of $\mathbf{x} (\in \partial\Omega)$ and t . If $\gamma(\mathbf{x}, t) = 0$, the conditions are said to be *homogeneous*, otherwise they are known as *non-homogeneous* boundary conditions.

Dirichlet boundary conditions are usually associated in groundwater flow with a body (or bodies) of surface water (rivers, lakes or oceans) that intersects an aquifer. A suitable Dirichlet boundary condition for Equation (2.14) will thus be of the form

$$\phi(\mathbf{x}, t) = \phi_1(\mathbf{x}, t) \quad (\mathbf{x} \in \partial\Omega_1, t > 0) \quad (2.17)$$

where $\phi_1(\mathbf{x}, t)$ is the *known* piezometric head in the body of surface water.

Neumann boundary conditions, also referred to as *flux boundary conditions*, are probably the most frequently used (and misused) type of boundary condition in groundwater flow phenomena. This type of boundary condition is usually associated with a flux of material across the boundary Ω . A suitable Neumann condition for Equation (2.14), would thus be of the form

$$\mathbf{q}(\mathbf{x}, t) \cdot \mathbf{n} = -[\mathbf{K} \nabla \phi(\mathbf{x}, t)] \cdot \mathbf{n} = q_n(\mathbf{x}, t) \quad (\mathbf{x} \in \partial\Omega_2, t > 0) \quad (2.18)$$

where \mathbf{n} is the outwardly directed unit vector, normal to the boundary $\partial\Omega$, see Figure 2-2.

Cauchy boundary conditions are usually associated with semi-permeable boundaries in groundwater flow phenomena. Boundaries of this type occur where a thin layer of low permeable material separates a porous domain and a body of water, e.g., at the bottoms of recharge ponds (artificial and natural), rivers and lakes. A Cauchy boundary condition is usually expressed in the form

$$\mathbf{n} \cdot \mathbf{K} \nabla \phi(\mathbf{x}, t) + K_l \phi(\mathbf{x}, t) = K_l \phi_0(\mathbf{x}, t) \quad (\mathbf{x} \in \partial\Omega_3, t > 0)$$

when applied to Equation (2.14), where ϕ_0 is the piezometric head in the semi-permeable layer and $K_l = K_0/l$, with l the thickness and K_0 the vertical hydraulic conductivity of the semi-permeable layer.

A Cauchy boundary is a rather special kind of boundary and not easy to apply in groundwater flow problems. It was consequently not implemented in the numerical flow models discussed in Chapters 6 and 7.

It is important to note that the types of boundary conditions can be mixed freely when applied to a given differential equation. The only constraint is that the conditions should cover the boundary, Ω , fully.

Although the three types of boundary conditions introduced above are the only boundary conditions allowed for, by the theory of partial differential equations, there is

nothing that prohibits a change in boundary condition from one type to another as time progresses. Two types of boundary conditions, that occur quite frequently in groundwater flow phenomena, and precisely do this, are *precipitation-evaporation* and *seepage boundary conditions*. These conditions will now be discussed in more detail.

2.4.3 Precipitation/Evaporation Boundary Conditions.

Precipitation and evaporation boundaries are usually associated with the surface of the earth. They differ mathematically only in the sense that the fluxes associated with them have opposite directions. However, since the physical processes involved are quite different, the boundaries are usually treated as separate boundaries.

In deriving the conceptual model for groundwater flow, it is customarily assumed that fluxes out of the domain represent a loss, and fluxes into the domain a gain in the volume of water contained by the domain (Botha *et al.*, 1990). Precipitation thus should be considered as a positive flux, even though it is directed towards the earth's surface. However, such an interpretation is in direct contrast to the routine interpretation of 'up' as positive in a right handed Cartesian coordinate system. Many discussions of groundwater flow therefore sometimes use a coordinate system rotated through 180°. However, this convention will not be followed here. The positive z -axis will always be taken as normal to the earth's surface in the direction of the atmosphere.

To derive suitable expressions for precipitation events, consider the situation of an unsaturated soil surface with a hydraulic conductivity \underline{K}_0 , subject to a rainfall intensity R . Everyday experience indicates that on reaching the earth's surface, the rain immediately begins to infiltrate, if the surface is not saturated. However, in heavy rainstorms, the rain tends to form ponds on the surface rather than infiltrate. This phenomenon, known as *ponding*, can be explained as follows.

Rainwater can only infiltrate into the soil surface if the normal rainfall intensity is larger than or equal to the normal flux through the surface. This situation can be described mathematically through the inequality

$$\mathbf{n} \cdot \mathbf{R} = \mathbf{n} \cdot \mathbf{k}R \geq \mathbf{n} \cdot \underline{K}_0 \nabla \phi$$

where \mathbf{k} is the unit Cartesian vector in the z -direction and R the intensity of the rain. This yields the non-homogeneous Neumann condition

$$\mathbf{n} \cdot \underline{K} \nabla \phi = \mathbf{n} \cdot \mathbf{k}R \quad (2.19)$$

as the condition R must satisfy in order for water to infiltrate the soil surface. The soil's ability to transmit water is not without a limit, however. This limit is reached, for any value of $\nabla \phi$, when the soil becomes saturated, i.e., when the hydraulic conductivity of the surface, \underline{K}_0 say,

is equal to its saturated hydraulic conductivity, \underline{K}_s . The rainfall boundary condition assumes in this case the form

$$\mathbf{n} \cdot \underline{K}_s \mathbf{k} = \mathbf{n} \cdot \mathbf{k} R \Rightarrow \mathbf{n} \cdot [N_s - R] \mathbf{k} = 0$$

There is thus a limit to the rate at which a soil can absorb rain, given by

$$R = N_s, \quad \text{or} \quad R = K_s$$

in the case of anisotropic and isotropic soils respectively, where N_s is the saturated equivalent of

$$N = \sqrt{N_x^2 + N_y^2 + N_z^2} \quad (2.20)$$

with

$$N_x = n_x K_{xx} + n_y K_{yx} + n_z K_{zx}$$

$$N_y = n_x K_{xy} + n_y K_{yy} + n_z K_{zy}$$

$$N_z = n_x K_{xz} + n_y K_{yz} + n_z K_{zz}$$

and K_{uv} the uv -th component of \underline{K} . As soon as this limit is reached, the rain begins to pond and the boundary condition has to be changed to the Dirichlet condition

$$\phi(\mathbf{x}, t) = \phi_p(\mathbf{x}, t) = h_p(\mathbf{x}, t) + z_0 \quad (2.21)$$

where $h_p(\mathbf{x}, t)$ is the depth of the ponded water on the surface, shown in Figure 2-3.

The earth's surface loses water through either one of two phenomena: *evaporation* and *transpiration*. Although there are situations where one of the processes completely dominates the other (bare soil surfaces and dense forests, for example), they usually occur simultaneously, hence the designation *evapotranspiration*. Evapotranspiration is first controlled by the atmospheric conditions prevalent at the surface of the earth. However, just as the infiltration rate of rain is controlled by the hydraulic properties of the soil, so is evapotranspiration. For no matter how large the atmospheric evaporation demand (AED) may be, the earth's surface cannot supply more water than what can be transmitted through the upper soil layers, or plant roots. The actual rate of evapotranspiration, E , is thus controlled by an inequality of the form

$$\mathbf{n} \cdot \underline{K}_0 \nabla \phi \geq \mathbf{n} \cdot \mathbf{E}$$

and not the AED. The boundary condition to be used with evapotranspiration is thus the non-homogeneous Neumann condition

$$\mathbf{n} \cdot \underline{K} \nabla \phi = \mathbf{n} \cdot \mathbf{E} = \mathbf{n} \cdot \mathbf{k} E \quad (2.22)$$

However, the ability of a soil to yield water, is limited by its residual water contents, θ_r , or

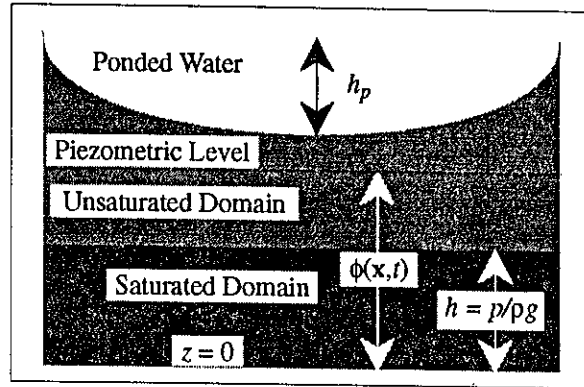


Figure 2-3 Definition of the various symbols used in describing the distribution of water on and in the earth's subsurface.

the equivalent residual matric head, h_r . Evapotranspiration is thus also limited by an inequality of the form

$$n \cdot [N_r - E]k \geq 0$$

where N_r is the equivalent of N in Equation (2.20) when $\mathbf{K} = \mathbf{K}_r$, the residual hydraulic conductivity of the soil. If this condition cannot be satisfied, the boundary condition has to be changed to the Dirichlet condition

$$\phi(\mathbf{x}, t) = \phi_r(\mathbf{x}, t) = h_r(\mathbf{x}, t) + z_o \quad (2.23)$$

It is thus of the utmost importance that the modeller of groundwater flow should have a good knowledge of the prevailing climatic conditions if he is to prescribe effective boundary conditions for evapotranspiration.

Experimental evidence suggests that precipitation is always accompanied by evapotranspiration from the earth's surface. However, the magnitude of evapotranspiration is then usually much smaller than the rainfall intensity, with the result that it can be neglected. The only noteworthy exception to this rule is that of a barren hot surface, where the rain may evaporate the moment it reaches the soil surface.

2.4.4 Seepage Boundary Conditions

A phreatic aquifer can be divided naturally into three domains: a *permanently unsaturated*, a *drainable* and a *permanently saturated domain*, see Figure 2-4. As used here, the term drainable domain refers to an unsaturated part of the aquifer that becomes saturated during recharge events. The drainable domain can thus be characterized as a domain that will tend to replenish the unsaturated and saturated domain, when water is withdrawn from the latter. The drainable domain is thus not static.

The drainable domain in a phreatic aquifer is often exposed to the atmosphere along valleys, the shores of oceans and lakes and river banks. Water will thus tend to drain from the domain towards the atmosphere, if the domain is saturated, $h(\mathbf{x}, t) > 0$; thereby creating a *seepage face*, see Figure 2-4. This situation can be described mathematically through a Dirichlet boundary condition of the form

$$\phi(\mathbf{x}, t) = \phi_0(\mathbf{x}, t) = z \quad (2.24)$$

This condition must, however, be changed to

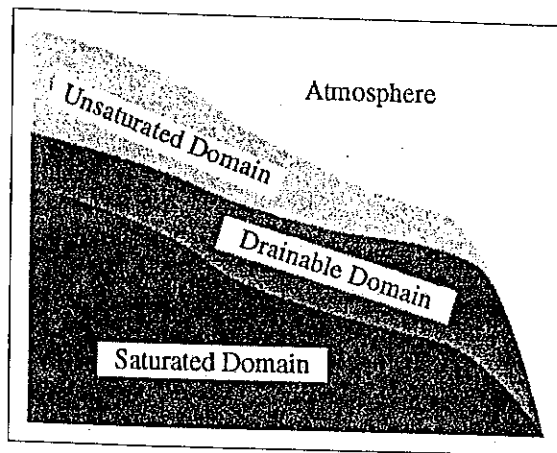


Figure 2-4 Schematic representation of the different domains in a phreatic aquifer.

a rainfall or evaporation boundary condition, as soon as the domain becomes unsaturated, i.e., if the pressure head $h(\mathbf{x}, t) \leq 0$. The correct boundary condition to use with a seepage face is thus either a Dirichlet condition, given by Equation (2.24), and a rainfall or evaporation boundary as described by Equations (2.19) to (2.21), and Equations (2.22) to (2.23), respectively.

It is impossible to determine the state of the soil surface in advance for precipitation, evaporation, or seepage boundaries. These boundary conditions can thus only be applied iteratively.

2.5 SOURCES AND SINKS

Boreholes are often represented as point sources when solving the two-dimensional equivalent of Equation (2.14) (Botha *et al.*, 1990). This is achieved by expressing the source term, $f(\mathbf{x}, t)$ of Equation (2.14), in the form

$$f(\mathbf{x}, t) = Q(t)\delta(\mathbf{x} - \mathbf{x}_0)$$

where \mathbf{x}_0 is the position of the point source, $Q(t)$ the rate at which water is discharged from the aquifer and $\delta(\mathbf{x} - \mathbf{x}_0)$ the Dirac delta function, defined by the equation

$$\int_{\Omega} g(\mathbf{x})\delta(\mathbf{x} - \mathbf{x}_0)d\mathbf{x} = g(\mathbf{x}_0)$$

This approach can, unfortunately, no longer be applied in the case of Equation (2.14), since the thickness of the aquifer cannot be neglected. One has thus to use either a line source, which cannot be represented easily by a Delta function, or another approach.

The first possibility would be to determine $f(\mathbf{x}, t)$ directly from its definition in Equation (2.13). However, this implies that the volume of the aquifer from which the water is withdrawn must be known, which is never the case. Vos (1984) circumvent the problem by equating the volume of porous material with the total volume of the aquifer. This may be true for a uniform aquifer, but not for a heterogeneous layered aquifer.

A borehole is not part of the aquifer, but forms a boundary of the aquifer, as can be seen by comparing Figures 2-2 and 2-5. It would thus be mathematically more correct to treat a borehole as a boundary to the aquifer and not as a source or sink. The only difficulty associated with this interpretation is what type of boundary condition to use in practice.

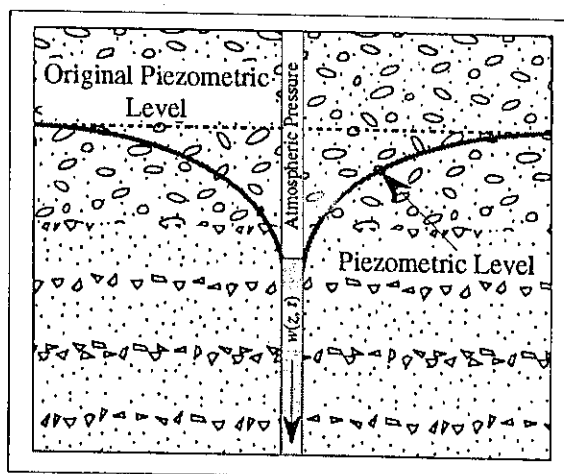


Figure 2-5 Distribution of the piezometric head near a borehole, before and after pumping was initiated.

A possibility, that immediately presents itself, is to consider the borehole as a seepage face, since a borehole is open to the atmosphere. However, a borehole usually contains a certain volume of water in it. The Dirichlet boundary condition in Equation (2.24) has thus to be changed to

$$\phi(\mathbf{x}, t) = \phi_b(\mathbf{x}, t) = w(z, t) \quad [h(\mathbf{x}, t) \geq 0] \quad (2.25)$$

where $w(z, t)$ is the water pressure head along the side of the borehole, see Figure 2-6.

At first sight it would seem as if this approach does not allow one to specify a discharge rate for the borehole. However, this is not true. To see this, let $Q(\mathbf{x}, t)$ be the rate at which water is discharged from the borehole and $Q_a(\mathbf{x}, t)$ the rate at which the aquifer discharges water to the borehole, subject to the boundary condition in Equation (2.25). The water level in the borehole will clearly rise, if $Q(\mathbf{x}, t) < Q_a(\mathbf{x}, t)$, with a corresponding increase in $w(z, t)$, and conversely. The effect that $Q(\mathbf{x}, t)$ has on the borehole, and thus the aquifer, is therefore implicitly contained in $w(z, t)$.

An interesting situation arises in the case of a fully penetrating borehole, if $Q(\mathbf{x}, t)$ and $w(z, t)$ are both constant. This implies that $\nabla \phi_b(\mathbf{x}, t)$ (and thus the Darcy flux through the side of the borehole) must be constant, whenever $w(z, t) = w_0 \geq d$, where d is the thickness of the aquifer, see Figure 2-6. These assumptions allow one to replace the Dirichlet condition in Equation (2.25) with the more manageable Neumann boundary condition

$$q_n(\mathbf{x}, t) = \frac{\text{total discharge}}{\text{total area of borehole}} = \frac{Q(\mathbf{x}, t)}{2\pi r d} \quad (2.26)$$

where $q_n(\mathbf{x}, t)$ is the normal Darcy flux through the side of the borehole and r the radius of the borehole (Huyakorn and Pinder, 1983).

The Neumann boundary condition in Equation (2.26) is, strictly speaking only valid for a confined aquifer, *continuously in contact with the borehole*. It cannot be used for a phreatic, or discontinuous multi-layer aquifer, such as the one shown schematically in Figure 2-7.

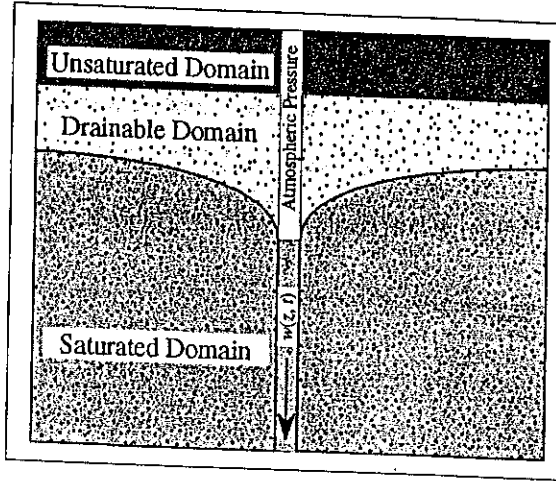


Figure 2-6 Illustration of the different saturation zones near a borehole drilled into a single layer aquifer.

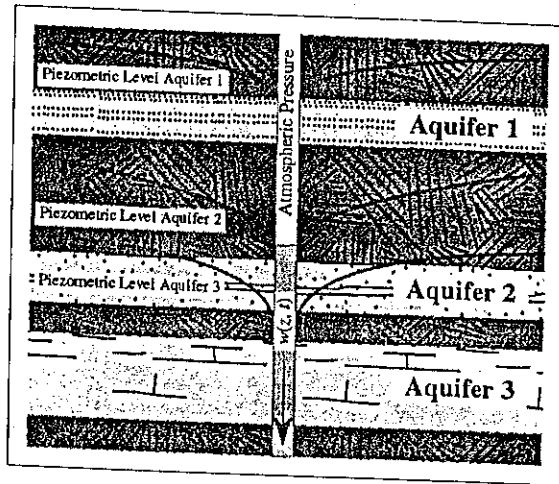


Figure 2-7 Graphical idealization of a multi-layer aquifer.

There is one aspect of treating a borehole as a seepage boundary that needs to be considered in more detail, before leaving this discussion—the evaporation condition. The water that leaves a seepage face, when the evaporation condition applies, will invariably be in the form of water vapour. Therefore, it would seem to be more correct not to take this loss into account, when calculating $w(\mathbf{x}, t)$ in Equation (2.25) for a phreatic or discontinuous multi-layer confined aquifer.

A seepage boundary can only be applied iteratively, as noticed in Section 2.4.4. Since the present investigation was more concerned with continuously layered confined aquifers, the Neumann condition, Equation (2.26), is the only condition implemented for boreholes in the numerical models discussed in Chapters 6 and 7.



CHAPTER 3

THE CONCEPTUAL MODEL FOR GROUNDWATER CONTAMINATION

3.1 GENERAL

The previously held belief by man that waste buried in the soil surface is safely disposed of, is today responsible for one of the greatest threats to the earth's potable water resources. What man did not seem to realize, is that the waste may be dissolved by water infiltrating into the earth's surface and accumulate in the groundwater. From there it can be transported, over vast distances, to enter rivers, streams and lakes that feed the surface reservoirs.

Groundwater is to some extent better protected from pollution than surface water, by the unsaturated zone of the earth's surface. However, this property and the slow speed at which groundwater normally moves, make it very difficult to clean a contaminated aquifer.

It is possible to clean a contaminated aquifer by pumping the contaminated water out. Nevertheless, the procedure can be simplified and streamlined, if it is supplemented with a conceptual model of the aquifer (Princeton University Water Resources Program, 1984; Kauffmann and Kinzelbach, 1990). Such a model can also be extremely useful in an evaluation of the impact that existing and new waste disposal sites may have on the environment (Huyakorn *et. al.*, 1984).

The conceptual model most widely used in the study of groundwater pollution today, is the *hydrodynamic dispersion equation*. This equation contains one dependent variable—the concentration of dissolved solids—and at least two relational parameters—flow velocity and the dispersion coefficient. Since groundwater flow velocities can be obtained directly from the flow model, see Chapter 2, they will not be discussed here.

Many of the pollutants found in groundwater are chemically reactive. These reactions should thus be included in the conceptual model whenever there is a possibility for them to occur. This is not difficult, if the chemical reaction rates of the reactions are known. The only problem is that these reaction rates are often not known and that they, moreover, vary considerably from one aquifer to another. The present model was therefore restricted to the two most common types of reactions—*adsorption and decay*. This assumption introduces two additional relational parameters into the model. These relational parameters, which are related to the concentration of the pollutant, are discussed in Section 3.2, together with the hydrodynamic dispersion tensor. This is followed by a discussion of the actual conceptual model and its associated boundary conditions in Section 3.3.

3.2 BASIC TRANSPORT PROCESSES IN GROUNDWATER

3.2.1 Introduction

The conceptual model for hydrodynamic dispersion, in use today, is described in a number of books and treatises (Bear and Bachmat, 1990; Botha *et. al.*, 1990; Dagan, 1989; and Bear, 1979). The present discussion will therefore be limited to aspects that are particularly important in the development of a numerical, mass transport model.

3.2.2 Basic Principles

A physical phenomenon can only be studied quantitatively, if at least one of its characteristic features can be measured. The most fundamental feature in groundwater flow is certainly the concentration of the dissolved solids; i.e., the quantity of solids dissolved in a unit volume (or mass) of water. The measure conventionally used in measuring concentration in groundwater pollution studies is the *volumetric concentration*, defined as

$$c = (m_s/v)$$

where m_s is the mass of dissolved solids in the volume of fluid v .

The concentration of a non-reactive dissolved solid is usually not influenced by the solid itself, or the physical properties of the container. There are, however, two well-known exceptions to this rule: (a) where the mass of a dissolved solid tends to decay exponentially with time (as in the case of radioactive materials) and (b) where the solid is adsorbed by the walls of the container. The reaction rate of the first type of reaction can be conveniently expressed through an equation of the form

$$Dm_s(t) = -\lambda m_s(t)$$

where $m_s(t)$ is the number of ions in solution at time t and λ , the *decay constant*, is a *characteristic constant* of the decaying chemical compound. This type of reaction can thus be easily incorporated into the conceptual model. The same is, unfortunately, not true in the case of adsorption, since this does not depend on the concentration alone, but also on factors such as the temperature and acidity of the solution. Nevertheless, the available experimental data indicate that the fraction of dissolved solids, s , adsorbed by a porous medium can be described by a relation, or *isotherm*, of the form (Bear, 1979)

$$s = m_a/(m_a + m_s) = m_a/m_b = f(c, t)$$

where m_a is the mass of dissolved solids adsorbed by a volume of porous material with mass m_s and total mass m_b .

The isotherms observed in groundwater pollution studies can be quite complex. The present model was therefore limited to materials whose adsorption properties can be described by the simple *Freundlich* isotherm (Bear, 1979)

$$s = K_d c$$

where K_d is known as the *volumetric distribution coefficient*.

3.2.3 The Dispersion Coefficient

Experimental evidence indicates that a pollutant starts to disperse in all directions as soon as it is introduced into an aquifer, see Figure 3-1. Although very little is known of the physical processes that are responsible for this behaviour, one obvious candidate is *molecular diffusion*. This form of dispersion can be described mathematically through a *Fickian* type of equation

$$\mathbf{J}_m = -\theta \underline{\mathbf{D}}_m \nabla c \quad (3.1)$$

where \mathbf{J}_m is the molecular diffusive flux and

$$\underline{\mathbf{D}}_m = \underline{\mathbf{T}} \mathcal{D}$$

the *molecular diffusion tensor*. The diffusion tensor thus consists of two factors: the *ordinary diffusion coefficient* of the substance, \mathcal{D} , and the *tortuosity tensor*, $\underline{\mathbf{T}}$. The tortuosity tensor was introduced by Scheidegger (1974) to account for the tortuous paths a molecule has to travel in a porous medium.

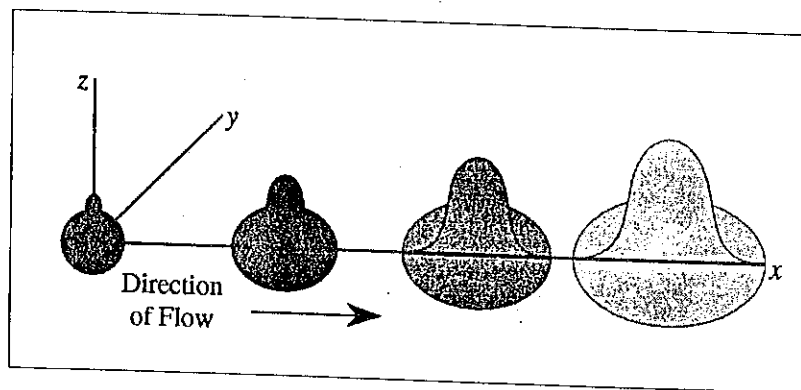


Figure 3-1 Dispersion of a slug of pollution introduced into an aquifer with flow restricted to the x-direction as a function of time.

The molecule of a dissolved solid can be expected to collide frequently with the matrix, when moving through a porous medium. Such a collision must change the velocity of the colliding molecule, according to Newton's second law of motion. These changes in velocity could obviously also contribute to the dispersion. The problem with this interpretation is that

the changes in velocity occur on the pore or *microscopic level*; a quantity very rarely observed in groundwater investigations. However, it is not unreasonable to assume that the microscopic velocity, \mathbf{v}^* , is related to the seepage velocity of groundwater through the equation

$$\theta \mathbf{v}^* = \mathbf{q} + \mathbf{q}_0$$

where θ denotes the volumetric water contents of the medium, \mathbf{q} the usual Darcy velocity and \mathbf{q}_0 deviations in $\theta \mathbf{v}^*$ from \mathbf{q} , caused by the collisions between the dissolved molecules and porous matrix. By using this assumption the mass flux of dissolved solids per unit area of porous medium can be expressed as

$$\mathbf{J}_h = \mathbf{J}_a + \mathbf{J}_d = c(\mathbf{q} + \mathbf{q}_0) \quad (3.2)$$

The terms $\mathbf{J}_a = c\mathbf{q}$ and $\mathbf{J}_d = c\mathbf{q}_0$ are consequently often referred to as the *advective* and *dispersive fluxes*, respectively. Notice that \mathbf{J}_a is caused by the usual flow of the water, while \mathbf{J}_d is caused by the collisions between the dissolved molecule and the porous matrix.

Based on his examination of a number of laboratory experiments, Bear (1972) suggests that the dispersive flux can be described mathematically by the equation

$$c\mathbf{q}_0 = -\theta \mathbf{D}_d \nabla c \quad (3.3)$$

where ρ is again the density of the fluid. Bear (1972) also uses a number of theoretical arguments to show that the ij -th component of the *dispersion tensor*, \mathbf{D}_d , is given by

$$\theta D_{d(i,j)} = \alpha_T q \delta_{ij} (\alpha_L - \alpha_T) q_i q_j / q \quad (3.4)$$

where q is the magnitude of the Darcy velocity, \mathbf{q} , q_i ($i = 1, 2, 3$) its three Cartesian components and

$$\delta_{ij} = \begin{cases} 1 & (i = j) \\ 0 & \text{otherwise} \end{cases}$$

the Kronecker delta. The two parameters, α_L and α_T , are known as the *longitudinal* and *transverse dispersivities*, respectively. It may seem strange that there are only two parameters, even though hydrodynamic dispersion is a three-dimensional phenomenon. However, experimental and observational experience indicates that dispersion is of the same magnitude, in the plane perpendicular to the main direction of flow.

It is interesting to note that the molecular diffusion and the dispersive flux are linear functions of ∇c . The total flux of dissolved solids, attributable to hydrodynamic dispersion, is thus given by the sum of Equations (3.1) and (3.2) and conventionally expressed as

$$\mathbf{J} = \mathbf{J}_m + \mathbf{J}_h = -\rho \theta \mathbf{D}_h \nabla c$$

where

$$\mathbf{D}_h = \mathbf{D}_m + \mathbf{D}_d \quad (3.5)$$

is known as the *coefficient of hydrodynamic dispersion, or dispersion tensor*.

3.3 THE HYDRODYNAMIC DISPERSION EQUATION

3.3.1 General

There are a number of methods that can be used to derive the hydrodynamic dispersion equation (Botha *et. al.*, 1990; Bear and Verruijt, 1987; Voss, 1984; Huyakorn and Pinder, 1983; and Bear, 1979, 1972). Although these equations are all equivalent mathematically, there are some subtle differences in their physical interpretation. The computer program developed in this investigation was consequently based on the *hydrodynamic dispersion* or *mass transport* equation, as it is sometimes called,

$$D_t(\theta c + \rho_b K_d c) + \nabla \cdot (\mathbf{q}c) = \nabla \cdot (\theta \mathbf{D}_h \nabla c) - \lambda(\theta c + \rho_b K_d c) + f c_s \quad (3.6)$$

where c_s is the concentration of the source term and $f(\mathbf{x}, t)$ its strength. This form of the hydrodynamic dispersion equation is the one used in the majority of published numerical models.

Equation (3.6) is nothing else than a mathematical description for the law of mass conservation as it applies to the masses of the dissolved solids *and* fluid. However, each of the components must also satisfy the law separately. The possibility thus exists that Equation (3.6) contains a number of redundant terms. That this is the case has been shown by Botha *et. al.* (1990). The program for mass transport in Chapter 8 was consequently based on the reduced equation

$$(\theta + \rho_b K_d) D_t c + \mathbf{q} \nabla c = \nabla \cdot (\theta \mathbf{D}_h \nabla c) - \lambda(\theta + \rho_b K_d) c + f(c_s - c) \quad (3.7)$$

There are four basic assumptions that should be taken into account when using Equation (3.7), in groundwater contamination studies. These are: (a) deformations of the porous medium can be neglected, (b) the flow is density independent, (c) the concentration of the pollutant decays exponentially and (d) reactions between the pollutant and aquifer material can be described by a simple Freundlich isotherm. Equation (3.7) can be simplified somewhat under certain conditions, for example when working with stable materials, or a conservative tracer, the terms containing λ (or K_d) can be dropped.

3.3.2 Initial and Boundary Conditions

The hydrodynamic dispersion and groundwater flow equations are both parabolic partial differential equations, see Equations (3.6) and (2.12) respectively. The initial and boundary conditions to use with Equation (3.6) are, therefore, very similar to those of Equation (2.12).

The initial condition can thus again be expressed as

$$c(\mathbf{x}, 0) = c_0(\mathbf{x}) \quad (\mathbf{x} \in \Omega) \quad (3.8)$$

while the boundary conditions will be a combination of either a Dirichlet condition

$$c(\mathbf{x}, t) = c_1(\mathbf{x}, t) \quad (\mathbf{x} \in \partial\Omega_1, t > 0) \quad (3.9)$$

with c_1 a known function of \mathbf{x} and t , a Neumann condition

$$\mathbf{n} \cdot \theta \underline{\mathbf{D}} \nabla c(\mathbf{x}, t) = \mathbf{n} \cdot c_0 \mathbf{q}_0(\mathbf{x}, t) \quad (\mathbf{x} \in \partial\Omega_2) \quad (3.10)$$

and a Cauchy condition

$$\mathbf{n} \cdot [\mathbf{q}c - \theta \underline{\mathbf{D}} \nabla c(\mathbf{x}, t)] = \mathbf{n} \cdot c_0 \mathbf{q}_0(\mathbf{x}, t) \quad (\mathbf{x} \in \partial\Omega_3) \quad (3.11)$$

where c_0 is the concentration of dissolved solids in the boundary flux $\mathbf{q}_0(\mathbf{x}, t)$. Although these boundary conditions can be applied in the same manner as those of the flow equation, there are a few subtle differences that need to be taken care of. For example, a homogeneous Neumann boundary condition is often used in the modelling of groundwater flow (Pinder and Gray, 1977), especially when the boundaries of an aquifer are not known precisely. However, there are very few (if any) natural materials that are not subject to molecular diffusion processes. The use of a homogeneous Neumann boundary condition in modelling a contaminated aquifer, could therefore lead to a considerable overestimation of the contamination, if the condition does not apply. Indeed, all indications are that one should never use a homogeneous Neumann boundary condition in the modelling of hydrodynamic dispersion, unless there is sufficient observational evidence to support it.

An aquifer is often contaminated by a sudden leak, or spill, of hazardous materials at the earth's surface. Since the concentration of the materials can usually be determined, it would be quite natural to use a Dirichlet type boundary condition in such a situation. However, Batu and Van Genuchten (1990) has pointed out recently, that such an approach can also lead to an overestimate of the pollution, and that a Cauchy type condition would be more appropriate in such a situation.

Another fallacy often committed in the modelling of hydrodynamic dispersion is to use the same type of boundary condition with the dispersion equation than the one used with the flow equation. However, this need not be true in general as the following argument will show. In the case of groundwater flow a Neumann boundary condition can be regarded as a control of the mass of fluid that enters or leaves the domain, Ω , but not in the hydrodynamic dispersion. Here the flux of mass is controlled by the Cauchy condition, as an application of Equations (3.1) and (3.2) to both sides of the boundary will show. A Neumann boundary condition in the flow equation should thus always be replaced with a Cauchy boundary condition in the dispersion equation.

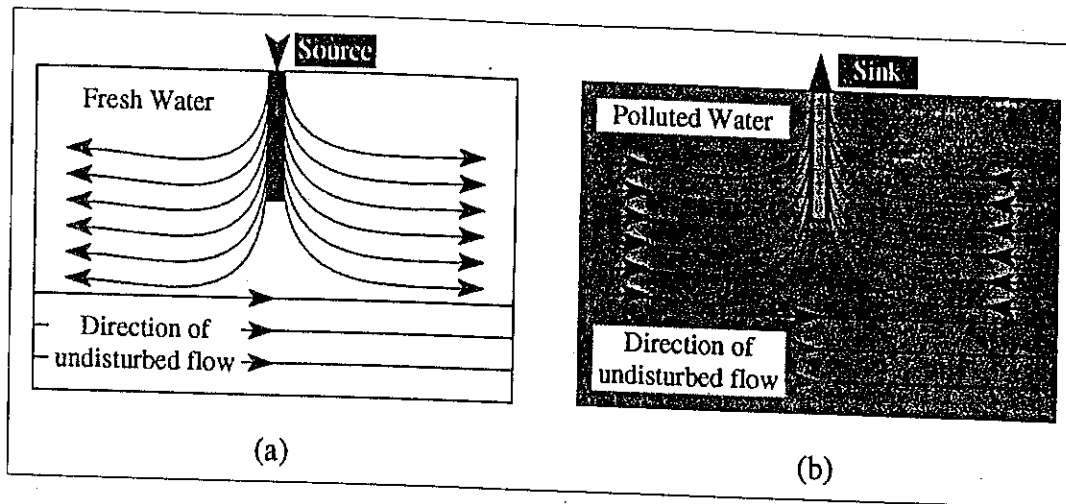


Figure 3-2 Vertical cross-sections through (a) a clean aquifer with a pollution source and (b) a polluted aquifer with a sink.

3.3.3 Sources and Sinks in Hydrodynamic Dispersion

It is rather interesting to compare the source term of the flow and hydrodynamic dispersion equations. The source term for the flow equation is a simple function, $f(\mathbf{x}, t)$, that changes sign when a source is replaced by a sink, *but does not vanish* (unless the source or sink itself vanishes). The source term in the dispersion equation, $f(\mathbf{x}, t)(c_s - c)$, consists on the other hand of two factors: the first of which describes the strength of the source (sink) and the second the difference in concentration between the source (sink) and aquifer. Since a sink, by its very definition, withdraw water from an aquifer; this water must have exactly the same concentration as the water in the aquifer, i.e., $c_s \equiv c$, see Figure 3-2. The source term thus vanishes from Equation (3.6) whenever a sink(s) is present in the aquifer. Care should thus be exercised with the source term, when using the hydrodynamic dispersion equation as the governing equation for contaminant transport

CHAPTER 4

NUMERICAL APPROXIMATIONS

4.1 GENERAL

The major objective of this project was to evaluate the differences between two- and three-dimensional conceptual models in the simulation of groundwater phenomena. This could only be achieved with models that use the minimum assumptions and approximations. Since very few analytical solutions are known for the three-dimensional flow and dispersion equations, numerical methods had to be used for the solution of the governing equations.

There are a number of analytical solutions and computer programs (Botha *et al.*, 1990; Voss, 1984; Walton, 1984; McDonald and Harbaugh, 1983; Davis and Neuman, 1983; Pinder 1974) available at the Institute for Groundwater Studies, suitable for the simulation of groundwater flow phenomena. However, the computer programs for three-dimensional phenomena are all based on a number of *ad hoc* assumptions that do not satisfy the needs of this investigation. It was consequently necessary to develop new computer programs for three-dimensional flow and dispersion phenomena. Some of the algorithms used for this purpose had to be developed from scratch. The discussion in this chapter will therefore be devoted mainly to these algorithms. The programs themselves are described in Chapters 6 through 8, where they are also used to discuss some relations between two- and three-dimensional conceptual models.

A review of the literature (Botha and Pinder, 1983; Zienkiewicz, 1977; Pinder and Gray, 1977) indicated that the Galerkin finite element approximation would be the most efficient method to use for the present purpose. Although the basis functions for the two-dimensional Galerkin finite element approximation are widely discussed in the literature (see the references cited above), the same cannot be said of the three-dimensional basis functions. A more detailed discussion of the tri-linear basis functions, used in this investigation, are therefore included in Appendix A.

The numerical solution of the saturated and unsaturated flow and hydrodynamic dispersion equations is frequently discussed in the literature. However, no reference could be traced for the solution of the variably saturated flow equation, described by Equation (2.14). Work done earlier on the two-dimensional variably saturated flow equation (Botha, 1986), has shown that the method proposed by Allen (1985) for the unsaturated flow equation can be readily adapted for the variably saturated flow equation. This approximation and its specialization to the saturated flow equation are discussed in Section 4.2. The approximation for the hydrodynamic dispersion equation is discussed in Section 4.3.

4.2 DISCRETIZATION OF THE FLOW EQUATION

4.2.1 Variably Saturated Flow

As has been shown in Section (2.3.4) the relation between the moisture content and pressure head is highly non-linear. The governing equation for variably saturated flow

$$D_t[\rho\theta(\mathbf{x},t)] = \nabla \cdot [\rho\mathbf{K}(\mathbf{x},t)\nabla\phi(\mathbf{x},t)] + \rho f(\mathbf{x},t) \quad (2.12)$$

is thus also highly non-linear, at least in the unsaturated part of the domain.

It is rather unusual to try to solve a differential equation, such as Equations (2.12) and (2.14), with two dependent variables, $\theta(\mathbf{x},t)$ and $\phi(\mathbf{x},t)$. One possibility, to prevent this double-dependent variable formulation, is to replace $\theta(\mathbf{x},t)$ with $\phi(\mathbf{x},t)$. This can be done quite easily by using the moisture retention curve in Equation (2.7). Unfortunately, there does not exist an efficient numerical approximation for this ϕ -based equation that conserves mass (Milly, 1985). However, Allen (1985) and Celia *et al.* (1990) have shown that this difficulty can be avoided, if Equations (2.12), or (2.14), is used directly.

Allen's method is based on the observation that any function, such as $\rho\theta(\mathbf{x},t)$, can always be expanded over an interval $[t_n, t_{n+1}]$ in terms of the linear Lagrange interpolation polynomial as

$$\rho\theta(\mathbf{x},t) = l_n(t)\rho\theta(\mathbf{x},t_n) + l_{n+1}(t)\rho\theta(\mathbf{x},t_{n+1}) + E(\tau)$$

(Botha and Pinder, 1983). Substitution of this expression for $\theta(\mathbf{x},t)$, but without the error term $E(\tau)$, into Equation (2.12) and collocating the resulting equation at $t = t_{n+1}$, yields the non-linear, backward finite difference approximation

$$\rho\theta^{n+1}(\mathbf{x}) - \rho\theta^n(\mathbf{x}) = \Delta t \nabla \cdot [\rho\mathbf{K}(\mathbf{x},t_{n+1})\nabla\phi(\mathbf{x},t_{n+1})] + \Delta t \rho f(\mathbf{x},t_{n+1}) \quad (4.3)$$

where the superscripts, n and $n+1$, refers to an approximation of $\rho\theta(\mathbf{x},t)$ at times t_n and t_{n+1} , respectively.

Equation (4.3) is still a non-linear equation and must thus be solved iteratively. There are a number of methods that can be used for this purpose (Botha and Pinder, 1983). However, there exists a very effective Newton-Raphson type iteration method for the solution of Equation (4.3). To show this, let $h_m^{n+1}(\mathbf{x})$ be the solution of Equation (4.3) after m iterations at the time step t_{n+1} . The solution after $(m+1)$ iterations can then be expressed in the form

$$h_{m+1}^{n+1}(\mathbf{x}) = h_m^{n+1}(\mathbf{x}) + \delta h_{m+1}^{n+1}(\mathbf{x}) \quad (4.4)$$

where $\delta h_{m+1}^{n+1}(\mathbf{x})$ represents a presumably small correction to $h_m^{n+1}(\mathbf{x})$. Since $\theta^{n+1}(\mathbf{x})$ and $\mathbf{K}(\mathbf{x},t)$ are both functions of $h(\mathbf{x},t)$, see Equations (2.7) and (2.10), Taylor's theorem can be invoked to write

$$\rho\theta_{m+1}^{n+1} = \rho\theta_m^{n+1} + \delta h_{m+1}^{n+1} D_h \rho\theta_m^{n+1} \quad (4.5)$$

and

$$\rho\mathbf{K}_{m+1}^{n+1} = \rho\mathbf{K}_m^{n+1} + \delta h_{m+1}^{n+1} D_h \rho\mathbf{K}_m^{n+1} \quad (4.6)$$

Substitution of Equations (4.4) to (4.6) into Equation (4.3), now yield

$$\begin{aligned} [\rho\theta_m^{n+1} + \delta h_{m+1}^{n+1} D_h \rho\theta_m^{n+1} - \rho\theta^n] &= \Delta t \nabla \cdot [\{\rho\mathbf{K}_m^{n+1} + \delta h_{m+1}^{n+1} D_h \rho\mathbf{K}_m^{n+1}\} \nabla \{h_m^{n+1} + \delta h_{m+1}^{n+1} + z\}] \\ &\quad + \Delta t \rho f(\mathbf{x}, t_{n+1}) \end{aligned}$$

or, after rearranging the terms on the right-hand side and assuming that the terms

$$\Delta t \nabla \cdot [\delta h_{m+1}^{n+1} D_h \rho\mathbf{K}_m^{n+1} \nabla \{h_m^{n+1} + \delta h_{m+1}^{n+1} + z\}]$$

are of second order magnitude,

$$\begin{aligned} [D_h \rho\theta_m^{n+1} - \Delta t \nabla \cdot \{\rho\mathbf{K}_m^{n+1} \nabla\}] \delta h_{m+1}^{n+1} &= -[\rho\theta_m^{n+1} - \rho\theta^n] + \Delta t \nabla \cdot [\rho\mathbf{K}_m^{n+1} \nabla \phi_m^{n+1}] \\ &\quad + \Delta t \rho f(\mathbf{x}, t_{n+1}) \end{aligned} \quad (4.7)$$

Equation (4.7) has one major advantage above similar approximations for the variably saturated flow equation (Milly, 1985)—it conserves mass. To see this, consider the integral on the right hand side of Equation (4.7) over the domain Ω

$$\begin{aligned} \int_{\Omega} R_m^{n+1} d\Omega &= -\int_{\Omega} [\rho\theta_m^{n+1} - \rho\theta^n] d\Omega + \Delta t \int_{\Omega} \nabla \cdot [\rho\mathbf{K}_m^{n+1} \nabla \phi_m^{n+1}] d\Omega + \Delta t \int_{\Omega} \rho f(\mathbf{x}, t_{n+1}) d\Omega \\ &= -\int_{\Omega} [\rho\theta_m^{n+1} - \rho\theta^n] d\Omega + \Delta t \int_{\partial\Omega} [\rho\mathbf{K}_m^{n+1} \nabla \phi_m^{n+1}] \cdot \mathbf{n} ds + \Delta t \int_{\Omega} \rho f(\mathbf{x}, t_{n+1}) d\Omega \end{aligned}$$

where \mathbf{n} is a unit vector normal to the boundary ($\partial\Omega$) of Ω , and use was made of the divergence, or Gauss', theorem (Hildebrand, 1976). The three terms on the right hand side of this equation represent, respectively, a change in the water content of Ω , the flux of water through the boundary of Ω and the yield of sources (sinks) during the period Δt . The right hand side, therefore, represents in effect the mass balance for variably saturated flow. This means that if Equation (4.7) is iterated until R_m^{n+1} satisfies a prescribed tolerance, the solution of Equation (4.7), $\phi^{n+1}(\mathbf{x}, t)$ will also satisfy the law of mass conservation within this tolerance.

The only difficulty experienced with the practical application of Equation (4.7) is that the first term on the right hand side will vanish as soon as the domain becomes saturated. However, this is not a serious difficulty, since $D_t[\rho\theta(\mathbf{x}, t)]$ can also be expressed as

$$D_t(\rho\theta) = D_h(\rho\theta) D_t h$$

through the chain rule of differentiation. The first term on the right hand side of this equation can be written in a more convenient form by replacing θ with the water saturation, S_w , as defined in Section 2.3.3. This yields

$$\begin{aligned}
D_h(\rho\theta) &= D_h(\rho\epsilon S_w) = S_w D_h(\rho\epsilon) + \rho\epsilon D_h(S_w) \\
&= S_w[\epsilon D_p \rho + \rho D_p \epsilon] D_h p + \rho\epsilon D_h(S_w) \\
&= S_w[\epsilon \rho \beta + \rho(1-\epsilon)\alpha] \rho g + \rho\epsilon D_h(S_w) \\
&= \rho S_w[\rho g\{\epsilon\beta + \alpha(1-\epsilon)\} + \rho\epsilon D_h(S_w)] \\
&\equiv \rho S_w S_0 + \rho C(h)
\end{aligned}$$

where S_0 is the specific storativity of the medium, $C(h)$ the moisture capacity and Equation (2.2) was used, to express h in terms of p . The other two parameters

$$\alpha = (1-\epsilon)^{-1} D_p \epsilon \quad \text{and} \quad \beta = \rho^{-1} D_p \rho$$

are the compressibility coefficients of the medium and water, respectively. Substitution of this expression into Equation (2.12), and using the same assumptions as in the derivation of Equation (4.7), allows one to express Equation (4.7) in the form

$$\begin{aligned}
[\rho S_0 - \Delta t \nabla \cdot \{\rho \underline{\mathbf{K}}_m^{n+1} \nabla\}] \delta h_{m+1}^{n+1} &= -[\rho S_0 (h_m^{n+1} - h^n)] + \Delta t \nabla \cdot [\rho \underline{\mathbf{K}}_m^{n+1} \nabla \phi_m^{n+1}] \\
&\quad + \Delta t \rho f(\mathbf{x}, t_{n+1})
\end{aligned} \tag{4.8}$$

This is the approximation to use in the saturated domain of variably saturated flow.

It is important to note that Equations (4.7) and (4.8) have been derived for density-dependent flow. However, density-dependent flow will not be discussed in this report, as has already been stated in Section 2.5.1. The programs, described in Chapters 6 and 7, are consequently based on the density-independent versions of Equations (4.7) and (4.8).

Equations (4.7) and (4.8) are fundamentally just two elliptic partial differential equations. The finite element method is thus the most efficient method with which to solve them numerically (Botha and Pinder, 1983). This yields a system of linear equations, which can be expressed in matrix form as

$$(\mathbf{A} - \Delta t \mathbf{B}) \delta \mathbf{h}_{m+1}^{n+1} = \mathbf{C} + \Delta t (\mathbf{B} \Phi_m^{n+1} + \mathbf{D} + \mathbf{F}) \tag{4.9}$$

where \mathbf{A} and \mathbf{B} are matrices with elements

$$\begin{aligned}
a_{ij} &= \iiint_{\Omega} [C(h_m^{n+1}) + S_0 S_w(h_m^{n+1})] \varphi_i(\mathbf{x}) \varphi_j(\mathbf{x}) d\Omega \\
b_{ij} &= \iiint_{\Omega} \underline{\mathbf{K}}(h_m^{n+1}) \nabla \varphi_i(\mathbf{x}) \nabla \varphi_j(\mathbf{x}) d\Omega
\end{aligned}$$

and \mathbf{C} , \mathbf{D} , \mathbf{F} and Φ_m^{n+1} vectors with components

$$\begin{aligned}
c_i &= \iiint_{\Omega} (\zeta^n - \zeta_m^{n+1}) \varphi_i(\mathbf{x}) d\Omega \\
d_i &= \iint_{\partial\Omega} \mathbf{n} \cdot [\underline{\mathbf{K}}(h_m^{n+1}) \phi_m^{n+1}] \nabla \varphi_i ds = \iint_{\partial\Omega} q_n \nabla \varphi_i ds
\end{aligned}$$

$$f_i = \iiint_{\Omega} f(\mathbf{x}, t^{n+1}) \phi_i(\mathbf{x}) d\Omega$$

$$\phi_{m,i}^{n+1} = \phi_m^{n+1}(\mathbf{x}_i, t_{n+1})$$

The variable ζ is used here to denote either θ or $S_0 h$, while $\phi_i(\mathbf{x})$ denotes the i -th three-dimensional, finite element basis function. Care should thus be taken, not to confuse $\phi_i(\mathbf{x})$ and the piezometric head $\phi(\mathbf{x}, t)$. These algorithms have been implemented in the Program SUF3, discussed in Chapter 7, that can be used to simulate variably saturated flow.

4.2.2 Fully Saturated Flow

The primary basis, for the iteration schemes in Equations (4.7) and (4.8), is the assumption that the correction term δh_m^{n+1} will vanish if m is sufficiently large. The left hand sides of both equations must thus also vanish when this is true. Since z is independent of time, Equation (4.8) can be rewritten as

$$S_0(\phi_m^{n+1} - \phi^n) = \Delta t \nabla \cdot [\mathbf{K}_m^{n+1} \nabla \phi_m^{n+1}] + \Delta t f(\mathbf{x}, t_{n+1}) \quad (4.10)$$

in this case. However, this is exactly the well-known backward finite difference approximation for the fully saturated flow equation, Equation (2.15). This shows that Equation (4.8) is indeed the correct approximation to use with saturated flow in the model for variably saturated flow.

It is important to note that Equation (4.10) reduces to a linear elliptic equation for fully saturated flow, since \mathbf{K} does not depend on the piezometric head then. Because it is always easier to solve a linear than a non-linear differential equation (Botha and Pinder, 1983), a separate computer program, SAT3, was consequently developed for Equation (2.15). This program was again based on the Galerkin finite element approximation, described above, but this time with Equation (4.10) as basis. This program is used in Chapter 6 to discuss the behaviour of various types of saturated aquifers.

Experience, gained to date, indicates that the linear model executes from two to four times faster than the variably saturated model. However, the program does not provide for rainfall and seepage boundary conditions, because they can only be applied iteratively and the variably saturated model converges very quickly in the case of a saturated domain.

4.3 THE HYDRODYNAMIC DISPERSION EQUATION

The computer program developed for contaminant transport, SUM3, has as conceptual model the linear hydrodynamic dispersion equation

$$(\theta + \rho_b K_d) D_t c + \mathbf{q} \nabla c = \nabla \cdot (\theta \mathbf{D}_h \nabla c) - \lambda(\theta + \rho_b K_d) c + f(c_s - c) \quad (3.7)$$

It is important to note that Equation (3.7) contains four parameters (the three components of \mathbf{q} and θ) that depend on the flow field. Therefore, it cannot be solved if the solution of the flow equation is not known. Since the Galerkin finite element method was used to solve the flow equation, it would be advantageous to use the same method for Equation (3.7).

The first step in the discretization Equation (3.7) is to approximate $c(\mathbf{x}, t)$ with a linear Lagrange interpolation polynomial, over the interval $[t_n, t_{n+1}]$, and then collocate the approximation at the time step $t = t_{n+1}$. This yields again an elliptic type of equation, given by

$$(\theta^{n+1} + \rho_b K_d)(c^{n+1} - c^n) = \Delta t [\nabla \cdot (\theta^{n+1} \underline{\mathbf{D}}_h \nabla c^{n+1}) - \mathbf{q} \cdot \nabla c^{n+1} - \lambda(\theta^{n+1} + \rho_b K_d)c^{n+1} + f(c_s^{n+1} - c^{n+1})]$$

or after rearranging the terms

$$(\theta^{n+1} + \rho_b K_d)c^{n+1} + \Delta t [\mathbf{q} \cdot \nabla c^{n+1} - \nabla \cdot (\theta^{n+1} \underline{\mathbf{D}}_h \nabla c^{n+1}) - \lambda(\theta^{n+1} + \rho_b K_d)c^{n+1}] = (\theta^{n+1} + \rho_b K_d)c^n + \Delta t f(c_s^{n+1} - c^{n+1})$$

An application of the Galerkin finite element approximation to this equation again yields a system of linear equations, but this time of the form

$$(\mathbf{A} + \Delta t \mathbf{B})\mathbf{C}^{n+1} = \mathbf{A}\mathbf{C}^n + \mathbf{F} \quad (4.11)$$

where \mathbf{A} and \mathbf{B} ($= \mathbf{B}_1 + \mathbf{B}_2 + \mathbf{B}_3$) are matrices with elements

$$\begin{aligned} a_{ij} &= \iiint_{\Omega} (\hat{\theta}^{n+1} + \rho_b K_d) \varphi_i \varphi_j d\Omega \\ b_{ij}^1 &= \iiint_{\Omega} \varphi_i \mathbf{q} \cdot \nabla \varphi_j d\Omega \\ b_{ij}^2 &= \iiint_{\Omega} \hat{\theta}^{n+1} \underline{\mathbf{D}}_h \nabla \varphi_i \cdot \nabla \varphi_j d\Omega \\ b_{ij}^3 &= \lambda \iiint_{\Omega} (\hat{\theta}^{n+1} + \rho_b K_d) \varphi_i \varphi_j d\Omega \end{aligned}$$


and \mathbf{C}^n and \mathbf{F} are vectors with components

$$\begin{aligned} c_i^n &= c^n(\mathbf{x}_i) \\ f_i &= \iiint_{\Omega} f(c_s^{n+1} - c^{n+1}) \varphi_i d\Omega + \iint_{\partial\Omega} \varphi_i \mathbf{n} \cdot (\hat{\theta}^{n+1} \underline{\mathbf{D}}_h \nabla \hat{c}^{n+1}) ds \end{aligned} \quad (4.12)$$

It should be noticed that the source term has been kept on the right hand side of Equation (4.11). The reason for doing this is that the term vanishes in the case of a sink. However, it must be remembered that the term $f c^{n+1}$ in Equation (4.12) has to be transferred to the left hand side of Equation (4.11) in the case of a source.

Although the Galerkin approximation in Equation (4.11) is easy to apply in theory, it places a much greater burden on computing resources than the flow equation. The main

reason for this is that the coefficient matrix $(A + \Delta t B)$ is no longer a symmetric matrix. The full coefficient matrix has thus to be stored and not only its upper triangle, as for the flow equation (Huyakorn and Pinder, 1983). Moreover, the solution determined from Equation (4.11) tends to oscillate, unless the finite element grid is sufficiently refined (Bear and Bachmat, 1990; Huyakorn *et al.*, 1986a; Huyakorn and Pinder, 1983). The situation thus frequently arises where one has to use a more refined grid for Equation (4.11), than is necessary for the flow equation. Some of the existing computer programs (e.g., Yeh and Ward, 1981) allow one to use different grids for the flow and hydrodynamic dispersion equations. However, this practice tends to introduce interpolation errors into the computed concentrations and is also cumbersome to implement. This option was therefore not implemented in Program SUM3.



CHAPTER 5

THE GRID GENERATOR

5.1 GENERAL

The accuracy attainable with the finite element method in solving partial differential equations depends ultimately on the sizes of the elements in the grid used for this purpose. One has therefore often to refine the grid a number of times, before an acceptable solution is obtained.

The generation of a finite element grid is at best a very time consuming exercise, the more so the higher the dimensions of the problem are. A grid generator is thus almost a necessity when solving three-dimensional partial differential equations, with the finite element method. An attempt was made to develop a three-dimensional grid generator during this investigation, but abandoned when it was realized that the visual representation of such a grid requires a study on its own. The program KUBIK, developed by Pissanetzky (1984) for a mainframe computer, was consequently used in the present investigation. The source code of this program is freely available from the Computer Physics Communications Library in Dublin. It was thus relatively easy to adapt it for the microcomputers used in this investigation. This generator is discussed briefly in Section 5.2, while its practical application is illustrated in Section 5.3.

5.2 STRUCTURE OF THE GENERATOR

The main objectives of a grid generator are threefold: (a) to divide the domain of interest into a number of elements, (b) to compute the coordinates of the nodes of each element and (c) to number the nodes and elements uniquely. The generator, KUBIK, used in this study, has two very desirable properties, as far as the present study is concerned. The first is, that it was developed specifically for the hexahedral elements, discussed in Appendix A, and the second that it allows the user to divide the domain in subdomains, each with its own grid spacing. The last property is particularly useful in groundwater pollution studies.

The form of a finite element grid and the sizes of its elements depend very much on the problem for which it is required (Botha and Pinder, 1983). An automatic grid generator should therefore always be able to display the grid visually, so that the user can verify and change the grid interactively. The additional ability of KUBIK to rotate the visual display of the grid, is of considerable value in the generation of three-dimensional grids.

There are a number of methods that can be used to generate a finite element grid for a

given or *global* domain, Ω (Thompson, 1977). The simplest method is probably to choose suitable lines along the boundary of Ω and represent them as edges of a rectangular or *local* domain. The advantage of this procedure is that it is much easier to cover the local domain automatically with elements, than the irregular global domain. This is especially true if the coordinates of the local domain are expressed in terms of integers. These regular elements can then be transformed to the global domain, by associating their edge nodes with suitable global coordinates, chosen from the lines used to define the local domain. This method is also used by KUBIK.

It is standard practice in finite element work to number the nodes anti-clockwise around an element, and in such a way that the bandwidth of the coefficient matrix is minimized. As shown in Figure 5-1, a three-dimensional hexahedral element contains six boundary sides, or *facets* as they are sometimes called. A special numbering convention has therefore to be used in the generation of a three-dimensional finite element grid. KUBIK achieves this by numbering the nodes on every side of an element such that it appears anti-clockwise to an outside observer who looks directly towards that side, see Figure 5-1.

Two major changes were made to the original program KUBIK for the present study. The first one was to replace all the subroutine calls to a mainframe graphics library with calls to a personal computer graphics library, PLOT88®, available at the Institute for Groundwater Studies. The second one was to provide an interface that allows the user to specify which boundary sides (maximum three) of the domain must be drawn. The reason for doing this was to circumvent the inability of the original program to handle hidden lines and nodes. This revised program, called QBIK, was implemented on a IBM-compatible personal computer with 4 Mb of extended memory.

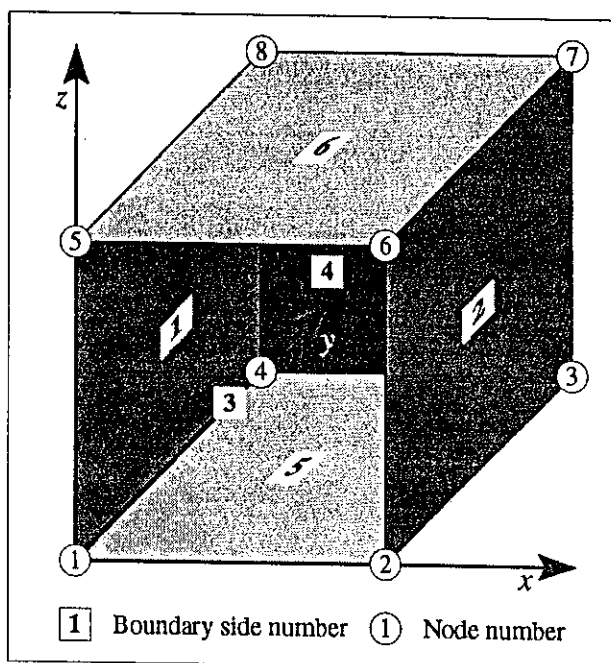


Figure 5-1 Example of a hexahedral element in three-space and the numbering convention used by KUBIK.

5.3 PRACTICAL APPLICATION OF PROGRAM QBIK

The example, chosen to illustrate the application of QBIK, is taken from the discussion of the unsaturated flow model in Chapter 7. This problem consists of a soil column subject to a

rainfall boundary condition on top, a seepage boundary on the left hand side and a fixed water level along the bottom edge of the left hand side, see Figure 5-2. The theory of finite elements (Botha and Pinder, 1983) indicates that such boundary conditions are best handled by using a grid with elements that increase gradually in size from these boundaries. This principle is illustrated graphically in Figure 5-2.

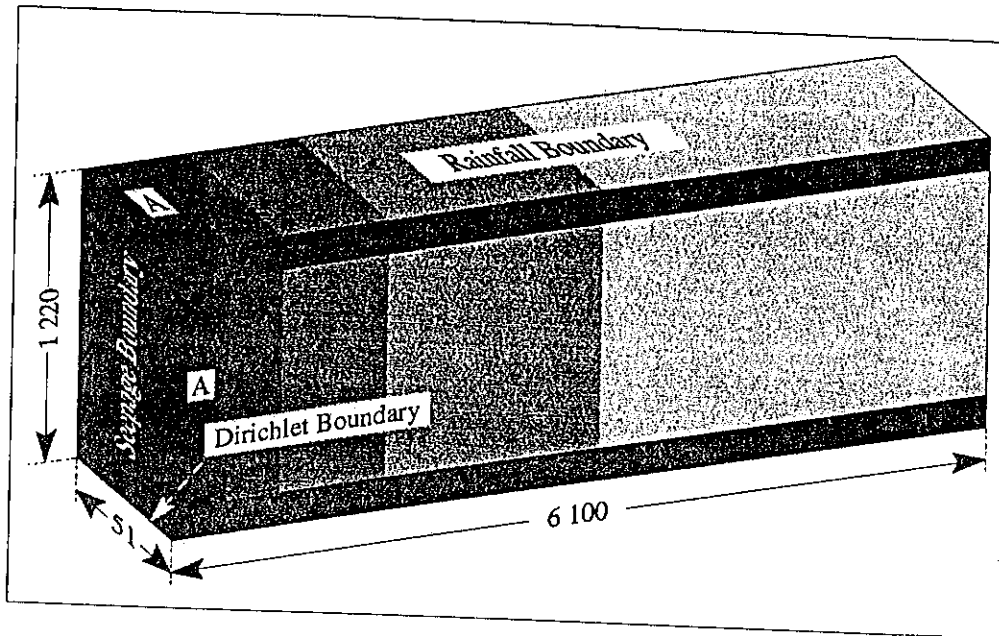


Figure 5-2 Schematic representation of the domain used in this discussion of Program QBIK. Dark grey areas represent subdomains that require more refined finite element grids.

The input to program QBIK is quite simple. All that the user needs to do, is to specify the coordinates of element nodes along the edges of the local domain and their associated global coordinates from the corresponding global domain, as in Table 5-1. The program then computes the nodal coordinates of all local elements by interpolation and transforms them to the global domain.

Table 5-1 Local and global coordinates used to generate the finite element grid in Figure 5-3 for subdomain A in Figure 5-2.

Local Coordinates			Cartesian Coordinates		
ξ	η	ζ	x	y	z
1	1	1	0,0	0,0	0,0
1	4	1	0,0	51,0	0,0
1	4	13	0,0	51,0	0,0
1	1	13	0,0	0,0	0,0
9	1	1	400,0	0,0	1 220,0
9	4	13	400,0	51,0	1 220,0
9	4	13	400,0	51,0	1 220,0
9	1	13	400,0	0,0	1 220,0

Program QBIK also allows the user to vary the sizes of elements across the global

domain. This can be achieved, by merely dividing the global domain into separate subdomains, and to specify a different distribution of local elements in each of these subdomains. For example, one can divide the domain of Figure 5-2 into the different subdomains delineated by the different shades of grey in Figure 5-3 and then add them together. The user must of course be careful to ensure that the elements are continuous across the boundaries of two such subdomains, if he wants to use conforming elements.

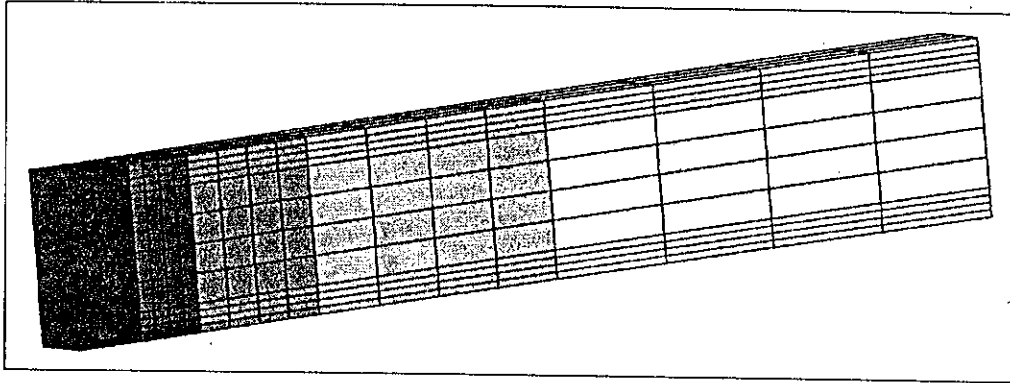


Figure 5-3 The finite element grid generated for the global domain in Figure 5-2, with Program QBIK. The different shades of grey denote the subdomains into which the domain was divided.

In conclusion it should be mentioned that Program QBIK is a very efficient program, as far as computer resources are concerned. This efficiency allowed us to generate all grids used in this report on a personal computer.



CHAPTER 6

THE SATURATED FLOW PROGRAM

6.1 INTRODUCTION

It is extremely difficult, if not impossible, to debug a computer program completely, especially one with the size of the programs developed for this investigation. Nevertheless, this does not free the developer from his responsibility to ensure that the program is, to the best of his knowledge, free of serious errors.

There are a number of methods that can be used in debugging a computer program for the simulation of a physical phenomenon. Four methods, frequently employed for this purpose, are:

- (a) To compare the output from the program with analytical solutions of simplified conceptual models for the phenomenon.
- (b) To ensure that the output from the program satisfies the convergence criteria of the numerical approximations used in the development of the program.
- (c) To ensure that the program satisfies the basic physical laws that govern the specific phenomenon, e.g., the law of mass conservation in fluid flow and mass transport.
- (d) To compare the output from the program with that from another, perhaps less sophisticated program.

The same approach was also followed in this investigation. The only difference is that the approximation, used for the solution of the groundwater flow equation, satisfies the law of mass conservation implicitly, see Section 4.2.1. More attention will, therefore, be paid to the other three methods in the discussion of the flow equation.

As shown by the discussion in Section 2.5, the saturated and unsaturated groundwater flow equations differ physically very little. The program, SUF3, for variably saturated flow, being the more complex, was therefore developed before the program, SAT3, for saturated flow. One reason for this approach was that it is easier to adapt the program of a general phenomenon to a more special phenomenon, than conversely. Another reason was that the variably saturated flow program can handle saturated flow conditions as well. The possibility thus existed that one program could handle all situations of interest in this investigation. However, it soon became clear that a separate saturated flow program would have definite advantages. For example, the saturated flow program executes much faster than the variably saturated flow program. Since the numerical approximations in the two programs are identical, the saturated flow program was used during the initial debugging phase. The discussion in this chapter will therefore be restricted to the saturated flow program SAT3.

The discussion starts with a comparison of the numerical three-dimensional flow model and two analytical solutions for the two-dimensional flow model in Section 6.2. The convergence rates of the numerical model in both time and space are then discussed in Section 6.3. This is followed by a comparison of Program SAT3 with the well-known program MODFLOW of McDonald and Harbaugh (1988) in Section 6.4. The significance of these comparisons for the application of two- and three-dimensional models is discussed in Section 6.5

6.2 COMPARISON OF THE NUMERICAL SATURATED FLOW MODEL WITH ANALYTICAL MODELS

No analytical solution of the three-dimensional groundwater flow equation, suitable for the debugging of Program SAT3, could be found in the available literature. The only alternative was thus to restrict the flow to the horizontal plane and compare the results with suitable two-dimensional analytic solutions. This approach is of course not without its difficulties. The majority of analytical solutions for groundwater flow problems [e.g., the Theis equation (Theis, 1935)], have been derived with the assumption that the borehole is a point source, centred in an infinite aquifer. These solutions therefore tend to infinity as the distance from the borehole tends to zero. The numerical solution, on the other hand, will always be finite, due the assumption that the borehole forms a Neumann boundary (See the discussion in Section 2.6.)

A boundary at infinity can be simulated on a computer either by an iterative method (Botha, 1971), or infinite elements (Zienkiewicz, 1977). The former method has the disadvantage that it can take a considerable number of iterations, before an acceptable approximation is found, while infinite elements need special procedures. Since all aquifers are finite in extent, it was not thought worthwhile to complicate the program further, by making provision for infinite boundaries.

Two analytical solutions for the two-dimensional flow equation that do not suffer from a boundary at infinity are those of Muskat (1946). These solutions, which are very similar to the Theis solution, have been derived with the assumption that the borehole, which discharges at a constant rate Q , is situated at the centre of a uniform aquifer with radius R , thickness d , hydraulic conductivity K and storativity S_0 . The first solution,

$$s(r, t) = \phi_0 - \phi(r, t) = \frac{Q}{\pi K d} \left[\frac{1}{2} \ln \frac{R}{r} - \sum_{i=1}^{\infty} \frac{J_0(\alpha_i r) \exp(-\alpha_i^2 \kappa t)}{\alpha_i^2 R^2 J_1^2(\alpha_i R)} \right] \quad (6.1)$$

where $J_0(z)$ and $J_1(z)$ are the zeroth and first order Bessel functions of the first kind, respectively and $\kappa = K/S_0$, while α_i must satisfy the equation

$$J_0(\alpha_i R) = 0 \quad (i = 1, 2, \dots)$$

This solution is valid for an aquifer subject to the initial piezometric level ϕ_0 and Dirichlet

boundary condition

$$\phi(R, t) = \phi_0 \quad (t \geq 0) \quad (6.2)$$

The second solution corresponds to the case where there is no flux of water across the outer boundary of the aquifer. This situation can be described mathematically by the homogeneous Neumann boundary condition

$$D_r \phi(R, t) = 0 \quad (t \geq 0) \quad (6.3)$$

The drawdown in such an aquifer is given by

$$s(r, t) = \phi_0 - \phi(r, t) = \frac{Q}{\pi K d} \left[\frac{1}{4}(\bar{r}^2 + 4\bar{t}) - \frac{3}{8} - \ln \bar{r} - \sum_{i=1}^{\infty} \frac{J_0(\chi_i \bar{r}) \exp(-\chi_i^2 \bar{t})}{\chi_i^2 J_0^2(\chi_i)} \right] \quad (6.4)$$

where

$$\chi_i = \alpha_i R, \quad \bar{r} = r/R, \quad \bar{t} = \kappa t/R^2$$

The other symbols all have the same meaning as before, except that α_i is now defined by the equation.

$$J_1(\alpha_i R) = 0$$

The Muskat solutions can be applied to any radially symmetric three-dimensional aquifer, such as the one shown in Figure 6-1, with the additional Neumann boundary conditions

$$D_z \phi(r, 0, t) = D_z \phi(r, 40, t) = 0 \quad (6.5)$$

(Botha *et.al.*, 1990). The first debugging of Program SAT3 was consequently based on this hypothetical aquifer, with parameters summarized in Table 6-1. The reason for this was that the radial symmetric Muskat solutions could be used to detect gross errors in the program.

The finite element grid used in the computation consisted of 36 angular slices, every one divided into curved elements with nodes at radial distances of 0,01; 0,05; 0,1; 0,5; 1; 2; 4; 8; 16; 32; 64; 128; 256; 512 and 768 m, and at heights of 0; 20 and 40 m. The borehole was

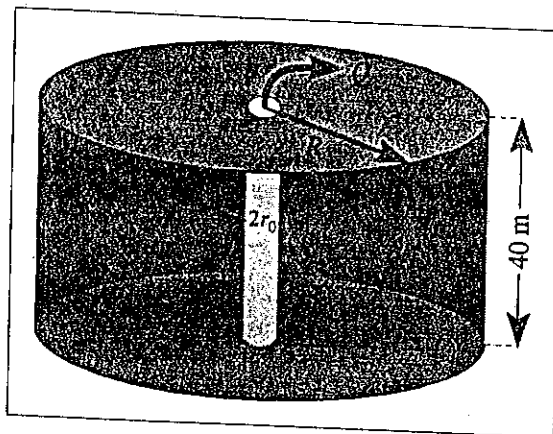


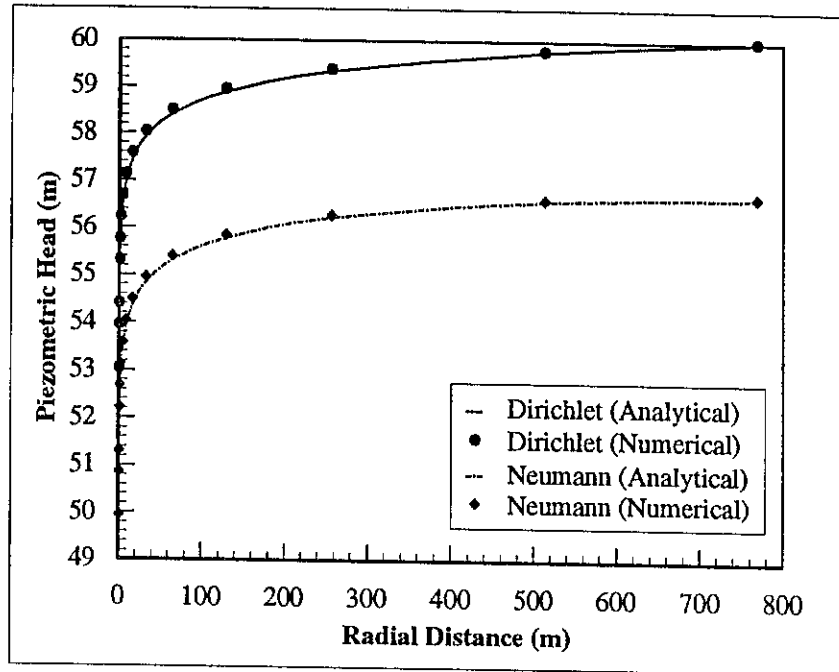
Figure 6-1 Schematic representation of the hypothetical aquifer used in debugging Program SAT3.

considered as a Neumann boundary with a non-zero flux given by Equation (2.26), while the time step was varied from 1 s to a maximum of 3 h with a multiplication factor of 1,50.

Table 6-1 Dimensions and hydraulic parameters of the aquifer used with the Muskat aquifer in debugging Program SAT3.

R (m)	d (m)	ϕ_0 (m)	Dirichlet Problem			Neumann Problem		
			K (m.d ⁻¹)	S_0 (m ⁻¹)	Q (m ³ .d ⁻¹)	K (m.d ⁻¹)	S_0 (m ⁻¹)	Q (m ³ .d ⁻¹)
768,0	40,0	60,0	1,0	$1,5 \cdot 10^{-5}$	172,8	4,0	$8,0 \cdot 10^{-6}$	691,2

As shown by the drawdowns in Figure 6-2, there is excellent agreement between the analytical and computed drawdowns, except in the vicinity of the borehole. One reason for this behaviour is the different methods used to account for the borehole in the two solutions—a point source in the analytical solution and a non-zero flux Neumann boundary in the numerical solution. It was thus

**Figure 6-2** Comparison of the analytical and numerical solutions of the Muskat aquifer as a function of the distance from the borehole ($t = 72$ h).

necessary to establish what influence the radius of the borehole may have on the numerical solution.

The possible influence of the finite radius (r_0) of the borehole on the numerical solution, was investigated by successively removing the elements at radial distances of 0,01; 0,1; 0,5 and 1,0 m from the finite element grid. The drawdowns, computed with a fixed time step of 0,5 (h), are compared with the analytical solutions of Equation (6.1) in Table 6-2. Although the approximation errors at small values of r are relatively large (at least from the numerical point of view), the results show that r_0 does not play a particularly important part in the solution. This behaviour accords with an earlier result of Bakkes and Botha (1982) that the influence of the singularity, caused by the representation of the borehole as a point source in the analytical solution, is restricted to a small area in the immediate vicinity of the borehole.

Two causes for concern remain, however. The first is the large numerical errors in Table 6-2 and the second the oscillations near $r = 64$ and 128 m. A natural impulse would be to ascribe this behaviour of the numerical solution to errors in the program. However, the possibility also exists that the finite element grid was too coarse, or that the time step was too

large. The only way to clarify the reason for such a behaviour is to study the convergence properties of the numerical approximation in more detail.

Table 6-2 Comparison of the analytic and computed piezometric heads in the aquifer of Figure 6-1 for the parameters in Table 6-1, with different values of r_0 . [$t = \Delta t = 0,5$ (h)]

Radial Distance (m)	Piezometric Head (m)		Approximation Error	Piezometric Head (m)		Approximation Error
	Analytical	Numerical		Analytical	Numerical	
$r_0 = 0,01$						
1	57,973	58,272	$-2,985.10^{-1}$	57,973	58,272	$-2,982.10^{-1}$
2	58,448	58,718	$-2,699.10^{-1}$	58,448	58,718	$-2,697.10^{-1}$
4	58,919	59,148	$-2,289.10^{-1}$	58,919	59,147	$-2,288.10^{-1}$
8	59,370	59,532	$-1,620.10^{-1}$	59,370	59,532	$-1,619.10^{-1}$
16	59,756	59,823	$-6,638.10^{-2}$	59,756	59,823	$-6,635.10^{-2}$
32	59,970	59,970	$-3,319.10^{-4}$	59,970	59,970	$-3,281.10^{-4}$
64	60,000	60,000	$-2,136.10^{-4}$	60,000	60,000	$-2,136.10^{-4}$
128	60,000	60,000	$+1,144.10^{-5}$	60,000	60,000	$+1,144.10^{-5}$
256	60,000	60,000	$+0,000.10^{+0}$	60,000	60,000	$+0,000.10^{+0}$
$r_0 = 0,5$						
1	57,973	58,267	$-2,935.10^{-1}$	57,973	58,255	$-2,821.10^{-1}$
2	58,448	58,715	$-2,661.10^{-1}$	58,448	58,706	$-2,577.10^{-1}$
4	58,919	59,145	$-2,264.10^{-1}$	58,919	59,139	$-2,208.10^{-1}$
8	59,370	59,531	$-1,606.10^{-1}$	59,370	59,528	$-1,576.10^{-1}$
16	59,756	59,822	$-6,586.10^{-2}$	59,756	59,821	$-6,469.10^{-2}$
32	59,970	59,970	$-2,441.10^{-4}$	59,970	59,970	$-4,578.10^{-5}$
64	60,000	60,000	$-2,174.10^{-4}$	60,000	60,000	$-2,174.10^{-4}$
128	60,000	60,000	$+1,144.10^{-5}$	60,000	60,000	$+1,144.10^{-5}$
256	60,000	60,000	$+0,000.10^{+0}$	60,000	60,000	$+0,000.10^{+0}$

6.3 CONVERGENCE OF THE NUMERICAL SOLUTION

6.3.1 General

There are two advantages in studying the convergence properties of a numerical method, when applied to a differential equation of the form

$$Lu(\mathbf{x}, t) = f(\mathbf{x}, t) \quad (6.6)$$

It allows one to: (a) track down programming errors and (b) chooses an optimal grid and time steps for the approximation (Zienkiewicz, 1977). To show this, let $\hat{u}(\mathbf{x}, t)$ be the finite element solution of Equation (6.6). If there are no numerical, or programming, errors in the program then one should have that (Botha and Pinder, 1983; Strang and Fix, 1973)

$$\lim_{\Delta\rho, \Delta t \rightarrow 0} \|u(\mathbf{x}, t) - \hat{u}(\mathbf{x}, t)\| \rightarrow 0$$

where $\Delta\rho = \max(\Delta x, \Delta y, \Delta z)$, with $\Delta x, \Delta y$ and Δz the element sizes in the x -, y - and z -directions respectively, and Δt the time step used in the discretization. It is thus possible to decide

whether a computer program contains programming, or other errors, by solving Equation (6.6) over a series of grids with various element sizes and time steps. Previous experience indicates that one can be confident with the approximation, if the errors decrease continuously with a refinement in either the grid, or time step, or both.

It would be ideal to use an analytic solution of Equation (6.6) in the convergence tests, but this is rarely possible in practice. Convergence studies are consequently often based on a numerical solution, obtained from a grid with suitably small values of t and ρ . This approach will thus also be used in the convergence studies discussed below, whenever the necessity arises.

6.3.2 Convergence in Time

The convergence rate of the numerical solution for the saturated flow equation was again studied with the hypothetical aquifer in Figure 6-1 and the parameter values in Table 6-1. The finite element grid was also kept the same in the horizontal plane, but the number of elements in the z -direction was increased from 2 to 3. Equations (6.2) and (6.5), with $\phi_0 = 60$ m, were again used as the initial and boundary conditions. Piezometric levels were computed, over a period of 2 hours, with time steps of 1, 5, 15, 30, 60 and 120 minutes.

The convergence rates of the numerical solution are displayed graphically in Figure 6-3. These rates are clearly in excellent agreement with the theoretical rate of $O(\Delta t)$ (Botha and Pinder, 1983) for the backward finite difference approximation of the time derivative, used in Program SAT3. As shown by the results in Figure 6-2, the numerical solution converges rapidly towards the analytical solution at large values of r . This explains the decrease in slope (m) of the convergence rate in Figure 6-3. These results suggest that there is no numerical or programming errors in the section of Program SAT3 that handles the time discretization.

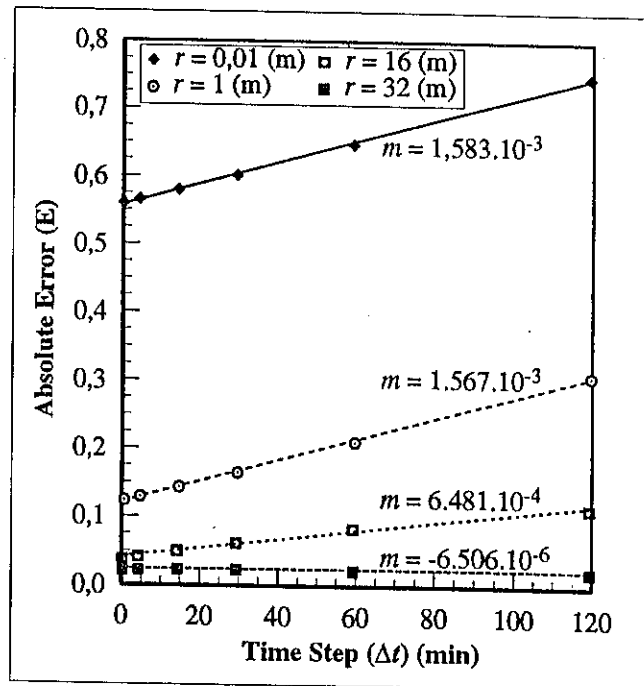


Figure 6-3 Convergence of the numerical solution for the saturated flow equation, as a function of time at different distances from the borehole.

6.3.3 Convergence in Space

The computer resources, available at that stage of the project, could not handle a more refined

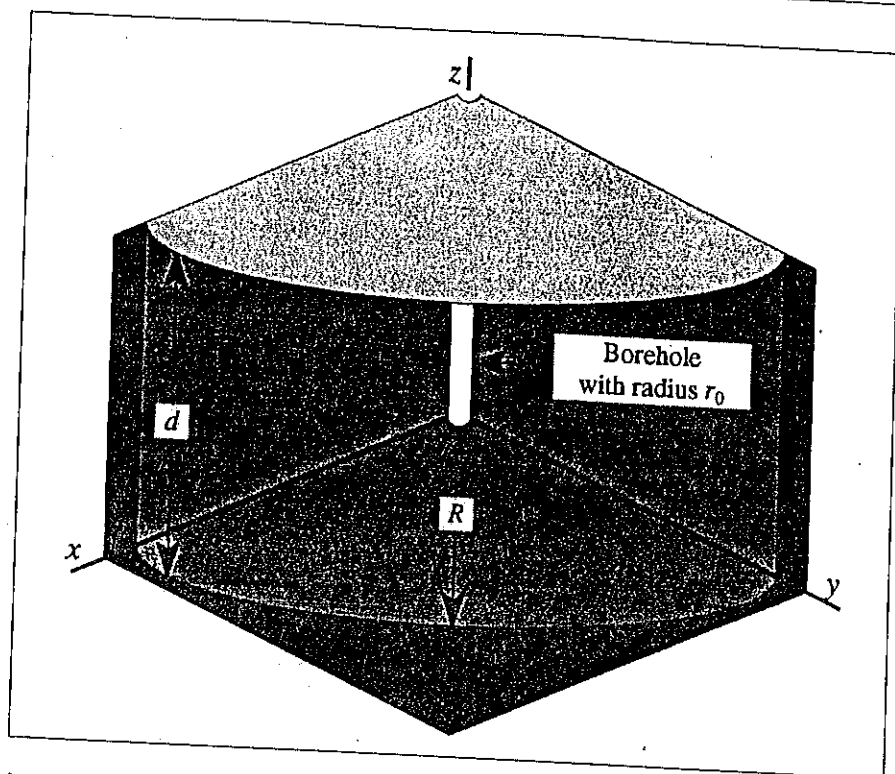


Figure 6-4 Hypothetical aquifer used in studying the convergence rate of Program SAT3 in space.

grid for the full aquifer. The quarter aquifer in Figure 6-4 was consequently used in the study of the spatial rate of convergence. The aquifer parameters, given in Table 6-1, were again used with this aquifer, except for the radius which was changed to 1 017 m, to obtain a better spacing in radial nodes. The diameter of the borehole was also fixed at 160 mm, which is the primary standard in South Africa. The grid used in this investigation was obtained by dividing the aquifer into angular slices of 10° and vertically in two elements, with lengths of 20 m each. (See Figure 6-5.)

A theoretical analysis (Botha and Pinder, 1983) shows that the finite element approximation error for the spatial part of the flow equation should be of the form

$$e_s = O(\rho_{\max}^2) \quad \text{where} \quad \rho_{\max} = \max(\Delta x, \Delta y, \Delta z) \quad (6.7)$$

and Δx , Δy and Δz are again the side lengths of a typical element. It would thus be ideal to keep the element sizes as equal as possible in an investigation of the spatial convergence rates. However, as shown in Figure 6-6, the increments in the xy -plane

$$\Delta x = (r_2 - r_1) \cos \theta \quad \text{and} \quad \Delta y = (r_2 + r_1) \sin \theta$$

are non-linear. It is therefore not easy to devise a grid for a radial domain with equal increments in the x - and y -directions. This difficulty was avoided to some extent by halving the radii of the elements repeatedly, until all the nodes in Figure 6-7 were assigned to an element. The final grid was obtained by reducing the angle (2θ) of the angular slices from 10°

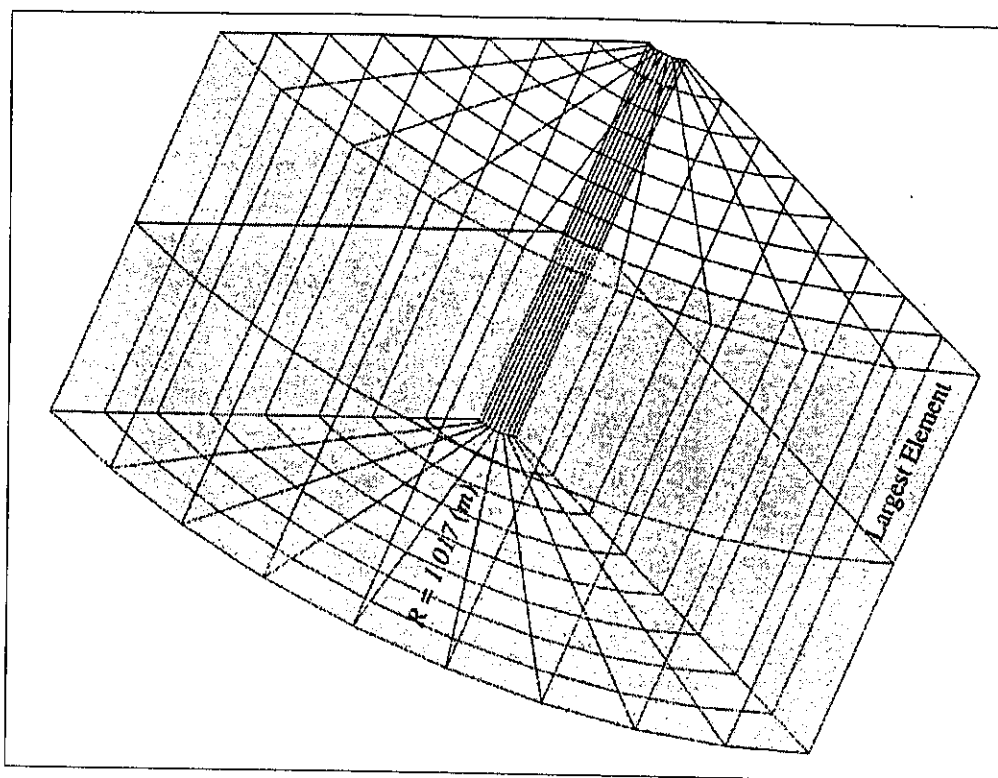


Figure 6-5 The radial finite element grid used with the hypothetical aquifer of Figure 6-4 in studying the spatial convergence of program SAT3.

to 5° . This approach yielded grids with maximum increments given in Table 6-3. The numerical solutions for three of the grids, with a constant time step of 1 h, are compared with

Table 6-3 Maximum sizes of elements used in studying the spatial convergence of program SAT3, for the hypothetical aquifer in Figure 6-4.

Grid No	$\Delta\rho_{max}$	Grid No	$\Delta\rho_{max}$	Grid No	$\Delta\rho_{max}$
1	527,018 994	2	298,415 288	3	209,415 893
4	183,152 073	5	107,108 379		

the Muskat solution, of Equation (6.1) in Figure 6-8.

A first impression of the results in Figure 6-8 is that the numerical solution of the saturated flow equation, computed with Program SAT3, only converges if $r > 70$ m. However, the influence of the logarithmic singularity in the analytical solution at the origin cannot be ignored completely. This possibility was investigated by comparing the convergence of the results for the $2\theta = 10^\circ$ grids, with that of the $2\theta = 5^\circ$ grid. The results for distances of 0,08; 1,0 and 9,0 m in Figure 6-9, show that the convergence rates do indeed satisfy the general quadratic behaviour, required by Equation (6.7).

An interesting feature of Figure 6-9 is that the numerical errors at the distances of 0,08 and 1,0 m tend to a limit as $\Delta\rho_{max}$ increases. This behaviour is contrary to the general theory of numerical approximation theory, but can probably be ascribed to the $\Delta\rho_{max}$ used in

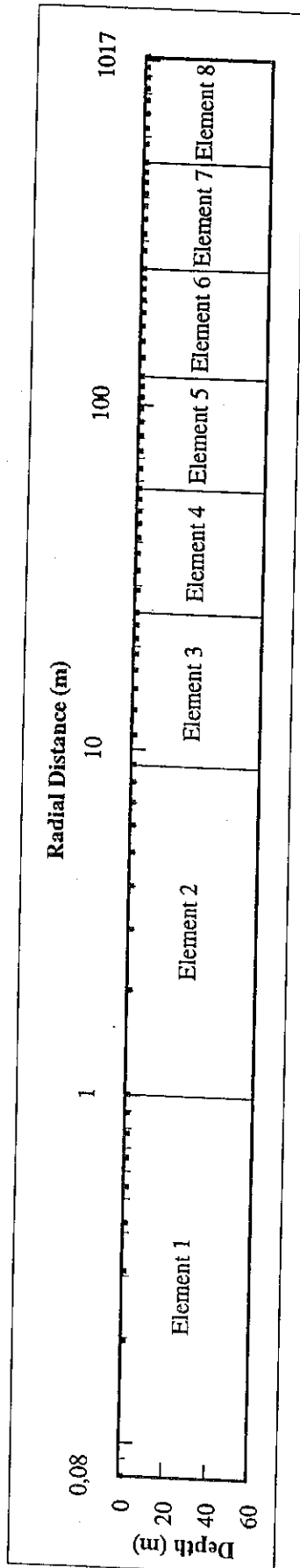


Figure 6-7 Radial spacings of the finite element grid, used in studying the spatial convergence of program SAT3, for the hypothetical aquifer in Figure 6-4.

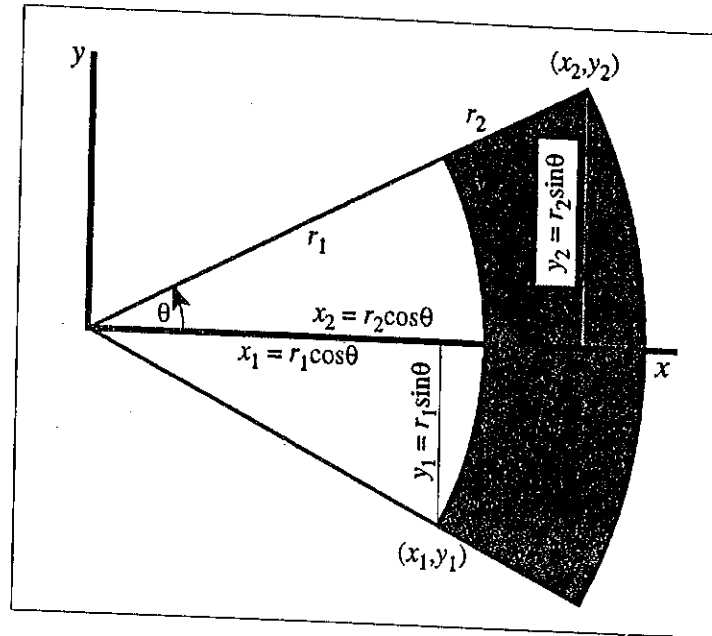


Figure 6-6 Schematic representation of a radial finite element in the horizontal plane of Figure 6-4.

drawing Figure 6-9, which is the diameter of the largest elements in the grid. These elements are all situated on the boundary of the domain, see Figure 6-5, their influence could therefore decrease after a certain distance.

6.4 COMPARISON OF SAT3 WITH MODFLOW

The program MODFLOW of the United States Geological Survey (McDonald and Harbaugh, 1988) is frequently used in the modelling of three-dimensional groundwater flow. Since the program is well documented and able to handle most of the boundary conditions met in practice, it is often considered as the industry standard in groundwater circles. It was thus thought worthwhile to compare Program SAT3 with MODFLOW, as a final check for possible numerical and programming errors.

One disadvantage of MODFLOW is that it is based on a finite difference approximation of the saturated flow equation. It cannot therefore handle Neumann conditions on curved boundaries with the same ease and accuracy as SAT3. The square, confined aquifer, presented graphically in Figure 6-10, was therefore chosen for this study.

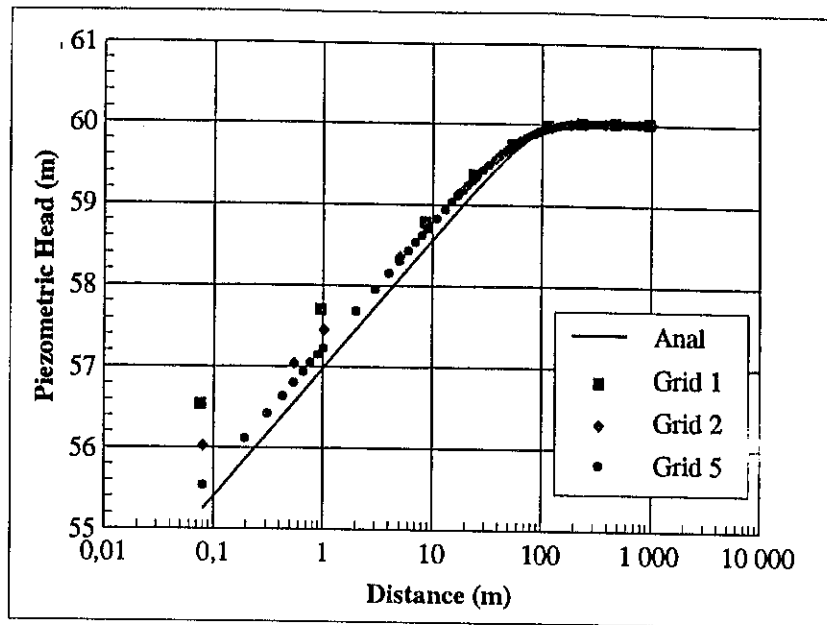


Figure 6-8 Spatial convergence of the program SAT3, for the hypothetical aquifer in Figure 6-4 and three of the grids in Table 6-3. ($\Delta t = 1$ h.)

It was assumed that the aquifer has the homogeneous parameters, given in Table 6-1, with zero-flux boundary conditions on all sides.

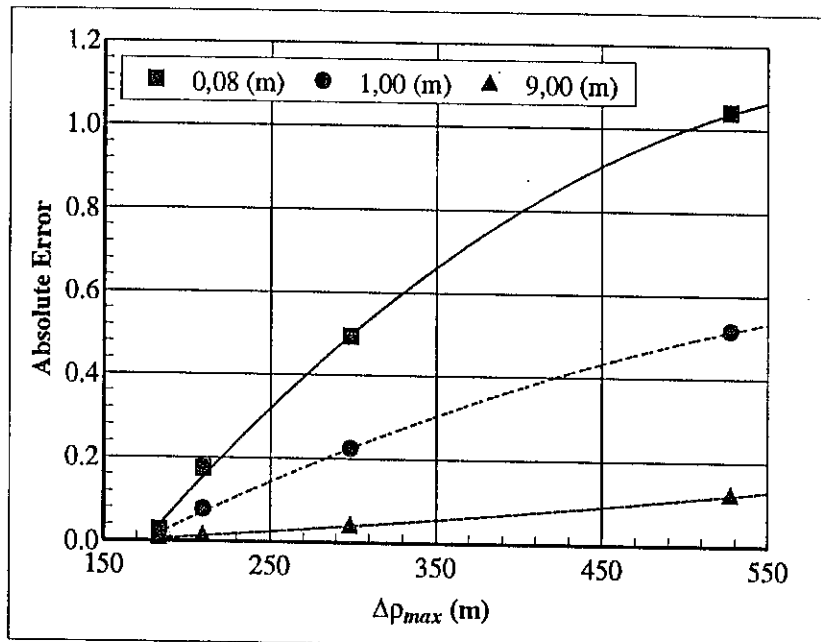


Figure 6-9 Convergence of the numerical solution of Equation 6-1, for three distances from the centre of the borehole.

Another disadvantage of MODFLOW is that it is restricted to an equally spaced grid in the xy -plane. A very fine grid of 250×250 nodes, had therefore to be used in the xy -plane, with four elements in the vertical direction, to ensure that the finite element and finite difference

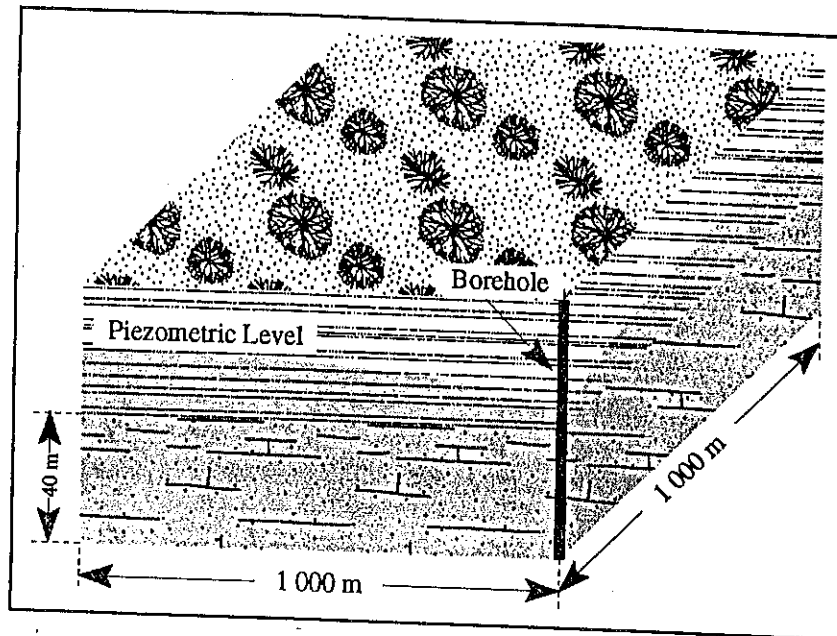


Figure 6-10 The hypothetical homogeneous aquifer used in comparing Programs SAT3 and MODFLOW.

solutions are comparable near the borehole.

Both programs were used to compute piezometric heads over a period of 72 hours with a fixed time step of 0,5 (h) and a pumping rate of $172,8 \text{ (m}^3\cdot\text{d}^{-1}\text{)}$. The results, which are summarized in Table 6-4, show that the two sets of piezometric heads are in excellent agreement. These results and the convergence properties of the solution for Muskat's problem can be taken as a clear indication that SAT3 does not contain serious numerical or programming errors.


Table 6-4 Computed piezometric heads for the aquifer in Figure 6-9 at diagonal distances of r (m) from the borehole as a function of time.

Time (h)	Piezometric Head (m)		Time (h)	Piezometric Head (m)	
	MODFLOW	SAT3		MODFLOW	SAT3
0,0	60,00	60,00	36,0	58,37	58,38
0,5	59,73	59,73	38,0	58,36	58,36
2,0	59,31	59,32	40,0	58,34	58,35
4,0	59,08	59,09	42,0	58,32	58,33
6,0	58,95	58,96	44,0	58,30	58,31
8,0	58,86	58,87	46,0	58,29	58,30
10,0	58,79	58,80	48,0	58,27	58,28
12,0	58,73	58,74	50,0	58,26	58,26
14,0	58,68	58,69	52,0	58,24	58,25
16,0	58,64	58,64	54,0	58,23	58,24
18,0	58,60	58,61	56,0	58,21	58,22
20,0	58,57	58,57	58,0	58,20	58,21
22,0	58,53	58,54	60,0	58,18	58,19
24,0	58,51	58,51	62,0	58,17	58,18
26,0	58,48	58,49	64,0	58,16	58,16
28,0	58,46	58,46	66,0	58,14	58,15
30,0	58,43	58,44	68,0	58,13	58,14
32,0	58,41	58,42	70,0	58,12	58,12
34,0	58,39	58,40	72,0	58,10	58,11

6.5 DISCUSSION

The results above indicate that there is no cross programming or numerical errors in Program SAT3 and that the program can be used with confidence in the simulation of three-dimensional saturated, groundwater flow problems.

It is not mathematically correct to compare the solution of two- and three-dimensional conceptual models. This is especially true, if the two-dimensional model has been derived from the corresponding three-dimensional model by a mathematical reduction of dimensions (Bear, 1979; Botha *et. al.*, 1990). However, if zero-flux boundary conditions are applied along two parallel sides of a uniform, confined aquifer, the three-dimensional model reduces to a two-dimensional model in the remaining dimensions. It is thus fair to interpret the preceding results as saying that there is no need to use a three-dimensional model, for a uniform, confined aquifer.



CHAPTER 7

THE UNSATURATED FLOW PROGRAM

7.1 INTRODUCTION

The approach to debug the saturated flow program before the variably saturated program, SUF3, had the advantage that the debugging of SUF3 could be limited to a study of the iteration convergence and the application of rainfall and seepage boundary conditions. However, one difficulty remained. No known analytical solution for unsaturated flow could be found in the literature. The only alternative was thus to search for a problem that had been solved with another numerical model. Such a problem is presented by the drainage problem, used by Davis and Neuman (1983) in the evaluation of their two-dimensional program, UNSAT2, for flow in a variably saturated medium. The problem has the added advantage that it requires exactly those boundary conditions, not included in Program SAT3. This problem is described and used in comparing Program SAT3 with UNSAT2 in Section 7.2. A study of the iteration and convergence rates of Program SUF3, in Section 7.3, was also based on the drainage problem.

7.2 THE DRAINAGE PROBLEM

7.2.1 Description of the Problem

The drainage problem originated from a series of laboratory experiments by Duke (1973) and Hedstrom *et al.* (1971), to obtain a better understanding of the drainage of agricultural soils and to design better subsurface drainage systems. In the experiment on which the model problem is based a flume 12 200×51×1 220 mm was packed with Poudre Sand, see Figure 7-1. The reason for using Poudre Sand was that its hydraulic properties have been studied extensively and are well documented (Davis and Neuman, 1983; Case *et al.*, 1983). The saturated hydraulic conductivity for the sand is: $K = 6,440 \cdot 10^{-5} \text{ (m.s}^{-1}\text{)}$, and its porosity $\varepsilon = 0,348$. The experimentally determined moisture retention curve of the sand, and its Van Genuchten approximation, given by Equation (2.9), is shown in Figure 7-2.

7.2.2 Comparison of Program SUF3 with Program UNSAT2

The first step in the evaluation of Program SUF3 was to apply it to the drainage problem, discussed above, and to compare the results with that of Program UNSAT2 (Davis and

Neuman, 1983). The same initial and boundary conditions, applied by Davis and Neuman

$$\begin{aligned}\phi(x,0) &= \phi_0(x) = 0 \\ \phi(0,y,0) &= 0 \quad (0 \leq y \leq 51) \\ q_n(x,y,z=1\,220) &= 103,5 \text{ (mm.d}^{-1}\text{)}\end{aligned}$$

were consequently used for this purpose.

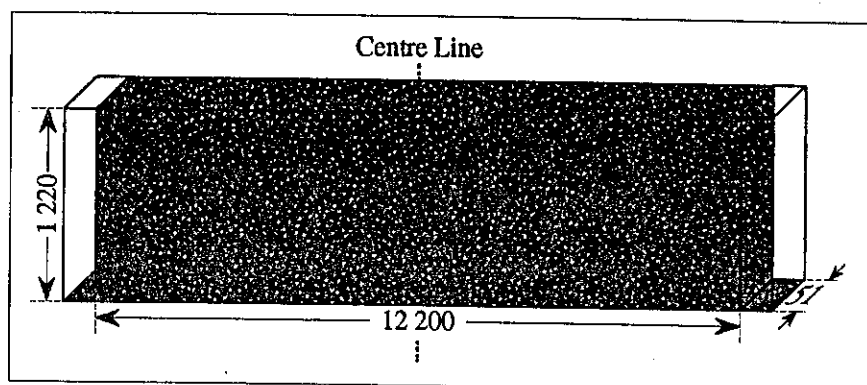


Figure 7-1 Schematic representation of the flume used by Duke (1973) and Hedstrom *et al.* (1971) in studying the drainage problem.

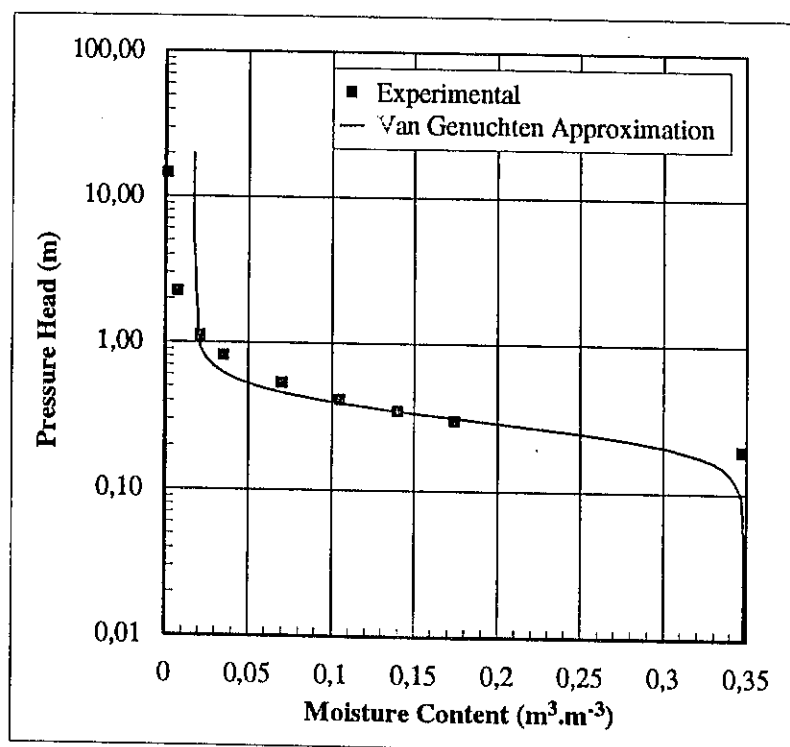


Figure 7-2 Graphs of the experimentally determined moisture retention curve and associated Van Genuchten approximation for Poudre Sand.

The flow system in Figure 7-1 will obviously be symmetrical about the centre line between the drainage ditches. It is thus natural to consider this centre line as the right hand

side boundary of the flow domain, and to prescribe a zero flux Neumann boundary condition along this side, as Davis and Neuman did. The same boundary condition was also prescribed along the two vertical faces of the flume to convert the problem to three-dimensions. This meant that Davis and Neuman's point Dirichlet boundary (at the intersection of the soil column and drain) had to be converted to a line boundary, and the seepage face and rainfall boundary to surfaces, see Figure 7-3.

Previous experience with Programs UNSAT2 and SUFF (an earlier two-dimensional version of Program SUF3) by Botha and Van Blerk (1990) have shown that the iteration convergence of both programs depends on the time step and maximum element size. Therefore, one would expect program SUF3 to behave in a similar fashion. Consequently, it was decided to base the finite element

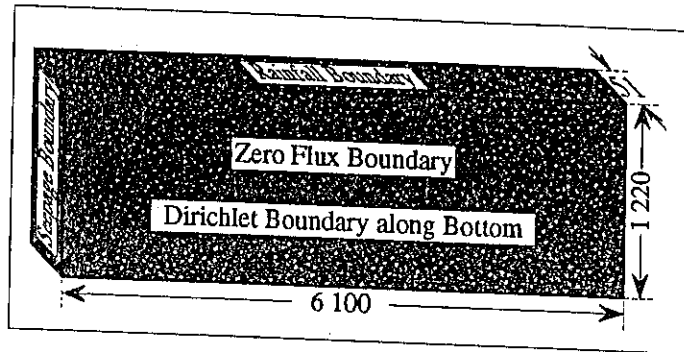


Figure 7-3 The physical dimensions and boundary conditions used with the drainage problem in the comparison of Programs UNSAT2 and SUF3.

grid for Program SUF3 on the one used by Davis and Neuman in their investigation of the drainage problem. This grid, of which a vertical cross-section is shown in Figure 7-4, differed only from the one of Davis and Neuman in that the four triangular elements, near the Dirichlet boundary, was replaced by seven rows of rectangular elements. This was done because both Programs QBIK and SUF3 cannot handle triangular elements. The grid was extended to three dimensions by repeating it three times along the other horizontal (y -axis). This yielded a grid with 1152×3 elements and 4900 nodes.

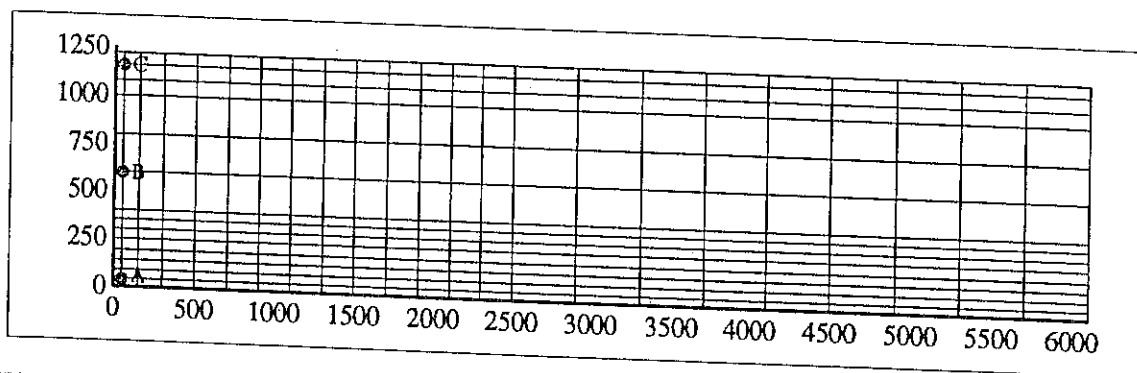


Figure 7-4 Vertical cross-section of the three-dimensional grid used with Program SUF3 in comparing it with Program UNSAT2.

Davis and Neuman (1983) used an initial step of $\Delta t = 0,005$ (d) in their investigation of the drainage problem. However, Program SUF3 did not converge within 5 iterations with the initial time step $\Delta t = 0,005$ (d) and iteration error of 0,01 (m). The initial time step in both programs was consequently reduced to 0,001 (d). This time step was kept constant until the

time $t = 0,005$, after which the time steps given by Davis and Neuman were used. The simulated elevations of the phreatic surface, $z(0) = z(h)|_{(h=0)}$, are compared graphically in Figure 7-5, after 1 and 8 d.

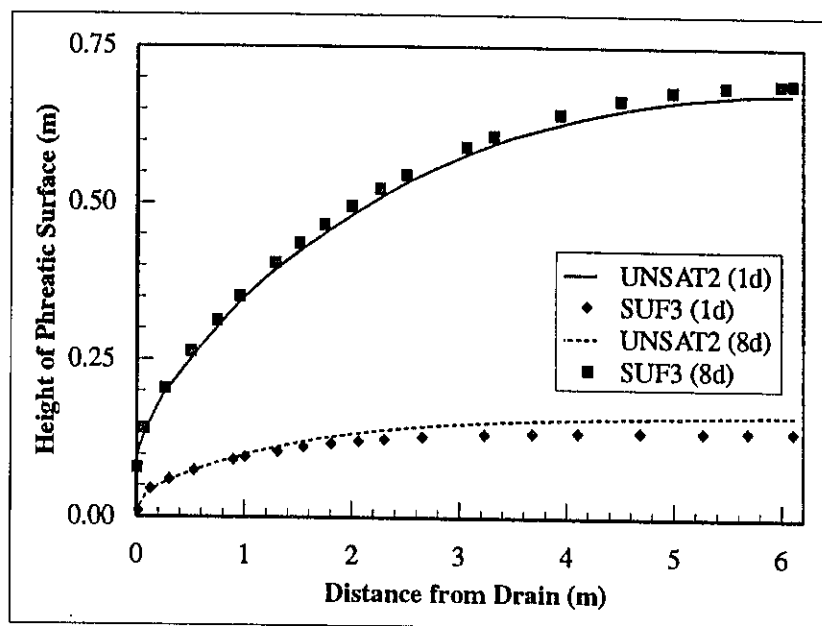


Figure 7-5 Comparison of the phreatic surfaces, $z(0)$, in the flume simulated with Programs SUF3 and UNSAT2 after 1 and 8 days.

Although the two phreatic surfaces in Figure 7-5 show the same general behaviour, there are significant differences, especially far from the drain. One reason for this behaviour is that the three-dimensional grid is more refined along the bottom boundary, than the two-dimensional one used by Davis and Neuman at distances far from the drain, see Figure 7-4. However, there is another one. Program UNSAT2 uses linear interpolation between the data points of the moisture retention curve to obtain values for the matric head, whereas SUF3 uses the Van Genuchten approximation. As can be seen from Figure 7-2, the experimental retention curve differs considerably from the Van Genuchten approximation near θ_r and θ_s . Since the phreatic surface coincides with θ_s , it would have been a surprise, if the two programs did yield identical phreatic surfaces.

Another indication that program SUF3 does not contain serious errors, is the way in which the two solutions behave with time. The variably saturated and saturated flow equations, see Equation (2.12), are essentially parabolic differential equations, although the variably saturated one is non-linear. The solution of a parabolic, partial differential equation always consists of two components: a smooth, stationary component and an exponentially, decaying, transient component (Botha and Pinder, 1983). The transient component usually decays very quickly with time, which leaves only the smooth stationary component at large times, see for example Equations (6.1) and (6.4). The numerical solution of a parabolic equation obviously must possess the same properties. (Otherwise the solution would not be

consistent, that is represent the true solution of the differential equation in all aspects.) Time-dependent approximation errors, such as errors made in approximating rainfall and seepage boundary conditions discretely, should thus decay with time. Therefore, one would expect the two solutions to converge towards one another in time, if other errors are ignored, which is exactly what happens in Figure 7-5.

7.3 CONVERGENCE OF THE NUMERICAL MODEL

7.3.1 Iteration Convergence

It is of the utmost importance to keep the number of iterations as small as possible in the numerical solution of a non-linear equation, such as the variably saturated flow equation. Indeed, it is usually considered ideal, if the number of iterations does not increase more rapidly than the inverse of the specified iteration error.

As shown by the discussion in Section 4.2.1, the iteration algorithm used in Program SUF3 conserves mass implicitly. Therefore, one would expect it to use fewer iterations than an algorithm that does not conserve mass. Unfortunately, it is extremely difficult to derive an explicit estimate for the number of iterations that the program will use. The iteration convergence was therefore investigated empirically.

The approach used for this purpose, was to solve the drainage problem for 480 s with different time steps and iteration errors and to count the number of iterations. These results, see Figure 7-6, show that the number of iterations increases logarithmically with the inverse of the iteration error, which is considerably less than the anticipated linear dependence. The iteration algorithm in Program SUF3, therefore must be considered as near optimum, if not optimum.

It is natural to interpret the

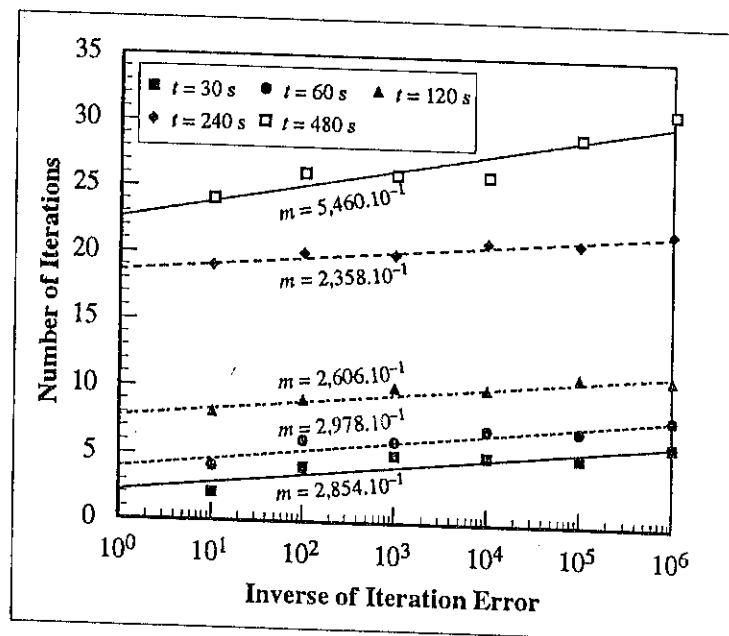


Figure 7-6 Convergence properties of the iteration algorithm in Program SUF3.

results in Figure 7-6 as indicating that any one of the time steps could be used in an actual simulation. Such an interpretation would not be correct, however. This can be seen by comparing the slopes of the lines in Figure 7-6. The sharp increase in slope of the $\Delta t = 480$ (s) line,

compared to the other, is a clear indication that there are significant approximation errors in the piezometric heads for this time step. This conjecture is confirmed by the comparison of piezometric heads in Table 7-1, at the three nodes, A, B and C in Figure 7-4. The error is especially noticeable for the matric head at Node C.

Table 7-1 Comparison of the matric heads, at $t = 480$ (s), computed with Program SUF3 for the same time steps used in Figure 7-6.

Iteration Error	Matric Heads		
	10^{-6}	10^{-3}	10^{-1}
Node	Time Step = 480 (s)		
A	-3,999 993.10 ⁻⁰²	-3,999 993.10 ⁻⁰²	-3,999 994.10 ⁻⁰²
B	-6,002 041.10 ⁻⁰¹	-6,002 041.10 ⁻⁰¹	-6,002 019.10 ⁻⁰¹
C	-1,716 785.10 ⁺⁰⁰	-1,716 720.10 ⁺⁰⁰	-1,702 288.10 ⁺⁰⁰
Node	Time Step = 240 (s)		
	10^{-6}	10^{-3}	10^{-1}
A	-4,000 000.10 ⁻⁰²	-4,000 000.10 ⁻⁰²	-4,000 000.10 ⁻⁰²
B	-6,002 913.10 ⁻⁰¹	-6,002 913.10 ⁻⁰¹	-6,002 901.10 ⁻⁰¹
C	-2,046 178.10 ⁺⁰⁰	-2,046 173.10 ⁺⁰⁰	-2,038 526.10 ⁺⁰⁰
Node	Time Step = 120 (s)		
	10^{-6}	10^{-3}	10^{-1}
A	-4,000 006.10 ⁻⁰²	-4,000 006.10 ⁻⁰²	-4,000 006.10 ⁻⁰²
B	-6,003 510.10 ⁻⁰¹	-6,003 510.10 ⁻⁰¹	-6,003 095.10 ⁻⁰¹
C	-2,309 397.10 ⁺⁰⁰	-2,309 362.10 ⁺⁰⁰	-2,107 468.10 ⁺⁰⁰
Node	Time Step = 60 (s)		
	10^{-6}	10^{-3}	10^{-1}
A	-4,000 008.10 ⁻⁰²	-4,000 008.10 ⁻⁰²	-4,000 008.10 ⁻⁰²
B	-6,003 866.10 ⁻⁰¹	-6,003 866.10 ⁻⁰¹	-6,003 645.10 ⁻⁰¹
C	-2,486 581.10 ⁺⁰⁰	-2,486 380.10 ⁺⁰⁰	-2,368 873.10 ⁺⁰⁰
Node	Time Step = 30 (s)		
	10^{-6}	10^{-3}	10^{-1}
A	-4,000 008.10 ⁻⁰²	-4,000 008.10 ⁻⁰²	-4,000 008.10 ⁻⁰²
B	-6,004 053.10 ⁻⁰¹	-6,004 053.10 ⁻⁰¹	-6,003 984.10 ⁻⁰¹
C	-2,587 287.10 ⁺⁰⁰	-2,587 253.10 ⁺⁰⁰	-2,541 125.10 ⁺⁰⁰

The solution of non-linear equations can be a time consuming and expensive process. Preference is consequently given to iteration methods that use the least number of iterations. This philosophy, unfortunately, does not apply necessarily to the solution of a time-dependent, non-linear partial differential. Consider for example the two time steps $\Delta t = 30$ (s) and $\Delta t = 240$ (s). As can be seen from Table 7-1, there is not a very big difference between the matric heads, computed with these time steps, if node C is disregarded for the moment. Since the time step $\Delta t = 30$ (s) requires only 6 iterations for an iteration error of 10^{-6} , against the 22 of $\Delta t = 240$ (see Figure 7-6), $\Delta t = 30$ (s) would seem to be the time step to choose. However, it would take 8 steps, and thus approximately 48 iterations, just to reach a time of 240 (s) with $\Delta t = 30$ (s)! On the other hand, if one would really like to achieve an error 10^{-3} , for all matric heads, the matric heads for the point C in Table 7-2 indicate that one should not use a time step > 30 (s). There is thus no *a priori* best time step to use in the simulation of variably saturated flow. The best that can be done, is to experiment with the time step, before choosing one for a specific purpose.

The previous investigation of the time step was only concerned with the time step that would ensure convergence of the non-linear iteration method. It should thus not be confused

with the convergence of the solution in time. This convergence, and the convergence in space, are discussed in the next section.

7.3.2 Convergence in Time and Space

As pointed out in Section 6.1, Program SUF3 uses the same numerical algorithms as Program SAT3. One, therefore, would not expect the convergence properties of Program SUF3 in space and time to differ significantly from that of Program SAT3. However, since the present problem is non-linear, there is a possibility that the convergence may not be linear across the domain of the problem.

The convergence of Program SUF3, as a function of the time step, was investigated by solving the drainage problem with the grid in Figure 7-7, for time steps of 1, 2, 4, 8, 16 and 32 s. The reason for using this grid was that experiments had shown that it yielded a more accurate solution near the rainfall boundary, than the one in Figure 7-4.

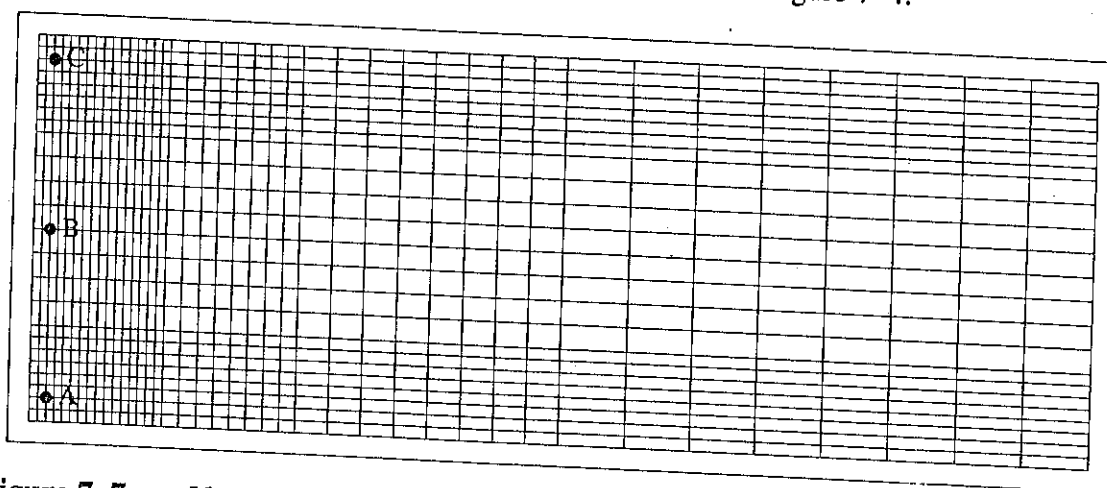


Figure 7-7 Vertical cross-section of the three-dimensional grid used to investigate the convergence of Program SUF3 as a function of the time step.

The convergence results for the last four time steps, at the three nodes, A, B and C in Figure 7-7, are shown in Figure 7-8 and Table 7-2, using the matric heads for $\Delta t = 1$ s as reference values. These results indicate that the convergence is still linear, but that there is a considerable variation in the values of the errors. This is especially true of the largest errors, associated with the matric head at point C near the rainfall boundary.

The spatial convergence of Program SUF3 was investigated with three grids—the grid in Figure 7-7 and two derivatives. The first derivative, see Figure 7-9, was obtained by doubling, and the second by halving the element sizes in the vertical plane of the grid given in Figure 7-7. The number of elements in the y-direction, was kept at three, however. The grid in Figure 7-9 (b), with its 19 012 nodes and 13 824 elements, is the largest grid that the available computing facilities could handle.

The convergence of Program SUF3 was investigated by solving the drainage problem

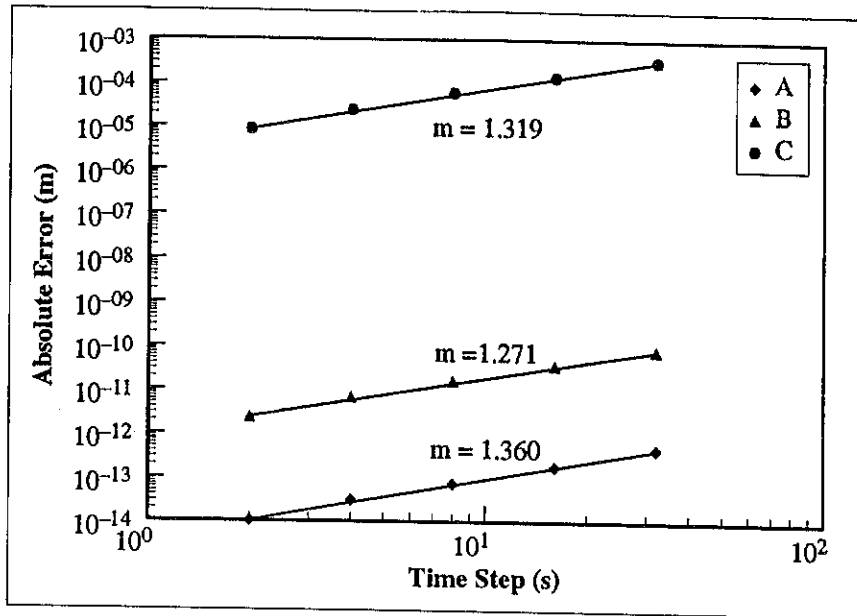


Figure 7-8 Convergence of Program SUF3 for the drainage problem as a function of the time step.

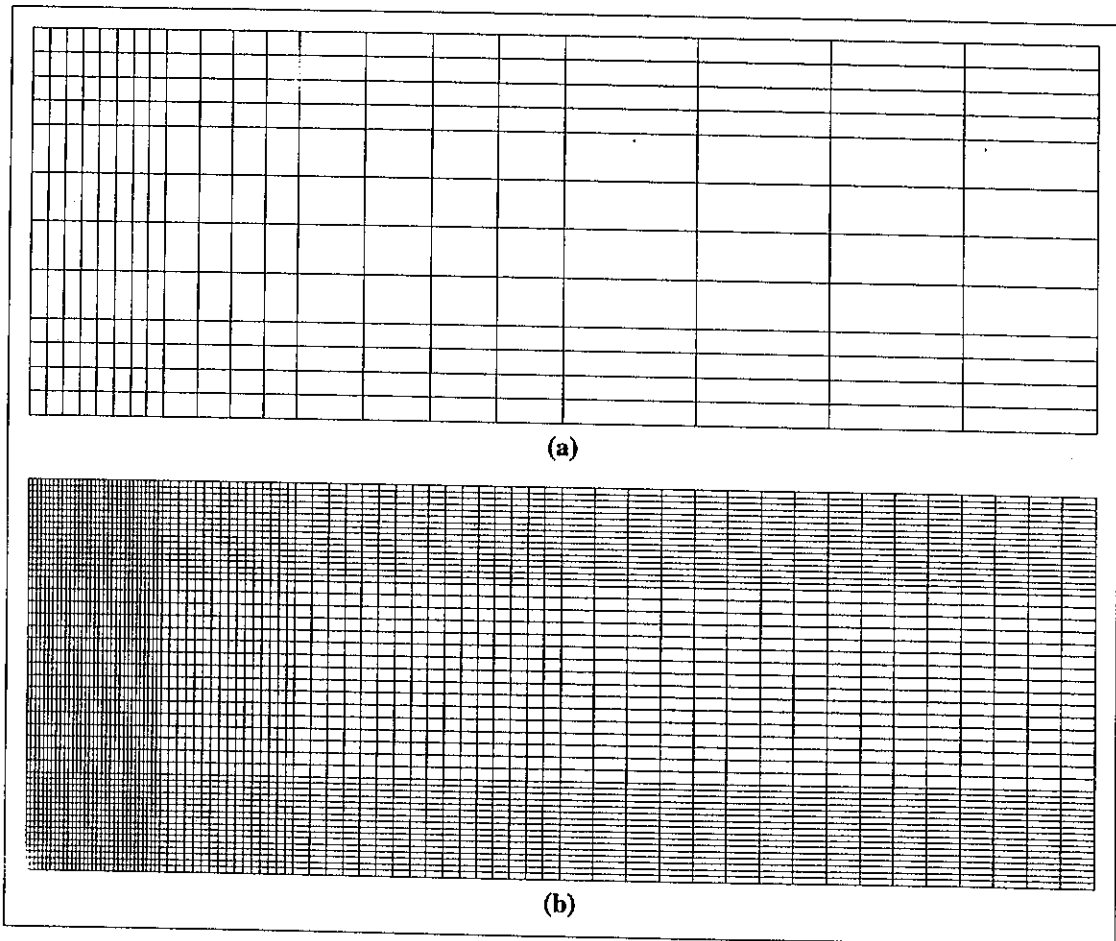


Figure 7-9 Vertical cross-sections of the three-dimensional grids used to investigate the convergence of Program SUF3 as a function of the element size.

with all three grids and a time step of 600 (s). The same problem was also solved with the grid

in Figure 7-9 (b) over a period of 600 (s) with a time step of 60 (s) for reference purposes. The absolute error between this solution and those of the other grids at the three nodes A, B and C in Figure 7-7, are compared graphically in Figure 7-10. The solution, therefore, does indeed converge with a refinement of the grid, but non-linearly. This is illustrated by the considerable differences in the powers (m) of the power function, that fitted the data the best in a linear least squares sense, which are also given in Figure 7-10.

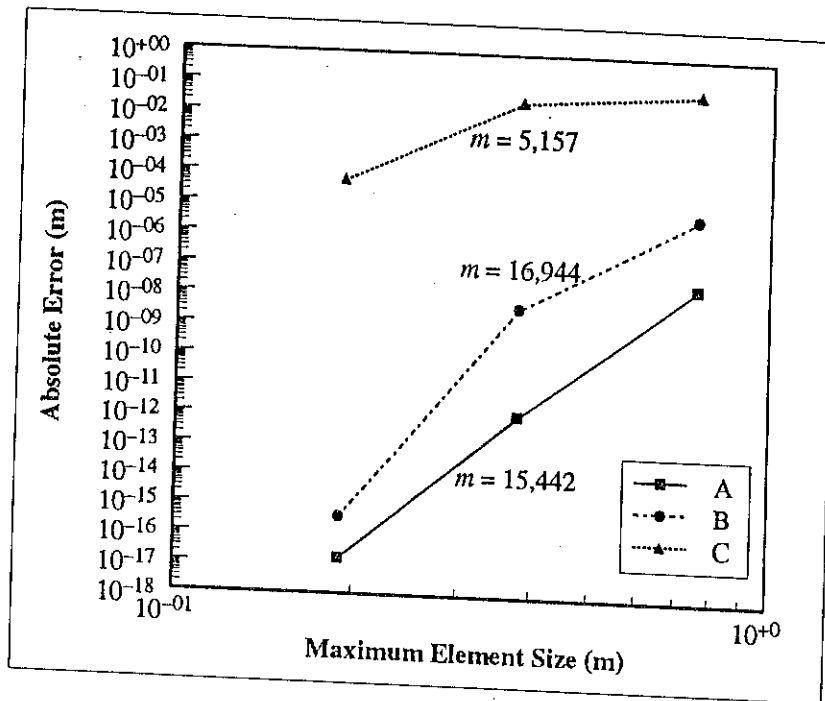


Figure 7-10 Graphical representation of the spatial convergence of Program SUF3.

7.4 CONCLUSIONS

The first conclusion to be drawn from the present investigation of the convergence of Program SUF3 is that care should be exercised in choosing an iteration error, time step and grid for the simulation of a variably saturated flow problem. The accurate representation of rainfall boundaries is particularly troublesome. For, as shown by both Figures 7-8 and 7-10, they are best represented with a differentially refined grid and a very small time step. This behaviour is consistent with observations by Botha (1986) and Hutson (1983) that one has to use an extremely small time step and grid size, in a variably saturated flow model, to properly account for pressure gradients near a rainfall boundary.

CHAPTER 8

THE MASS TRANSPORT PROGRAM

8.1 INTRODUCTION

The computer program to simulate the movement of contaminated groundwater in three dimensions was developed from the conceptual model, described in Chapter 2, and the algorithms in Chapter 4. The main reason for this was that use could be made of more modern and accurate numerical algorithms, than those found in existing programs.

The program, called SUM3, can simulate the movement of any conservative tracer, and non-conservative tracers that decay exponentially, or are adsorbed linearly by the porous medium. It was further assumed that the contaminant will only be present in small quantities, with the result that transport could be decoupled from the flow program. However, the program needs information on the groundwater velocities and water contents of the medium, from either of the programs SAT3 or SUF3. One of these programs must therefore be run before SUM3 can be used, or the user must supply suitable values for the velocities and water contents at all nodes.

The size of SUM3 is almost double that of Program SAT3 (or SUF3) for the same grid. The reason for this is that the coefficient matrix in the finite element approximation of the hydrodynamic dispersion equation is asymmetric, see Equation (4.9). The decoupling of transport and flow is thus fortunate, as it means that many simulations can still be done on personal computers and workstations. Nevertheless, more sophisticated computers will be needed for real world applications. In fact, all major simulations conducted with SUM3 during this investigation, were carried out on the vector computer of the University of the Orange Free State.

Program SUM3 can handle all types of sources and sinks, encountered in practice. The program also provides for three types of boundary conditions: time-dependent Dirichlet, Cauchy and rainfall conditions. The prescribed values of these boundary conditions must all be specified nodewise, along the boundary of the domain. Aquifer properties, on the other hand, must be specified for every soil type, present in the domain of interest, but the program also applies them nodewise.

The lack of suitable data precluded the application of Program SUM3 to an actual real world problem. However, various methods were used to debug the program extensively. These methods are described in Section 8.2. Extensive tests were also conducted on the convergence properties of the numerical algorithms, used in the program. These tests are described in Section 8.3.

8.2 DEBUGGING OF THE PROGRAM

8.2.1 The Model Problem

The philosophy used in debugging Program SUM3, was to compare the computed concentrations with analytical concentrations. The latter concentrations were derived from the solution of a semi-infinite, two-dimensional, model aquifer; discussed by Cleary and Ungs (1978). This model considers a clean aquifer, subjected to a finite strip source, along the side parallel to the y -axis, at the time $t = 0$. It is further assumed that the flow in the aquifer is uniform and in the direction of the x -axis, in other words perpendicular to the source, as in Figure 8-1. The analytical solution of Equation (3.7), subject to the boundary and initial conditions

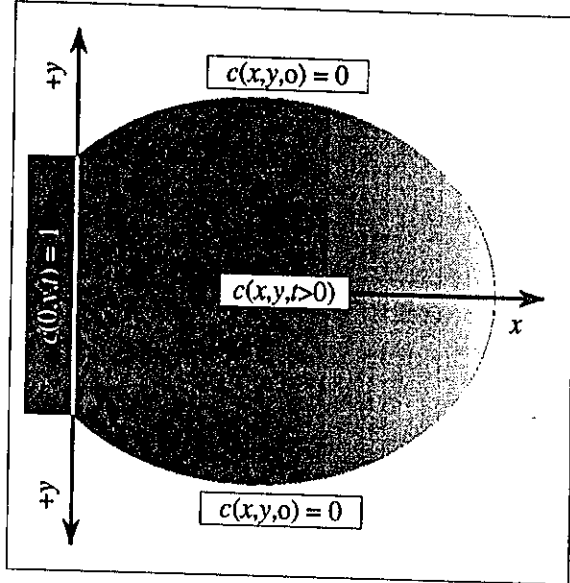


Figure 8-1 Graphical representation of the Cleary-Ungs two-dimensional strip source problem.

$$\begin{aligned}
 c(x, y, 0) &= 0 \\
 c(0, y, t) &= \begin{cases} c_0 \exp(-\gamma t) & (y_l \leq y \leq y_u) \\ 0 & \text{otherwise} \end{cases} \\
 D_x c(x, y, t) &= 0 \quad (x \rightarrow +\infty); \quad D_y c(x, y, t) = 0 \quad (y \rightarrow \pm\infty);
 \end{aligned} \tag{8.1}$$

is of the form

$$c(x, y, t) = c'(x) \exp[w(x, t)] \int_{\tau=0}^t u(x, \tau) [v_u(y, \tau) - v_l(y, \tau)] d\tau \tag{8.2}$$

where γ is a constant, taken as zero in the following discussion,

$$\begin{aligned}
 c'(x) &= \frac{c_0 x}{4\sqrt{\pi D_x}}; \quad w(x, t) = \frac{x q_x}{2 D_x} - \gamma t \\
 v_s &= \text{erf} \left[\frac{y_s - y}{2\sqrt{D_y \tau}} - \frac{q_y}{2} \sqrt{\frac{\tau}{D_y \tau}} \right] \quad (s = u, \text{ or } l) \\
 u(x, \tau) &= \frac{1}{\tau^3} \exp - \left[\left\{ \lambda - \gamma + \frac{q_x^2}{4 D_x} \right\} \tau - \frac{x^2}{4 D_x \tau} \right]
 \end{aligned}$$

and the other parameters are as defined in Chapter 3.

The model problem was adapted to three-dimensions, by extending the strip source over the full depth of the aquifer, and specifying a zero-flux concentration condition on its top and bottom boundaries. This aquifer is presented graphically in Figure 8-2.

The dimensions of the model aquifer had to be restricted to $8 \times 8 \times 2$ m to ensure that the initial debugging could be done on a personal computer. However, this meant that the contamination

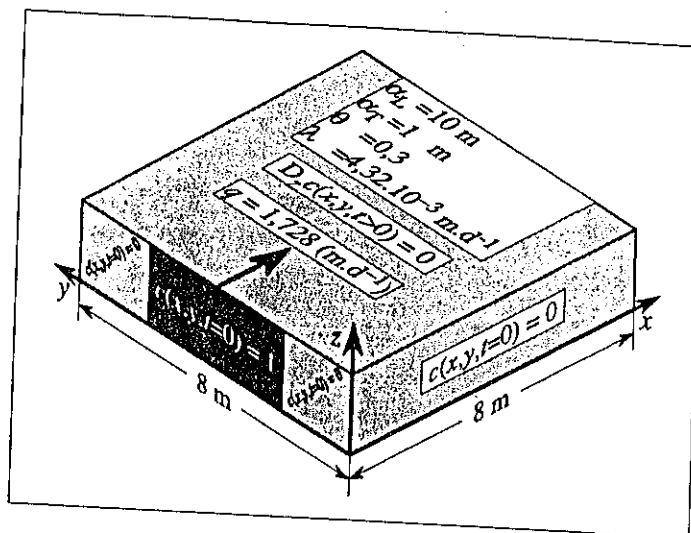


Figure 8-2 Graphical representation of the three-dimensional aquifer, and associated parameters, used in debugging program SUM3.

reached the vertical sides of the aquifer very quickly. Concentration values, computed with the analytical solution, were therefore prescribed as time-dependent Dirichlet boundary conditions on all four vertical sides of the aquifer.

8.2.2 Finite Element Approximation of The Model Problem

A plan of the finite element grid used in the computations is shown in Figure 8-3. The advantage of such a grid is that the element sizes can be easily changed. Four grids were used in this investigation. The first consisted of 8×8 horizontal elements, the second of 16×16 and the third of 32×32 elements. The second and third grids were generated by repeatedly halving the elements of the first grid, as indicated by the small divisions in Figure 8-3. For the fourth grid, two elements were added at each of the points marked with the symbol (\rightarrow) in Figure 8-3. This resulted in a grid with 34×36 horizontal elements.

The assumption that there is no vertical flow, implies that the spacing of the elements in the vertical will have no influence on the solution. The aquifer was therefore divided into two elements vertically, although one element would have been sufficient.

Simulations for the model problem were conducted for one day, with a constant time step of 0,031 25 d. The numerical solution, along the lines $(x, 4, 1)$ and $(4, y, 1)$ are compared graphically with the analytical solution in Figure 8-4.

The fits between the numerical and analytical solutions in Figure 8-4 are, with the exception of the $t = 0,062$ 5 d results, excellent. However, there is a rather straightforward explanation of this behaviour.

The hydrodynamic dispersion equation, Equation (3.7), is (like the variably saturated

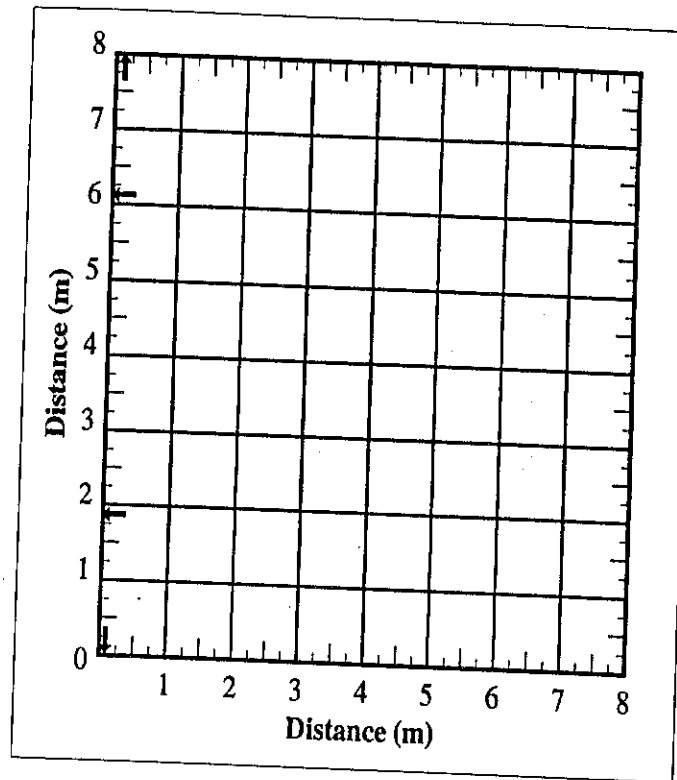


Figure 8-3 Plan view of the finite element grid, used with the aquifer of Figure 8-3, in debugging Program SUM3.

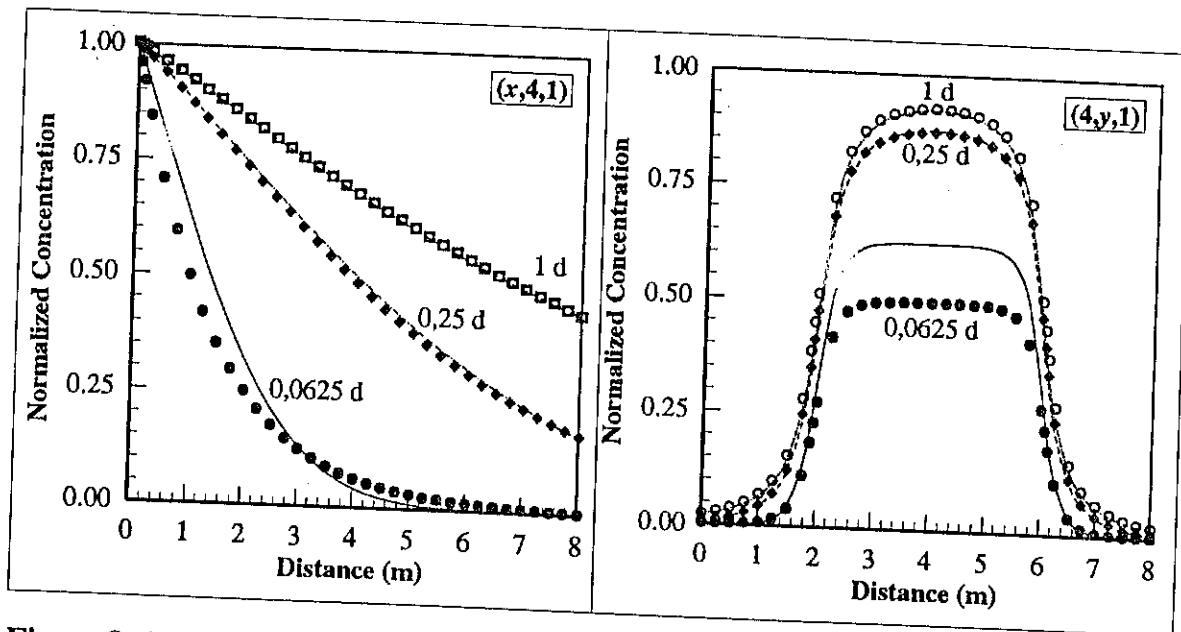


Figure 8-4 Comparison of the numerical and analytical solutions for the aquifer in Figure 8-2, along the lines $(x, 4, 1)$ and $(4, y, 1)$, at the times indicated.

flow equation) essentially a parabolic differential equation, especially for small values of the Darcy velocity (q). The same line of reasoning used in Section 7.2 to explain the behaviour of the phreatic surfaces in Figure 7-5, thus also applies here. This applies in particular to the inability of the numerical approximation to handle the discontinuity between the boundary and initial conditions in Equations (8.1) along the y -axis at the time $t = 0$. The numerical

solution in Figure 8-4 thus behaves exactly in the way one would expect theoretically.

8.3 CONVERGENCE OF THE NUMERICAL MODEL

8.3.1 Convergence in Time

Judging from the results in Figure 8-4 it would seem as if the numerical solution of the model aquifer converges quite rapidly in time. This conjecture was investigated by solving the model problem, over the $34 \times 36 \times 2$ element grid, for 1 d, with time steps varying between 0,031 25 and 1 d. The results are compared with the analytical solution of Cleary and Ungs in Table 8-1 and Figure 8-5.

Table 8-1 Absolute errors in the numerical solution of the model problem, along the lines (1, y, 1) and (4, y, 1), for different time steps. ($t = 1$ d)

Time Step (d)	Absolute Error	
	(1,y,1)	(4,y,1)
0,031 250	$1,167 \cdot 10^{-3}$	$2,538 \cdot 10^{-3}$
0,062 500	$1,005 \cdot 10^{-3}$	$2,010 \cdot 10^{-3}$
0,125 000	$5,506 \cdot 10^{-4}$	$5,454 \cdot 10^{-4}$
0,250 000	$1,008 \cdot 10^{-3}$	$4,325 \cdot 10^{-3}$
0,500 000	$7,174 \cdot 10^{-3}$	$2,105 \cdot 10^{-3}$
1,000 000	$3,272 \cdot 10^{-3}$	$6,734 \cdot 10^{-3}$

The results in Table 8-1 and Figure 8-5 confirm the anticipated convergence of the solution up to a time step of 0,125 d, after which the numerical solution began to diverge. This behaviour is not peculiar to Program SUM3, but has also been observed with other mass transport programs, such as Femwaste (Yeh and Ward, 1980), and even with programs for the groundwater flow equation. Numerical experiments conducted with these programs, have shown that the behaviour is caused by using a too coarse finite element grid, when solving equations that are subject to discontinuous boundary and initial conditions. In all

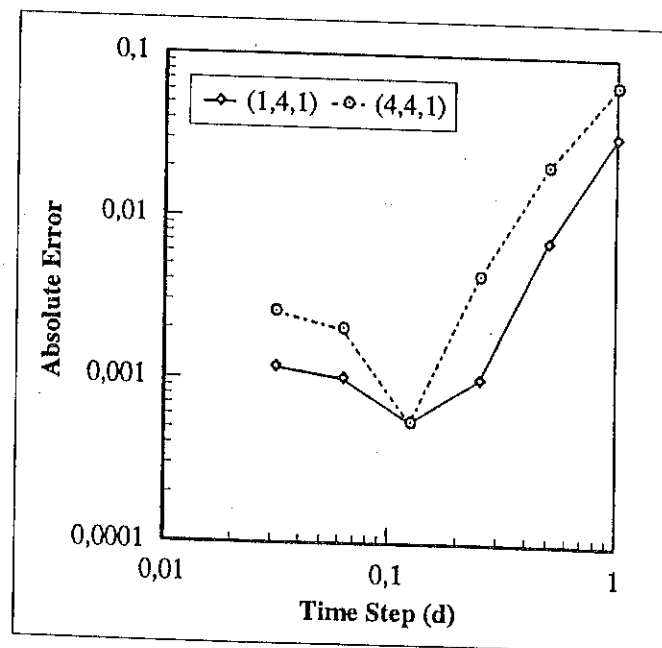


Figure 8-5 Convergence of the numerical solution obtained for the model equation with Program SUM3, as a function of the time step at the two points (1,4,1) and (4,4,1).

cases, encountered thus far, the divergence disappeared, when the finite element grid was

refined in the immediate neighbourhood of the discontinuity.

8.3.2 Convergence in Space

The computationally correct approach, towards the investigation of the spatial convergence of Program SUM3, would be to compare the numerical solution with the analytical solution of the model aquifer. However, the large differences between the analytical and numerical solutions of the model aquifer, at early times, made this impossible. The convergence tests, described below, were consequently all based on the solution of the (34x36x2) grid, with a time step of 0,125 d. The results of the tests, given in Table 8-2 and Figure 8-6, show that the convergence rate again satisfies the quadratic behaviour associated with linear elements.

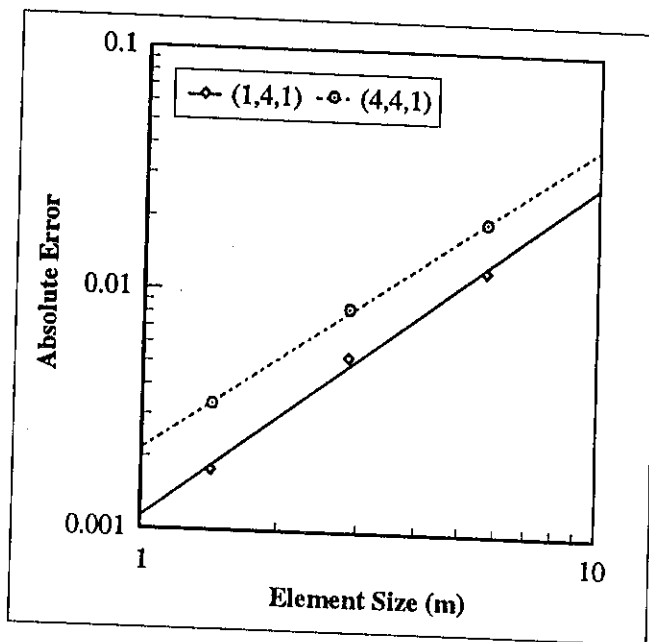


Figure 8-6 Convergence of Program SUM3 for the model aquifer as a function of the element size, at the time $t = 0,25$ d.

Table 8-2 Absolute errors in the concentrations, computed with SUM3, for three grids in Figure 8-3, with a constant time step of 0,25 (d), at the nodes (1,4,1) and (4,4,1).

Element Size	Absolute error	
	(1,4,1)	(4,4,1)
1	$1,755 \cdot 10^{-3}$	$3,308 \cdot 10^{-3}$
2	$5,274 \cdot 10^{-3}$	$8,350 \cdot 10^{-3}$
4	$1,227 \cdot 10^{-2}$	$1,945 \cdot 10^{-2}$

8.4 DISCUSSION

The convergence rates obtained for the model problem and the excellent agreement between the numerical and analytical solutions, at not too early times, indicate that Program SUM3 can be used with confidence in the simulation of groundwater contamination problems. This will especially be the case if suitable care is taken of discontinuities between the boundary and initial conditions.

CHAPTER 9

APPLICATION OF THE THREE-DIMENSIONAL SATURATED FLOW PROGRAM

9.1 GENERAL

The main purpose of the discussion in this chapter is to try to establish suitable criteria that can serve as guidelines in establishing when to use a two-dimensional and when a three-dimensional conceptual model in groundwater investigations. In the original proposal to the Water Research Commission it was anticipated that field data from the Atlantis and Zululand aquifers could be used for this purpose. Unfortunately, the necessary data were not available at the end of this contract period. The discussion to follow had, therefore, to be restricted (albeit reluctantly) to hypothetical aquifers. However, such an approach has its own advantage, as it allows one to study the effects of different aquifer properties separately.

The discussion in Chapter 2 shows that the conceptual models for saturated and variably saturated flow, differ only in that the first model is linear, while the second is non-linear. Any variation in the physical nature of the aquifer, therefore, must have similar effects on both models. Although the hydrodynamic dispersion equation, Equation (4.11), contains three independent relational parameters, α_L , α_T and \mathcal{D} , these parameters always appear in conjunction with the flow velocity (see the discussion in Chapter 3). One would, therefore, expect that the flow velocity will play an important role in a mass transport model. Previous experience with two-dimensional mass transport models (Botha, 1990, 1986) has shown that this is indeed the case. Therefore, it is not unreasonable to assume that if a three-dimensional model has to be used for the flow, one must also use a three-dimensional mass transport model. The discussion to follow will, therefore, be restricted to a study of the saturated flow equation.

There are two main differences between two- and three-dimensional conceptual models for groundwater phenomena: the vertical dimension allowed for in the latter model, and a different interpretation of the relational parameters (Botha *et al.*, 1990). Any differences in the results of the two models should thus be especially noticeable, when the physical properties of an aquifer vary in the vertical direction. Since an aquifer (or pumping) test is the major tool to investigate such variations today, attention will also be given to these tests in the discussion to follow.

The simplest hypothetical aquifer is a single layer aquifer of uniform thickness. This aquifer was used in Section 9.2 to investigate the influence of the hydraulic parameters (conductivity and storativity) on the water-levels. Three aquifers were considered for this purpose: a homogeneous aquifer, an aquifer whose parameters vary quadratically with depth

and one whose parameters follow a Gaussian distribution. This is followed by a discussion of two- and three-layered aquifers in Section 9.3. The results are summarized in Section 9.4.

9.2 THE SINGLE-LAYER AQUIFER

9.2.1 The Homogeneous Uniform Aquifer

The theory of the reduction of dimensions (Botha *et al.*, 1990) indicates that there should be no difference between the results of two- and three-dimensional models, when applied to a homogeneous uniform aquifer. This hypothesis was tested by fitting the water-levels computed for the three-dimensional homogeneous uniform aquifer in Section 6.2 to the Theis (1935) and Muskat (Equation 6.1) type curves, for two sets of hydraulic parameters and pumping rates, given in Table 9-1. The first set of parameters (the same as those used in Section 6.2) was chosen to ensure that the drawdown cone does not reach the boundary of the aquifer, and the second that it does. The solutions for a three day period, observed at a distance of 11 m from the

pumping hole, are shown in Figure 9-1 as a function of time. The fitted parameters are compared with the prescribed model parameters in Table 9-1.

The results in Table 9-1 show that there is no significant difference between the prescribed

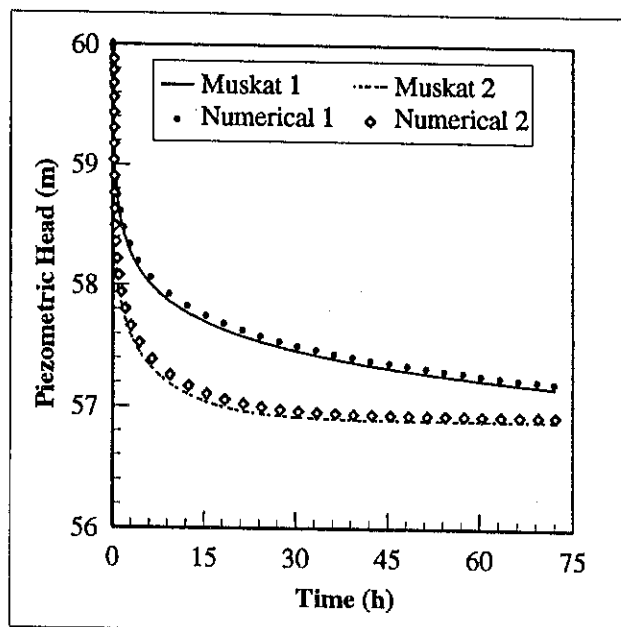


Figure 9-1 Comparison of the Muskat solution in Equation (6.1) and the piezometric levels computed with SAT3 for the hydraulic parameters in Table 9-1.

Table 9-1 Hydraulic conductivity (K) and specific storativity (S_0) values, determined from fits of the Muskat and Theis type curves to the piezometric levels of Figure 9-1.

Type Curve	K (m.d ⁻¹)	S_0 (m ⁻¹)	Pumping rate (m ³ .s ⁻¹)
Three-dimensional Model	1,000	1,437.10 ⁻⁵	2,0.10 ⁻³
Muskat	0,998	1,598.10 ⁻⁵	
Theis	1,000	1,598.10 ⁻⁵	
Prescribed value	4,000	8,000.10 ⁻⁵	8,0.10 ⁻³
Muskat	4,038	8,799.10 ⁻⁶	
Theis	4,470	6,413.10 ⁻⁶	

hydraulic parameters, and those derived from fitting type curves to the solution of the three-dimensional model, if the drawdown does not reach the boundary. However, the Theis parameters are less accurate in the case where the drawdown do reach the boundary, as one would expect, since the Theis curve was derived for an infinite aquifer. This shows that one can use a two-dimensional model with confidence in the analysis of a homogeneous uniform aquifer, *provided that the model satisfies the basic geometrical properties of the aquifer.*

9.2.2 An Aquifer with Quadratically Distributed Parameters

In this aquifer it was assumed that the hydraulic parameters and pumping rate vary with depth according to the function

$$f(z) = a(z+1)^2 \quad (9.1)$$

where $a = 5.10^{-3}$, 5.10^{-8} and $1,25.10^{-5}$ for K , S_0 and Q respectively, and z is measured from the bottom of the aquifer.

A common assumption in the analysis of aquifer tests with a two-dimensional type curve is that the fitted parameters represent an average, across the thickness of the aquifer, of their three-dimensional equivalents. This hypothesis was tested by comparing the drawdowns, simulated over a period of three days, with the parameter values in Equation (9.1) and their average values, defined by the equation

$$\bar{f}(z) = (1/40) \int_0^{40} a(z+1)^2 dz$$

Judging from the comparison of prescribed and average values in Table 9-2, one would intuitively expect the drawdowns at the top and bottom of the aquifer to differ considerably from those computed for the average parameters. However, the results in Figure 9-2 show that this is not the case. The piezometric heads computed with the variable and average parameters, were exactly the same at all elevations.

Table 9-2 Comparison of the quadratically distributed hydraulic conductivity, specific storativity and pumping rates at a few depths in a hypothetical aquifer with their average values.

Depth (m)	$K(z) (m.d^{-1})$	$S_0(z) (m^{-1})$	$Q(z) (m^3.s^{-1})$
$z = 0$	0,005	$5,000.10^{-8}$	$1,250.10^{-5}$
$z = 20$	2,205	$2,205.10^{-5}$	$5,513.10^{-3}$
$z = 40$	8,405	$8,405.10^{-5}$	$2,101.10^{-2}$
Average value	2,872	$2,872.10^{-5}$	$7,179.10^{-3}$

There are two reasons that can be advanced for this behaviour. The first is the way in which the parameters have been prescribed—low values at the top and large values at the bottom. Less water was therefore pumped from the top than the bottom of the aquifer. The second reason is that

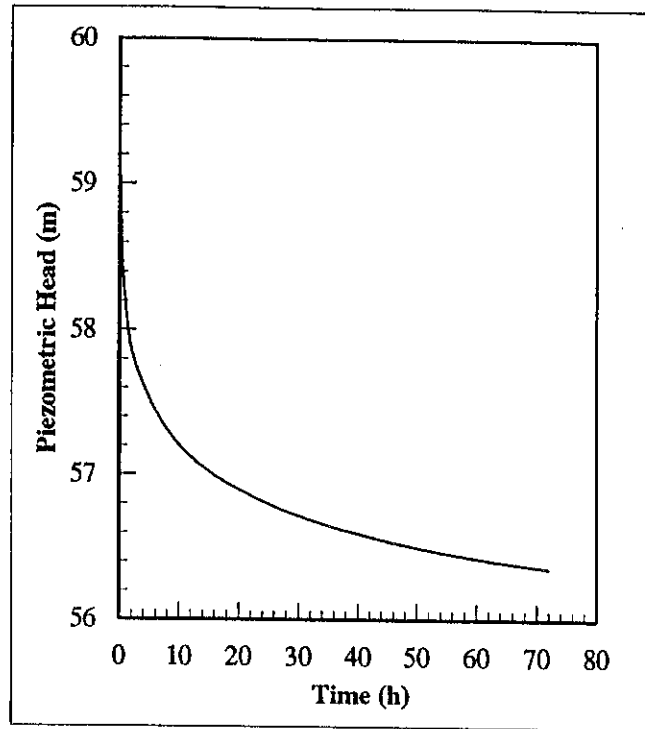


Figure 9-2 Computed piezometric heads in the model aquifer for the average hydraulic parameters at all elevations, as a function of the time.

the borehole penetrated the aquifer fully. There was this no area along the borehole where pressure could build up. A second numerical experiment was therefore performed, to try to establish what are the contribution of each of the two causes on the observed piezometric levels.

9.2.3 An Aquifer with Gaussian Distribute Parameters

In this experiment the specific storativity of the aquifer was distributed in the form of a Gauss curve

$$S_0(z) = a_0 \exp[-(z - b)^2 / c_0^2] \quad (a_0 = 1,0 \cdot 10^{-4}, b = 15, c_0 = 11,555 \text{ m}) \quad (9.2)$$

while the hydraulic conductivity was distributed antisymmetrical Gaussian

$$K(z) = k_h - a_h \exp[-(z - b)^2 / c_h^2] \quad (k_h = 4,1; a_h = 4; b = 15; c_h = 10,413 \text{ m}) \quad (9.3)$$

as shown in Figure 9-3. The pumping rate was taken as $Q = 2,5 \cdot 10^{-3} K$. Values of these parameters, at a few representative elevations above the reference datum, and their height-averaged values are given in Table 9-3. Incidentally, it is interesting that the average values of S_0 and K occur at $z = 24,70$ and $24,28$ m, respectively, and not at $z = 20$ m as is conventionally assumed in the analysis of aquifer tests with two-dimensional models (Kruseman and De Ridder, 1991).

The piezometric heads computed for three elevations in an observation borehole, at a distance of 11 m from the pumped borehole, are compared with those for the average

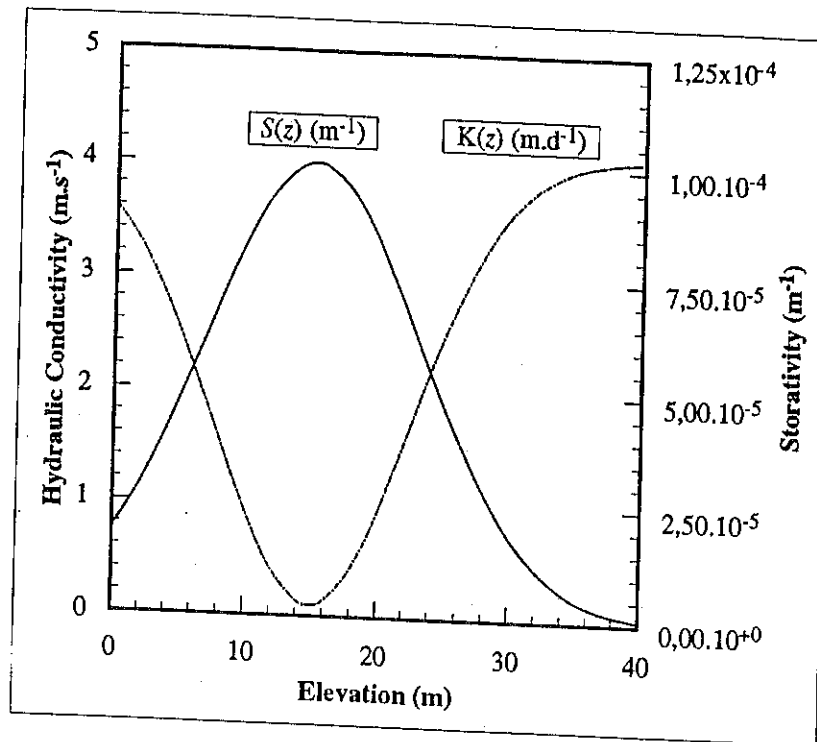


Figure 9-3 Graphs of the of S_0 and K as functions of elevation above the bottom of the aquifer.

Table 9-3 Values of S_0 , K and Q at a few elevations above the bottom of the aquifer and their average values computed from Equations (7.1) and (7.2).

Height (m)	$K(z)$ (m.d ⁻¹)	$S_0(z)$ (m ⁻¹)	$Q(z)$ (m ³ .s ⁻¹)
0	3,598	$1,854.10^{-5}$	$8,994.10^{-3}$
15	0,100	$1,000.10^{-4}$	$2,500.10^{-4}$
20	0,924	$8,292.10^{-5}$	$2,309.10^{-3}$
35	4,000	$5,000.10^{-6}$	$1,000.10^{-2}$
40	4,087	$9,271.10^{-7}$	$1,022.10^{-2}$
Average value	2,293	$4,945.10^{-5}$	$5,733.10^{-3}$

parameters in Figure 9-4.

It is clear from Figure 9-4 that the heterogeneous parameters have indeed an influence on the values of the piezometric heads, but that this influence is restricted to early times. This behaviour is more noticeable in graphs of the piezometric head versus elevation, as in Figure 9-5. The deviations sometimes observed, when fitting water-levels to theoretical type curves at early times, may thus be ascribed to non-homogeneous aquifer parameters.

The influence that the depth of a borehole may have on the behaviour of the piezometric heads, was investigated by restricting borehole in Figure 6-3 to a depth of 24 m. Graphs of the piezometric heads for various elevations in the aquifer, at a distance of 11 m from the pumped borehole and 72 hours of pumping, are shown in Figure 9-6. These results obviously differ considerably from that of the fully penetrating borehole in Figure 9-4. The most striking difference between the two graphs is that the piezometric heads for the partial penetrating borehole never converge towards the average value. However, the results in

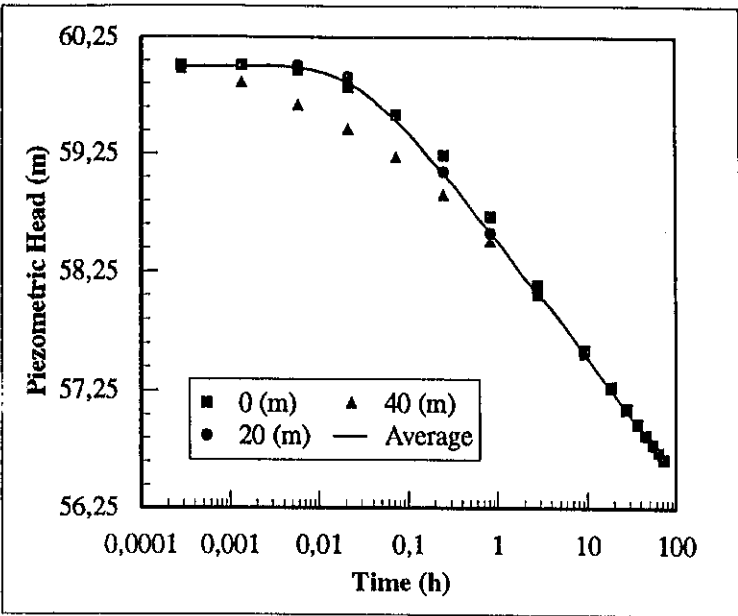


Figure 9-4 Graphs of the piezometric heads at three elevations in an observation borehole, 11 m from the pumped borehole, computed with the Gaussian distributed hydraulic parameters. The piezometric heads for the average parameters are also shown for comparison.

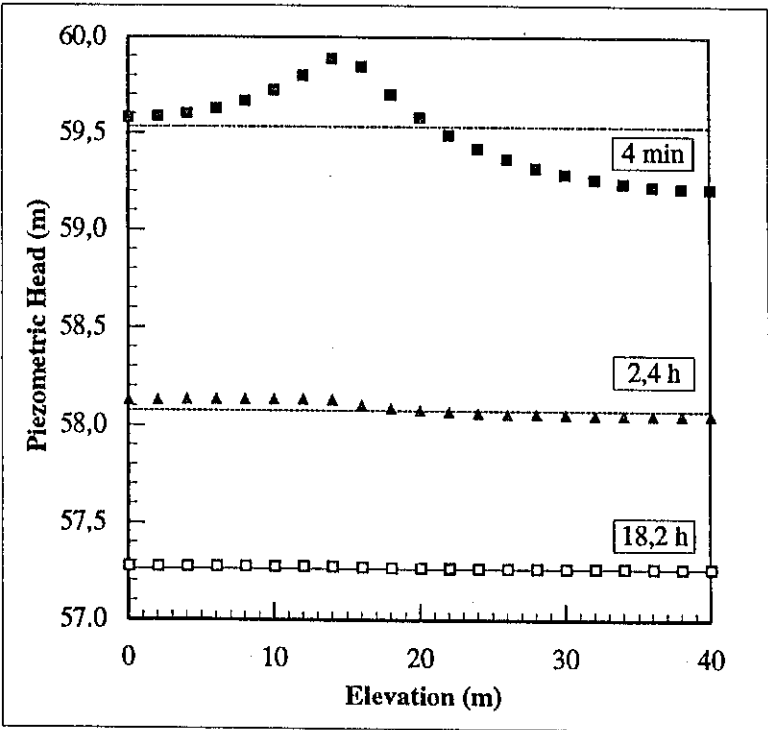


Figure 9-5 Profiles of the piezometric levels in an aquifer with Gaussian distributed hydraulic parameters, and of an aquifer with parameters equal to the average (constant) values of the Gaussian parameters.

Table 9-4 show that the two sets of average values also differ considerably. Care must therefore be exercised, when analysing data from partially penetrating boreholes in a heterogeneous aquifer, with a two-dimensional conceptual model. This applies in particular

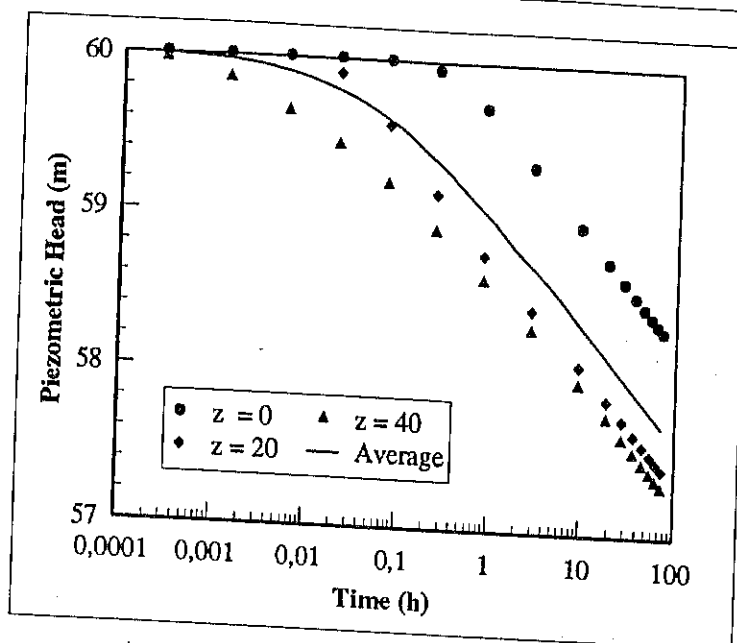


Figure 9-6 Graphs of the piezometric heads for various elevations in the aquifer, with a partially penetrating borehole, at a distance of 11 m from the pumped borehole and 72 hours of pumping.

Table 9-4 Average piezometric heads, observed in a heterogeneous aquifer, with (a) a fully and (b) a partially penetrating pumped borehole.

Time (h)	Average Piezometric Heads (m)	
	(a)	(b)
0,000 277 778	59,999 972	59,995 785
0,001 319 444	59,999 962	59,972 557
0,005 772 569	59,988 021	59,906 919
0,020 801 866	59,859 784	59,797 097
0,071 525 743	59,533 629	59,623 376
0,242 718 828	59,084 530	59,366 533
0,820 495 490	58,588 002	59,051 944
2,770 491 722	58,076 217	58,710 066
9,234 300 818	57,564 616	58,352 459
18,234 300 820	57,262 818	58,138 559
27,234 300 820	57,084 482	58,011 758
36,234 300 820	56,958 431	57,922 032
45,234 300 820	56,861 070	57,852 691
54,234 300 820	56,781 828	57,796 240
63,234 300 820	56,715 110	57,748 705
72,000 000 000	56,657 627	57,707 749

to the analysis of aquifer test data, with conventional type curve methods.

9.3 MULTI-LAYER AQUIFERS

9.3.1 General

The majority of South African aquifers, especially those in the Karoo sediments, are conventionally assumed to be multi-layered. The discussion in this section will therefore be

directed towards the study of multi-layer aquifers.

Two models of multi-layer aquifers, shown schematically in Figure 9–7, were used for this investigation. The aquifer in Figure 9–7(a) consisted of two water-bearing formations, with different hydraulic parameters, while the one in Figure 9–7(b) consisted of two water-bearing formations with the same hydraulic parameters, but separated through a semi-confining layer. The prescribed boundary and initial conditions were in both cases taken as

$$\phi(r, \theta, z, 0) = 0; \quad \phi(R, \theta, z, t > 0) = 60$$

$$D_z \phi(r, \theta, 0, t > 0) = 0; \quad D_z \phi(r, \theta, 40, t > 0) = 0$$

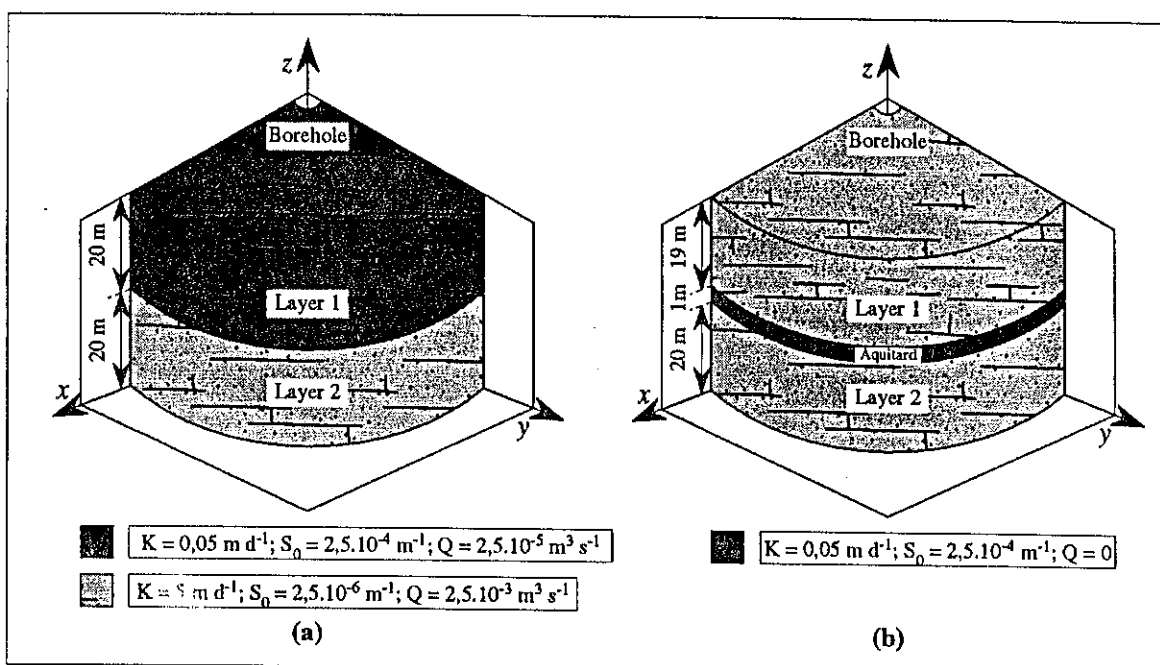


Figure 9–7 Graphical representation of the model aquifers used in the study of multi-layer aquifers.

The finite element grid of Figure 6–5 was again used in the discretization the aquifers, but with a different number of nodes in the vertical direction. The two-layer aquifer was divided vertically into 20 equally spaced elements, and the three-layer aquifer into 20 variably spaced elements, with nodes as given in Table 9–5.

Two-layer aquifers occur frequently in unconsolidated, sedimentary deposits. The Atlantis aquifer in the Cape Province is probably the best known example of such an aquifer in South Africa (Müller and Botha, 1986; Wright, 1991). Unfortunately there is, not much information on three-layer aquifers available in South Africa. However, Boehmer (1991) suggested that the discrepancies between S -values obtained from aquifer tests and recharge studies in the Karoo aquifers, observed by Kirchner *et al.* (1991), can be explained by a three-layer aquifer. His main idea is that recharge is confined to an upper aquifer with a high S_0 , but low K value, and that the aquifer tests were conducted in a lower laying confined aquifer with a high K , but low S_0 value.

Table 9-5 Vertical spacing of the elements in the finite element grid used with the aquifer in Figure 9-7(b).

Node	Elevation	Node	Elevation	Node	Elevation	Node	Elevation
1	0,000	2	2,500	3	5,000	4	7,500
5	10,000	6	12,500	7	15,000	8	17,50
9	20,000	10	20,250	11	20,500	12	20,750
13	21,000	14	23,375	15	25,750	16	28,125
17	30,500	18	32,875	19	35,250	20	37,625
21	40,000						

9.3.2 The Two-layer Aquifer

The values of the aquifer parameters, K and S_0 , used in the investigation of the two-layer aquifer, were chosen such that the initial piezometric head of 60 m was not lowered by more than 5 m, during the simulation period. The yield was again distributed evenly over the length of the borehole and prescribed as a Neuman boundary condition. The normal flux, q , for aquifer 1 is, for example, given by

$$q = Q/2\pi rl = 2,487.10^{-4} \text{ m.s}^{-1}$$

where $r = 0,08$ m is the radius of the borehole and $l = 20$ m the thickness of the aquifer.

Two numerical experiments were conducted with the two-layer aquifer, with the assumption that the yield in each aquifer was proportional to its hydraulic conductivity, given in Figure 9-7(a). In the first experiment it was assumed that the borehole was not cased. Water could, therefore, enter the borehole along its full length.

The computed piezometric heads in the centre of each aquifer and 11 m from the pumped borehole, are compared graphically in Figure 9-8 with the depth-averaged piezometric head, defined as

$$\bar{\phi}(x, y, t) = (\Delta z_n/80) \sum_{n=1}^{n_e} [\phi(x, y, z_u, t) + \phi(x, y, z_l, t)]_e$$

where $\phi(x, y, z_m, t)$ ($m = u, l$) is the piezometric head at the upper (or lower) vertical node of the e -th element in the z -direction, and n_e is the number of elements in the z -direction. The reason for including the average piezometric heads, in Figure 9-8, is that they correspond theoretically to the water-levels in an open borehole (Botha *et al.*, 1990).

Two results that follow immediately from Figure 9-8 are: (a) it took a considerable time for the piezometric heads in the upper aquifer to respond to variations in the piezometric levels of the lower aquifer, and (b) the piezometric heads in both aquifers ultimately approach the average value. However, this behaviour should not be surprising, if it is kept in mind that the hydraulic conductivity of the lower aquifer was considerably larger than that of the upper aquifer.

The fact that the piezometric heads in both aquifers ultimately approach the average value, suggested that it may not be too wrong to analyse aquifer tests from such aquifers with

conventional two-dimensional type curves. The program AQTESOLVE, developed by Gerarghty and Millar (1990) was consequently used to fit a Theis type curve to the drawdowns, derived from the average piezometric heads. The results are shown in Table 9-6. Although there is good agreement between the fitted and prescribed T -values, the fitted S -value is more than two times less than the prescribed value. This is rather disturbing, since it means that the

fitted S -value will always underestimate the water bearing capacity of the aquifer.

There is obviously no reason to fit a Theis type curve to the drawdowns, except that it is the one commonly used in the analysis of aquifer tests. Indeed, the results in Figure 9-9 show that the Neuman type curve, for a phreatic aquifer (Neuman, 1975), fitted the data much better. (The Neuman curve actually yielded the best fit of all the curves available in AQTESOLVE.) This shows that one should not try to fit a type curve to aquifer test data, *without a sound knowledge of the physical properties of the aquifer.*

Table 9-6 Comparison of the prescribed hydraulic parameters and those derived from fitting a Theis type curve to the average drawdowns in Figure 9-8.

	T ($\text{m}^2.\text{d}^{-1}$)	S
Prescribed	101,00	$5,050.10^{-3}$
Fitted	130,56	$1,828.10^{-3}$

Table 9-7 Aquifer parameters obtained by fitting the average piezometric heads in Figure 9-9 to the Neumann type curve for a phreatic aquifer.

Prescribed Parameters		Neumann Parameters	
K (lower) ($\text{m}.\text{d}^{-1}$)	5,0	K_{xy} ($\text{m}.\text{d}^{-1}$)	3,65
K (upper) ($\text{m}.\text{d}^{-1}$)	$5,0.10^{-2}$	K_z ($\text{m}.\text{d}^{-1}$)	$3,86.10^{-2}$
S_0 (lower) (m^{-1})	$2,5.10^{-6}$	S_0 (m^{-1})	$3,00.10^{-6}$
S_0 (upper) (m^{-1})	$2,5.10^{-4}$	S_y	$3,00.10^{-4}$

As shown in Table 9-7, the numerical values of the Neuman parameters, for the fit in Figure 9-9, compare favourably with the actual prescribed parameters. It is thus tempting to

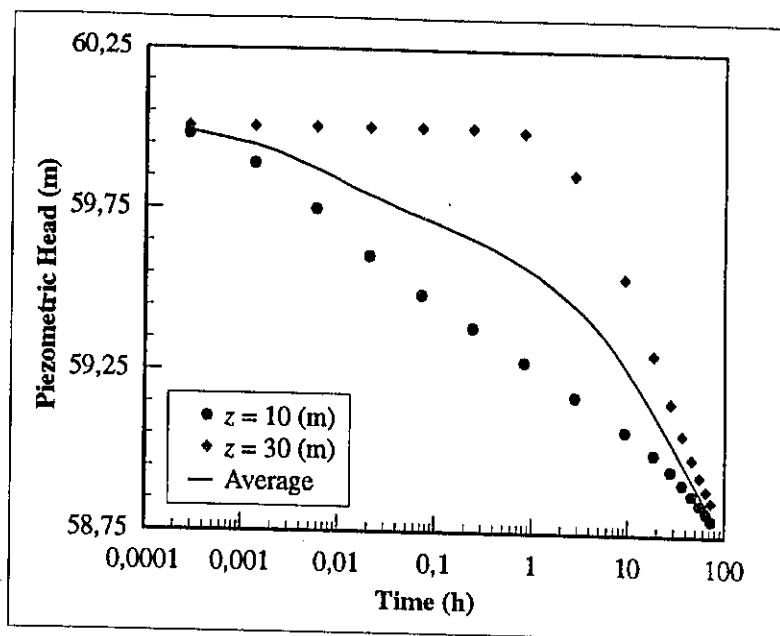


Figure 9-8 Computed piezometric heads at the centre of each layer in the two-layer aquifer and the vertically averaged piezometric head, when the pumped borehole penetrates both aquifers. (Distance from the pumped borehole = 11 m.)

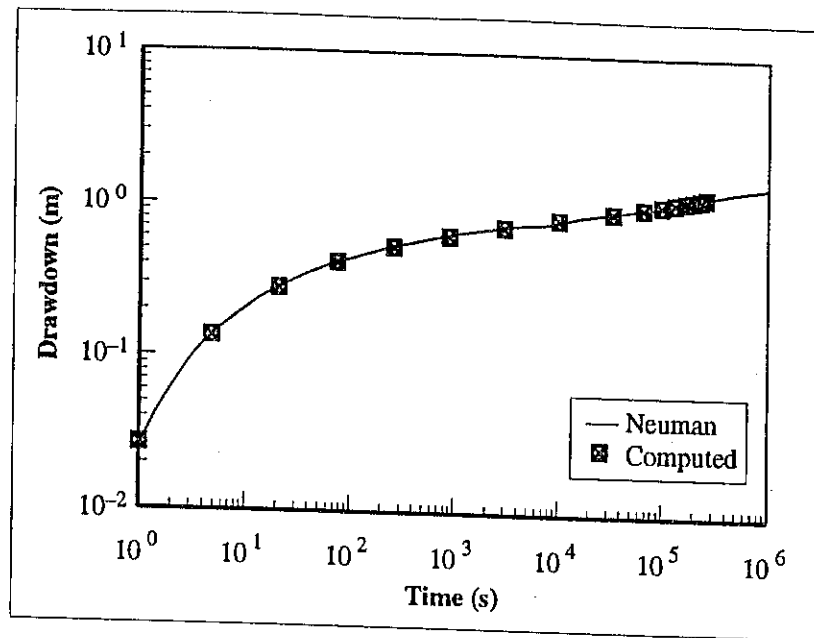


Figure 9-9 Comparison of the average piezometric heads computed for the two-layer confined aquifer and the Neumann type curve for a phreatic aquifer.

equate these two sets of parameters. However, this cannot be done, because the Neuman parameters have a completely different physical interpretation. These parameters, moreover, are only valid for a two-dimensional horizontal model.

In the second experiment, with the two-layer aquifer, if the borehole was assumed to be cased off in the upper aquifer. In other words, water was pumped only from the lower aquifer. As can be seen from Figure 9-10, the piezometric heads are very similar to those in Figure 9-8. However, there is one major difference—the piezometric heads, at the different elevations, do not converge to the average piezometric head. Serious errors could, therefore, be made, if

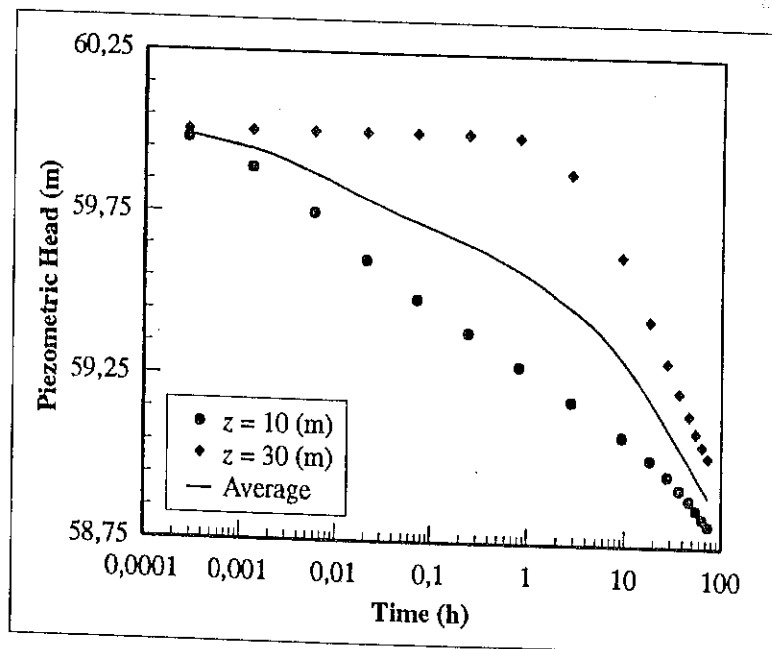


Figure 9-10 Computed piezometric heads at the centre of each layer in the two-layer aquifer and the vertically averaged piezometric head, if the upper aquifer was cased off. (Distance from the pumped borehole = 11 m.)

observed water-levels are equated with the average piezometric heads in such an aquifer.

Figure 9-11 displays the drawdowns, as a function of distance, of the two-layer aquifer, where the upper aquifer was cased off. A rather interesting conclusion, that follows

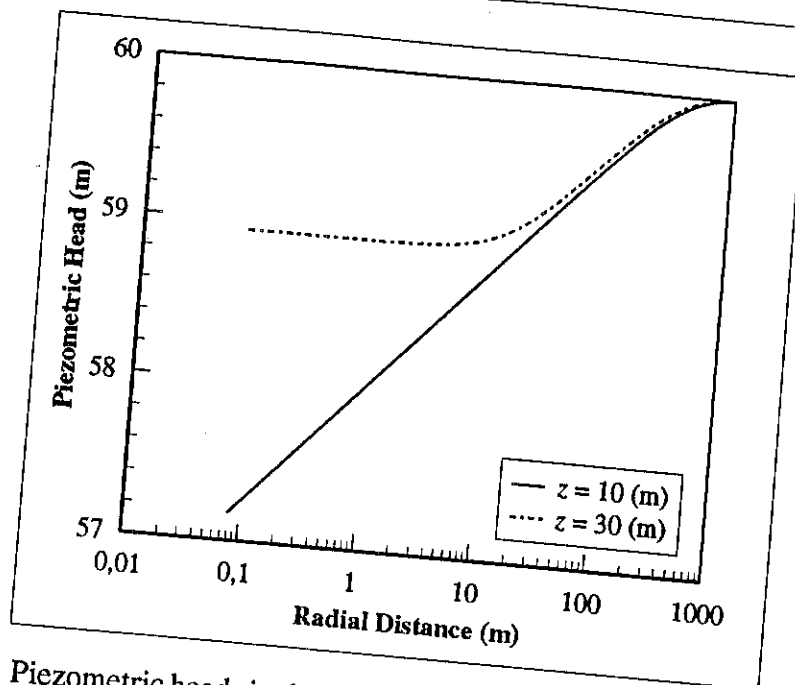


Figure 9-11 Piezometric heads in the hypothetical, two-layer aquifer as a function of the radial distance, after three days of pumping in the lower aquifer.

immediately from this graph, is that a production borehole (in a two-layer aquifer) may run dry before the upper aquifer is depleted, if pumping is restricted to the lower aquifer. This conclusion is confirmed by observations of piezometric heads in the Atlantis aquifer, shown in Figure 9-12 (Botha *et al.*, 1991; Wright, 1991). It would thus be wise to screen a production borehole across both aquifers in a two-layer aquifer, unless the water quality in one of the aquifers is unacceptable.

9.3.3 The Three-Layer Aquifer

The main purpose of this investigation was to see how does a confining layer influence the piezometric levels of an aquifer. The first simulation considered the situation where water is withdrawn along the full depth of the aquifer, and the second only from the bottom aquifer. The piezometric heads obtained from the simulations, at an

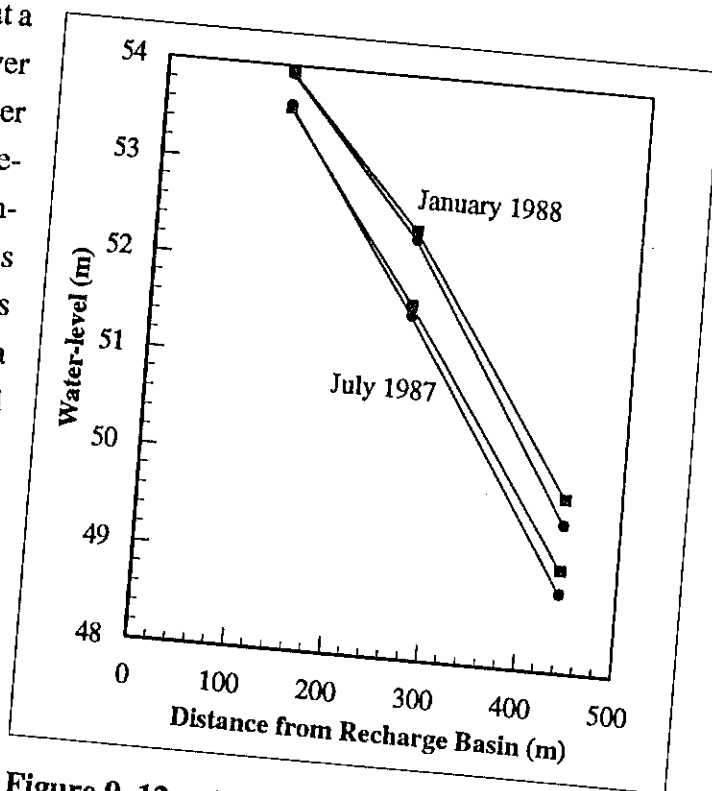


Figure 9-12 Piezometric levels observed in the well points WP02, 03, 09 and WP 01, 04, 10 at Atlantis in July 1987 and January 1988.

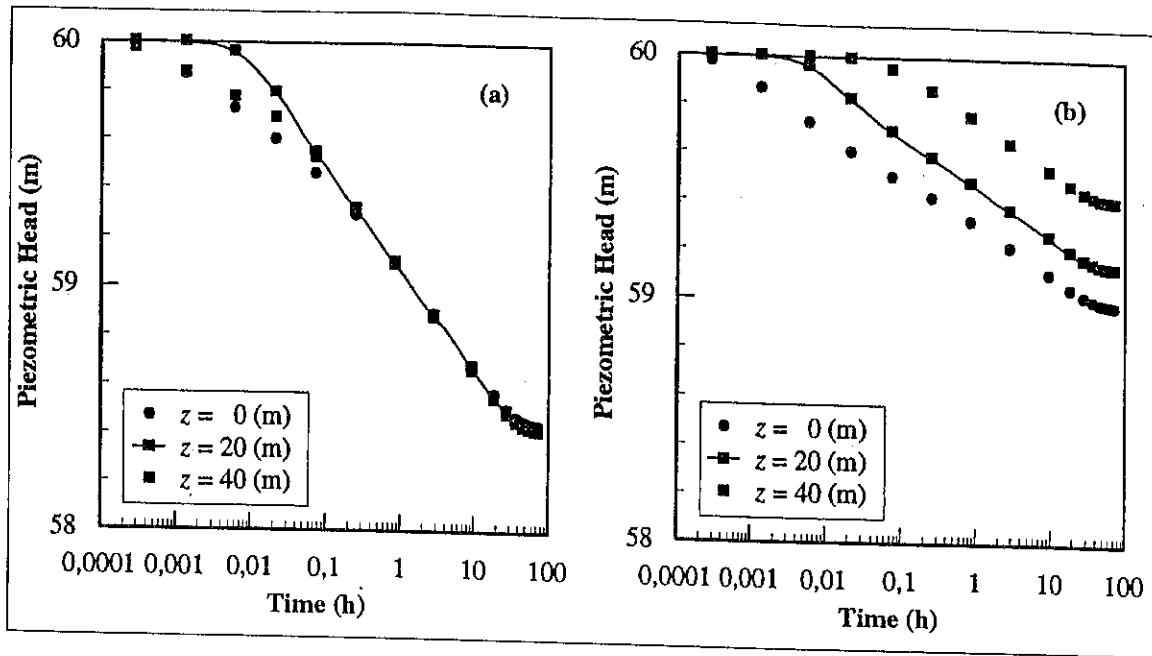


Figure 9-13 Computed piezometric heads in the three-layer aquifer as a function of the time; (a) when water is withdrawn from the full thickness of the aquifer and (b) only from the bottom layer.

observation point 11 m from the pumped borehole, are presented in Figure 9-13. A comparison of Figures 9-13 with Figures 9-8 and 9-10 shows that the piezometric heads of the three-layer aquifer behave similarly to the piezometric heads in a two-layer aquifer, if differences in the hydraulic parameters are neglected.

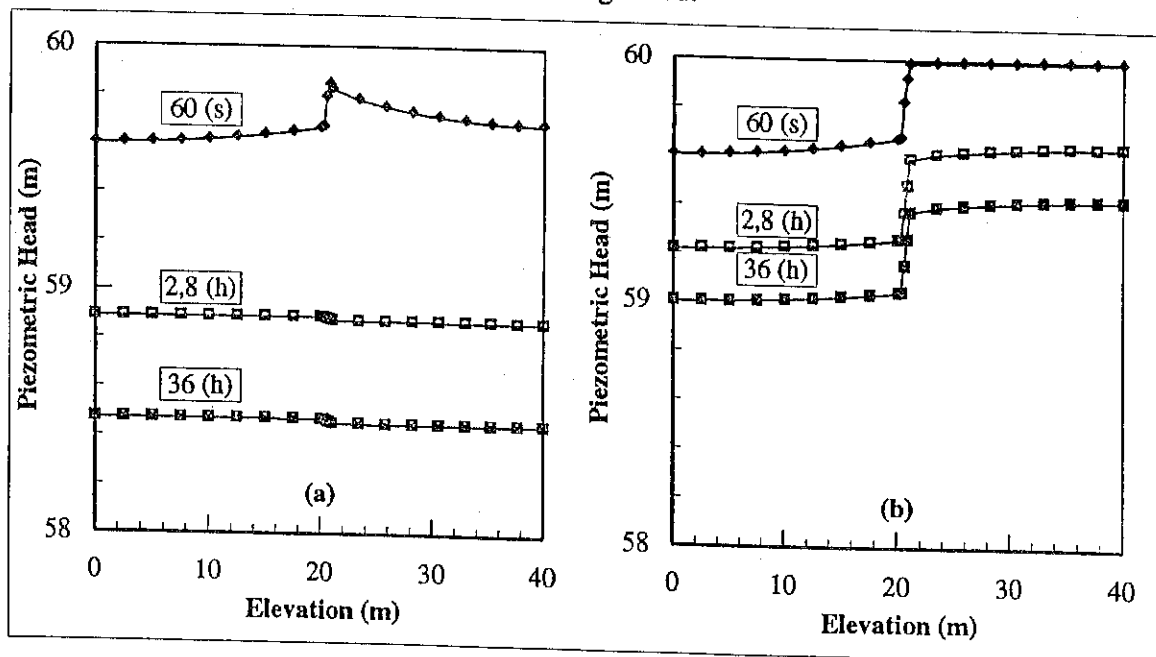


Figure 9-14 Vertical profiles of the piezometric heads in Figure 9-13.


The movement of water in an aquitard is conventionally assumed to be vertical when the ratio of its hydraulic conductivity, K_a , and that of the water bearing layers, K , is $\approx 0,01$ (Bear, 1979). Since the ratio of K_a to K , for the three-layer aquifer in Figure 9-7(b), is

precisely 0,01, it would be interesting to see how far the piezometric heads satisfy this assumption. The piezometric heads in Figure 9-14 show that this assumption would be valid, if water is withdrawn only from the bottom layer, but not when withdrawn across the full thickness of the aquifer. Indeed, Figure 9-14(a) shows that the vertical gradient in the piezometric head disappears almost completely, shortly after pumping began. It is of course possible that the present result is caused by the assumption that the confining layer can store water. However, it is difficult to see why the confining layer would in one case contribute significantly towards the water balance in the borehole and not in the second one, especially if it is kept in mind that water was withdrawn at the same rate from the bottom layer in both Figures 9-14(a) and 9-14(b). The only conclusion is thus that the confining layer has no influence on the piezometric heads, if it separated two aquifers with the same hydraulic parameters.

9.4 SUMMARY AND CONCLUSIONS

The main result of the present investigation of heterogeneous aquifers can be summarized in saying that it could be dangerous to place too much confidence in results derived from an analysis of their water-levels with a two-dimensional conceptual model. The only situation where such an analysis would be useful, is when observations are made with boreholes that penetrate the aquifer fully. These results confirm again, that it would be wise to obtain as much information as possible on the physical and geometrical properties of the aquifer, before analysing the results with a particular model.

It will obviously be extremely difficult to meet the conditions above in practical situations, with the observational techniques available today. Nevertheless, the present results leave one with no other choice. It may thus be worthwhile to try to develop better and cost effective observation methods, which would yield the data required by a three-dimensional model of these aquifers, rather than fiddle around with two-dimensional models. This applies especially to the multi-layered (perhaps multi-porous) aquifers in the Karoo sediments of South Africa.



CHAPTER 10

CONCLUSIONS AND RECOMMENDATIONS

10.1 CONCLUSIONS

The first primitive three-dimensional numerical models for groundwater flow phenomena were developed roundabout 1973, but it is only in the last couple of years that these models have been applied extensively in practical investigations. Strangely enough, though, is there nowhere in the available literature any reference to a comparative study of two- and three-dimensional models. The aim of the present study was to try to fill this gap, particularly to establish suitable criteria that can be used in deciding when to use a two-dimensional model and when a three-dimensional model in groundwater investigations. The reason for this is that a three-dimensional model requires considerably more observational data and computer resources, than a two-dimensional model. It thus stands to reason that one should prefer a two-dimensional model, whenever possible.

Although geohydrologists paid very little attention to three-dimensional models in the past, recent experience (Botha *et al.*, 1990) has shown that there are situations where the behaviour of an aquifer cannot be explained with a two-dimensional model.

The three-dimensional problems normally encountered in practice, cannot be solved analytically. It was thus necessary to solve the groundwater flow and mass transport equations numerically. There is no doubt that a finite difference approximation of these equations is the easiest to implement on a computer. The majority of computer models for three-dimensional groundwater phenomena, now available, are consequently based on this approximation. However, the approximation does not allow one to implement Neumann, Cauchy, or seepage boundary conditions; with ease. Moreover, some of the available computer models, especially those for variably saturated flow, do not conserve mass. The opportunity was therefore taken to develop completely new models.

There is very little physical difference between the conceptual models for saturated and unsaturated groundwater flow. The program for variably saturated flow, being the more complex, was therefore developed before the program for saturated flow. The main reason for this philosophy was that it is easier to adapt the program for variably saturated flow to saturated flow, than the other way round. Another reason was that the variably saturated flow program can handle saturated flow conditions as well. The possibility thus existed that one program could handle all situations of interest in this investigation. However, it soon became clear that a separate saturated flow program would have definite advantages. For example, the saturated flow program executes much faster than the variably saturated flow program.

Three programs were, therefore, developed during this investigation.

- Program SAT3 – for the simulation of saturated groundwater flow.
- Program SUF3 – for the simulation of variably saturated groundwater flow.
- Program SUM3 – for the simulation of saturated and variably saturated mass transport.

The programs were evaluated extensively by comparing their output with the two-dimensional analytical solutions of: (a) Muskat for a circular homogeneous aquifer in the case of SAT3, and (b) the infinite strip source problem of Cleary and Ungs (1978) in the case of SUM3. Program SAT3 was also compared with the 'industry standard' three-dimensional program for saturated flow, MODFLOW of McDonald and Harbaugh (1988). No analytical solution was available for the variably saturated flow problem at the time of the evaluation. Program SUF3 was therefore evaluated with the help of the two-dimensional variably saturated program UNSAT2 (Davis and Neuman, 1983).

In the original proposal to the Water Research Commission, it was anticipated that observational data from the Atlantis, Saldanha and Zululand aquifers could be used as examples for the practical implementation of the computer models. Unfortunately, the available data for these aquifers, at the end of the contract period, were not sufficient. Hypothetical aquifers had therefore to be used instead.

Three types of aquifers were used for this study: a single layer aquifer, a two-layer and a three-layer aquifer. The results of these investigations indicated that a two-dimensional model is really only suitable in the case of a homogeneous aquifer, with uniform thickness. However, there are a few special conditions where a two-dimensional model can be used for a heterogeneous aquifer. These are:

- (a) The aquifer must be approximately uniform and parallel with the soil surface.
- (b) Vertical anisotropy in the aquifer must be negligible.
- (c) The production and observation boreholes must penetrate the aquifer fully.
- (d) Water must be pumped from all layers in a multi-layer aquifer and not from one layer alone. In other words no water bearing formation must be cased off in production and observation boreholes.

It is not too difficult to satisfy the last two conditions, but it is unlikely that natural aquifers, especially those in hard-rock formations will satisfy the first two. Therefore, one most likely will have to analyse these types of aquifers with a three-dimensional model. This conclusion has obviously far reaching consequences for investigations of multi-layered aquifers, such as those in the Karoo sediments of South Africa. One particularly important consequence is that conventional observation methods, such as measuring water levels in partially (even fully) penetrating boreholes, cannot be used in the investigation of these heterogeneous aquifers. What is needed here, are methods that reveal the three-dimensional properties of the aquifer. This implies that one should use piezometers, and multi-level

samplers to measure piezometric heads and concentrations, respectively, in these aquifers.

The study of the two-layer aquifer with the same initial piezometric levels in both layers, but different hydraulic conductivities and storativities, yielded two interesting results. The first is that the piezometric level in the lower layer of a two-layer aquifer tends to decrease more rapidly than in the top layer, near a borehole, if the upper layer is cased off, even though the hydraulic conductivity of the lower layer is higher than that of the upper layer. The second is that the average drawdown in such an aquifer may resemble the type curve of a completely different kind of aquifer. These results have two important implications for the conventional analysis of aquifer tests with type curves.

- (a) It shows that the results of aquifer tests in heterogeneous aquifers may depend on both the depth at which the pump is installed and the distance(s) where observations are taken.
- (b) Drawdowns in heterogeneous aquifers should only be analyzed with conventional type curves, if the assumptions made in the derivation of the type curve, is justified by the physical nature of the aquifer.

9.2 RECOMMENDATIONS

The most important lesson learned from the present investigation is that nature is just too subtle for man to comprehend without suitable observational data. *The choice between two- and three-dimensional groundwater models, therefore, should never be based on mathematical arguments, or some preconceived ideas of the investigator, but observational evidence.* This conclusion leads to two natural approaches in groundwater investigations—the *descriptive approach and the quantitative approach*. The choice of which one of the two approaches to use, will ultimately be determined by the objective of the investigation. If the objective is merely to obtain a broad general qualitative description of an aquifer, the descriptive approach will be sufficient. However, if the objective is to utilize the aquifer efficiently, the quantitative method has to be used.

The descriptive approach has two advantages over the more quantitative approach: (a) it is relatively cheap and easy to implement and (b) it can supply a short term solution. Nevertheless, numerous studies, for example Cherry (1989), have shown that the descriptive approach may not provide a reliable framework for the efficient management of an aquifer.

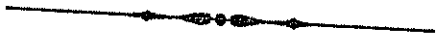
The previous statement should not be interpreted as if the quantitative approach is without any difficulties. Two particularly important aspects that must be taken into account in this approach are: (a) how accurately does the conceptual model represent the aquifer, and (b) what is the quality of the data supplied to the model. There is little doubt, that modern conceptual groundwater models are able to handle very complex phenomena. What is missing, however, is sufficient information on the physical and chemical properties of

aquifers and cost-effective methods to determine these properties. The last remark applies in particular to an aquifer test, which is the only method available now to study the physical properties and behaviour of an aquifer.

There exists a considerable body of data, particularly aquifer test data, in South Africa. These data have, unfortunately, been gathered and analyzed with the descriptive approach in mind. Nevertheless, it would be a considerable waste of time and money if the data are simply to be ignored. A more responsible approach in future, quantitative investigations of South African aquifers would thus seem to be as follows:

- (a) Re-evaluate the existing aquifer test data with conventional type curve methods and the three-dimensional models developed during this study, with the view to obtain a better insight into their physical properties.
- (b) Supplement the investigations in (a) with more refined field observations, such as ordinary and cross-borehole packer tests.
- (c) Pay more attention to the development of novel and versatile methods for the observation of the physical properties of an aquifer.

The implementation of the recommendations above, will certainly require more money and suitably trained personnel than the conventional descriptive approach. However, the history of science and engineering indicates that the rewards, from a determined effort to solve a given problem, usually outweigh the original cost.



APPENDIX A

THE THREE-DIMENSIONAL ISOPARAMETRIC TRANSFORMATION

A.1 DEFINITION

A fundamental concept in the finite element approximation of differential equations is the discretization of the *global domain*, $\Omega(x,y,z)$, into smaller (usually irregular) subdomains, or *elements* Ω_e . However, it is not easy to perform the necessary calculations, if Ω_e is not rectangular. The computations in finite element approximations are consequently preferably performed on rectangular elements in what will be called the *local domain*, $\Gamma(\xi,\eta,\zeta)$. This means that one must be able to transform the elements in global coordinates, $\mathbf{x} = \{x, y, z\}$, to elements in the local coordinates $\xi = \{\xi, \eta, \zeta\}$. Although there are various ways in which such a transformation can be performed, it is customary in finite element work to use an *isoparametric transformation* (Botha and Pinder, 1983; Huyakorn and Pinder, 1983; Pinder and Gray, 1977; Zienkiewicz, 1977). The isoparametric transformations for one- and two-dimensional elements are readily available in the references given above, but not for three-dimensional elements. The present discussion will therefore be restricted to the three-dimensional transformation.

To describe the isoparametric transformation in more detail, consider the hexahedral element, Ω_e (in global coordinates), and the cube, Γ_e (in local coordinates) of Figure A-1. It is well-known that any function, say $f(\xi)$, can always be interpolated by a set of Lagrange interpolation polynomials (Botha and Pinder, 1983). These polynomials have the property that they all vanish at a particular node of an element, except one, which assumes the value 1. It is thus quite easy to derive suitable expressions for them. For example, the polynomials associated with the unit cube $[0,1] \otimes [0,1] \otimes [0,1]$ in Figure A-1(b) can be expressed as

$$\varphi_{ijk}(\xi, \eta, \zeta) = [(1 - \xi_i) - (1 - 2\xi_i)\xi][(1 - \eta_j) - (1 - 2\eta_j)\eta][(1 - \zeta_k) - (1 - 2\zeta_k)\zeta] \quad (\text{A.1})$$

where $\xi_i, \eta_j, \zeta_k = 0$ or 1 , see Figure A-1(b).

The main advantage of Lagrange interpolation polynomials in finite element approximations, is not so much their ability to easily approximate a given function, but rather to define a simple map from the global onto the local space. This can be achieved by merely parametrizing the global coordinates in terms of the local coordinates as

$$x = \sum_{j=1}^N x_j \varphi_j(\xi, \eta, \zeta); \quad y = \sum_{j=1}^N y_j \varphi_j(\xi, \eta, \zeta); \quad z = \sum_{j=1}^N z_j \varphi_j(\xi, \eta, \zeta) \quad (\text{A.2})$$

where, l denotes the (i,j,k) -th of the N nodes in a finite element. ($N = 8$ for the unit cube

considered here.) It is for this reason that the transformation is known as an isoparametric transformation.

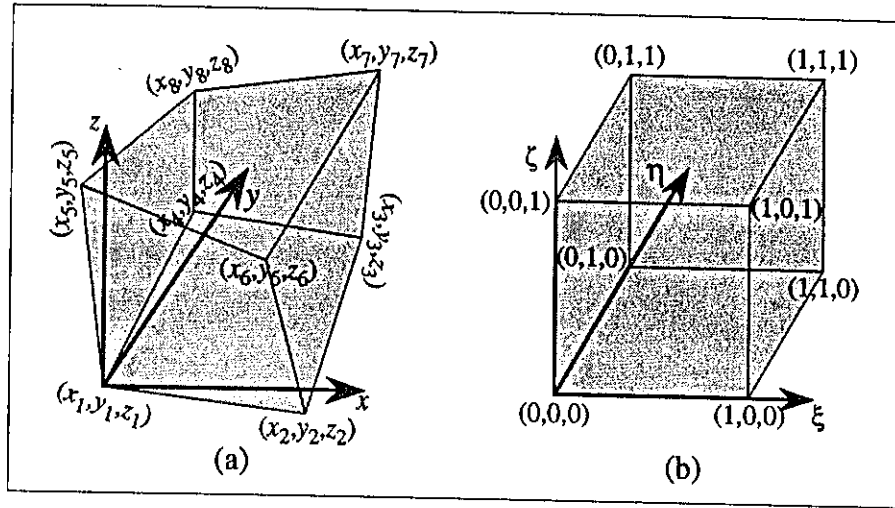


Figure A-1 Schematic representation of a three-dimensional finite element (a) in local and (b) in global coordinates.

A.2 TRANSFORMATION OF DERIVATIVES

The approximation of a differential equation by the finite element method does not only involve the transformation of function values, but also function derivatives (Botha and Pinder, 1983). Of particular importance in this connection are the first partial derivatives of a function. Consider therefore the function, $\varphi(\mathbf{x})$, which can also be expressed through the isoparametric transformation in Equation (A-2) in the form

$$\varphi(\mathbf{x}) = \varphi[x(\xi, \eta, \zeta), y(\xi, \eta, \zeta), z(\xi, \eta, \zeta)]$$

The chain rule of differentiation can now be invoked to express the first partial derivatives of $\varphi(\mathbf{x})$ as

$$\begin{pmatrix} D_{\xi}\varphi \\ D_{\eta}\varphi \\ D_{\zeta}\varphi \end{pmatrix} = \mathbf{J} \begin{pmatrix} D_x\varphi \\ D_y\varphi \\ D_z\varphi \end{pmatrix} \quad (\text{A.3})$$

where

$$\mathbf{J} = \begin{pmatrix} D_{\xi}x & D_{\xi}y & D_{\xi}z \\ D_{\eta}x & D_{\eta}y & D_{\eta}z \\ D_{\zeta}x & D_{\zeta}y & D_{\zeta}z \end{pmatrix} \quad (\text{A.4})$$

is the so-called Jacobi *matrix* of the transformation. This matrix and more particularly its determinant, also known as the *Jacobian* of the transformation,

$$J = \det(\mathbf{J}) = \begin{vmatrix} D_{\xi}x & D_{\xi}y & D_{\xi}z \\ D_{\eta}x & D_{\eta}y & D_{\eta}z \\ D_{\zeta}x & D_{\zeta}y & D_{\zeta}z \end{vmatrix} = \begin{vmatrix} D_{\xi}x D_{\eta}y D_{\zeta}z + D_{\xi}y D_{\eta}z D_{\zeta}x + D_{\xi}z D_{\eta}x D_{\zeta}y \\ -D_{\xi}x D_{\eta}z D_{\zeta}y - D_{\xi}y D_{\eta}x D_{\zeta}z - D_{\xi}z D_{\eta}y D_{\zeta}x \end{vmatrix}$$

is of paramount importance in any mapping. The reason for this is that a map is only possible if its inverse, and thus that of its Jacobi matrix

$$\mathbf{J}^{-1} = \frac{1}{\det(\mathbf{J})} \begin{pmatrix} D_{\eta}y D_{\zeta}z - D_{\zeta}y D_{\eta}z & D_{\eta}z D_{\zeta}x - D_{\eta}x D_{\zeta}y & D_{\eta}x D_{\zeta}x - D_{\zeta}x D_{\eta}y \\ D_{\xi}z D_{\zeta}y - D_{\xi}y D_{\zeta}z & D_{\xi}x D_{\zeta}z - D_{\zeta}x D_{\xi}x & D_{\xi}y D_{\zeta}z - D_{\zeta}y D_{\xi}x \\ D_{\eta}z D_{\xi}y - D_{\xi}z D_{\eta}y & D_{\eta}x D_{\xi}z - D_{\eta}z D_{\xi}x & D_{\eta}y D_{\xi}x - D_{\eta}x D_{\xi}y \end{pmatrix}$$

exists. This will be true iff $J \neq 0$.

The Jacobi matrix of the isoparametric transformation in Equation (A.2), and its Jacobian, can be computed readily by substituting Equation (A.2) in Equation (A.4) to obtain (Botha and Pinder, 1983; Zienkiewicz, 1977)

$$\mathbf{J} = \begin{pmatrix} D_{\xi}\phi_1 & D_{\xi}\phi_2 & \dots & D_{\xi}\phi_N \\ D_{\eta}\phi_1 & D_{\eta}\phi_2 & \dots & D_{\eta}\phi_N \\ D_{\zeta}\phi_1 & D_{\zeta}\phi_2 & \dots & D_{\zeta}\phi_N \end{pmatrix} \begin{pmatrix} x_1 & y_1 & z_1 \\ x_2 & y_2 & z_2 \\ \vdots & \vdots & \vdots \\ x_N & y_N & z_N \end{pmatrix}$$

where $D_{\tau}\phi_l$ denotes the τ -th derivative of the basis function $\phi_l(\xi, \eta, \zeta)$. Explicit expressions for these derivatives can be readily derived from expressions of the Lagrange interpolation polynomial used in the map. The expressions for the tri-linear polynomials of Equation (A.1) are, for example, given by

$$\begin{aligned} D_{\xi}\phi_{ijk}(\xi, \eta, \zeta) &= -(1-2\xi_i)[(1-\eta_j)-(1-2\eta_j)\eta][(1-\zeta_k)-(1-2\zeta_k)\zeta] \\ D_{\eta}\phi_{ijk}(\xi, \eta, \zeta) &= -(1-2\eta_j)[(1-\xi_i)-(1-2\xi_i)\xi][(1-\zeta_k)-(1-2\zeta_k)\zeta] \\ D_{\zeta}\phi_{ijk}(\xi, \eta, \zeta) &= -(1-2\zeta_k)[(1-\xi_i)-(1-2\xi_i)\xi][(1-\eta_j)-(1-2\eta_j)\eta] \end{aligned} \quad (\text{A.5})$$

A.2 TRANSFORMATION OF INTEGRALS

A.2.1 General

As shown by the discussion in Chapter 4, there are two types of integrals that play a very important part in the solution of a partial differential equation by the finite element method: volume integrals

$$V = \iiint_{\Omega} f(x, y, z) d\Omega \quad (\text{A.6})$$

and surface integrals

$$\mathcal{A} = \iint_{\partial\Omega} \mathbf{q}(x, y, z) \cdot \mathbf{n}(x, y, z) dA \quad (\text{A.7})$$

where $\mathbf{n}(x, y, z)$ is the outwardly directed unit vector, normal to the surface area dA . The integrals in Equations (A.6) and (A.7) obviously must also be mapped onto local coordinates, if the finite element approximation is computed in local coordinates. The discussion of these maps is simplified considerably by introducing the tangent vector to a space curve \mathcal{C} . Consider therefore first the vector

$$\frac{\Delta \mathbf{r}}{\Delta u} = \mathbf{i} \frac{\Delta x}{\Delta u} + \mathbf{j} \frac{\Delta y}{\Delta u} + \mathbf{k} \frac{\Delta z}{\Delta u}$$

where $\Delta \mathbf{r}$ is the difference of the two radii vectors \mathbf{r} and $\mathbf{r} + \Delta \mathbf{r}$ in Figure A-2 and Δu the line segment bounded by them. It is clear from Figure A-2 that the vector

$$\mathbf{T}_u = \frac{d\mathbf{r}}{du} = \lim_{\Delta u \rightarrow 0} \frac{\Delta \mathbf{r}}{\Delta u} = \mathbf{i} \frac{dx}{du} + \mathbf{j} \frac{dy}{du} + \mathbf{k} \frac{dz}{du} = \mathbf{i} D_u x + \mathbf{j} D_u y + \mathbf{k} D_u z \quad (\text{A.8})$$

will be tangential to the curve \mathcal{C} at the point P, hence the name tangent vector. It should be noticed that nothing had been said about the measure of u . The vector \mathbf{T}_u can thus be expressed conveniently in the form

$$\mathbf{T}_u = |D_u \mathbf{r}| \mathbf{e}_u = h_u \mathbf{e}_u \quad (\text{A.9})$$

where h_u is the magnitude of \mathbf{T}_u and \mathbf{e}_u a unit vector in the direction of \mathbf{T}_u .

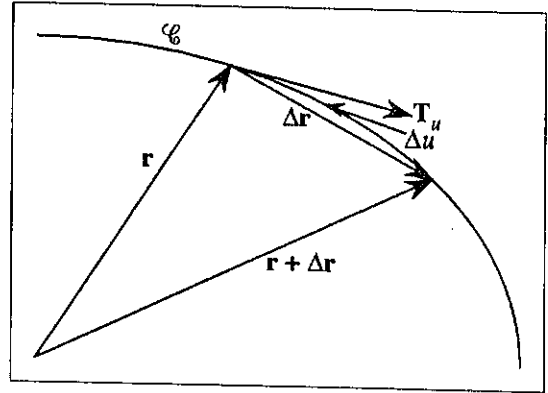


Figure A-2 Graphical representation of the tangent vector to a space curve.

A2.2 The Volume Integral

It is obviously easy to transform the integrand in Equation (A.6), given the relation between the old ($\mathbf{x} = \{x, y, z\}$) and new ($\mathbf{u} = \{u, v, w\}$) sets of coordinates. The transformation of the elementary volume element is, however, more complicated. Consider for this purpose the two coordinate systems in Figure A-3. The elementary radius vector, $d\mathbf{r}$, can now be expressed in terms of the new coordinates, \mathbf{u} , through the chain rule of differentiation as

$$\begin{aligned} d\mathbf{r} &= \frac{\partial \mathbf{r}}{\partial u} du + \frac{\partial \mathbf{r}}{\partial v} dv + \frac{\partial \mathbf{r}}{\partial w} dw \\ &= h_u d\mathbf{e}_u + h_v d\mathbf{e}_v + h_w d\mathbf{e}_w \end{aligned}$$

where use was made of the unit vectors defined by Equation (A.9). The variables \mathbf{u} can only serve as a set of coordinates, if v and w remain constant along the curve defined by $u(x, y, z)$

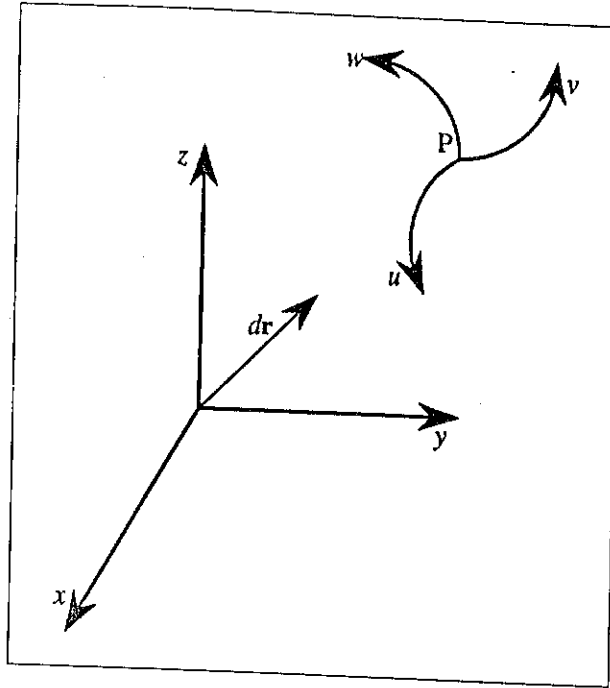


Figure A-3 Illustration of the two coordinate systems used in deriving an expression for the transformation of the volume integral.

and conversely. The differential $h_u du$ may thus be taken as the elementary arc length along the curve $u = u(x, y, z)$, and similarly for $h_v dv$ and $h_w dw$. The elementary volume element in a set of orthogonal coordinates, \mathbf{u} , is thus given by, see Figure A-4,

$$dV = h_u h_v h_w du dv dw = |(h_u d\mathbf{u} \mathbf{e}_u) \bullet (h_v d\mathbf{v} \mathbf{e}_v) \times (h_w d\mathbf{w} \mathbf{e}_w)| \quad (\text{A.10})$$

since $(\mathbf{e}_u \bullet \mathbf{e}_v \times \mathbf{e}_w) \equiv 1$, by definition. It is well-known that the triple product on the right hand side of Equation (A.10) can also be expressed in the form (Spiegel, 1959)

$$dV = \det(\mathbf{J}) du dv dw$$

where

$$\det(\mathbf{J}) = \begin{vmatrix} D_u x & D_u y & D_u z \\ D_v x & D_v y & D_v z \\ D_w x & D_w y & D_w z \end{vmatrix} = h_u h_v h_w$$

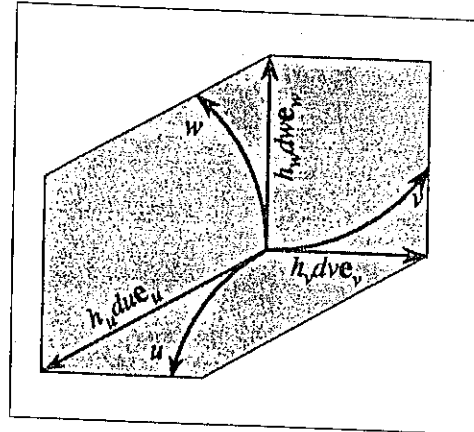


Figure A-4 Illustration of the elementary volume element in the transformed space.

is again the Jacobian of the transformation. The volume integral in Equation (A.6) can thus be expressed in the new coordinates as

$$V = \iiint_{\Omega'} F(u, v, w) \det(\mathbf{J}) d\Omega'$$

where Ω' denotes the volume in the new coordinate system and $d\Omega' = du dv dw$, with $F(u, v, w) = f(x(\mathbf{u}), y(\mathbf{u}), z(\mathbf{u}))$. As has been shown above, it is relatively simple to compute

$\det(\mathbf{J})$ in the case of an isoparametric transformation.

A.2.3 The Surface Integral

The transformation of the surface integral in Equation (A.7) is hampered, not only by the presence of the elementary surface area dA , but also the normal unit vector \mathbf{n} . Both these quantities must therefore be transformed to the new coordinate system. To achieve this, consider the coordinates (r, s) , in Figure A-5. The same line of reasoning used in the derivation of Equation (A.8) can now be used to construct the two tangential vectors

$$\begin{aligned} \mathbf{T}_r &= \mathbf{i}D_r x + \mathbf{j}D_r y + \mathbf{k}D_r z = h_r d\mathbf{r}e_r \\ \mathbf{T}_s &= \mathbf{i}D_s x + \mathbf{j}D_s y + \mathbf{k}D_s z = h_s ds\mathbf{e}_s \end{aligned} \quad (\text{A.11})$$

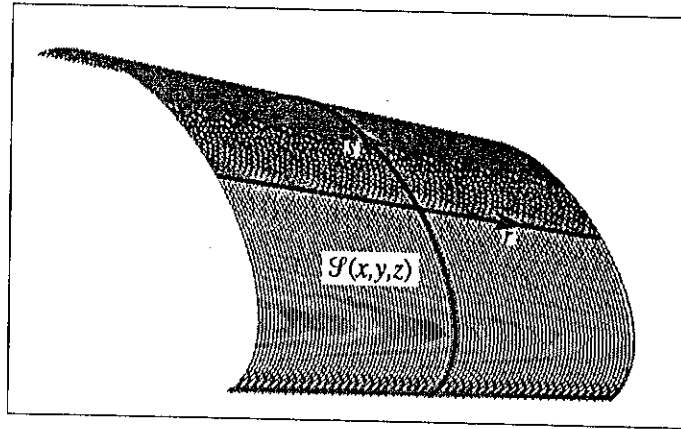


Figure A-5 Parametric coordinates on the surface of a three-dimensional surface.

The elementary surface area dA' to use in the transformation can thus be expressed as, see Figure A-6,

$$dA' = |\mathbf{T}_r \times \mathbf{T}_s| = h_r h_s dr ds \quad (\text{A.12})$$

where

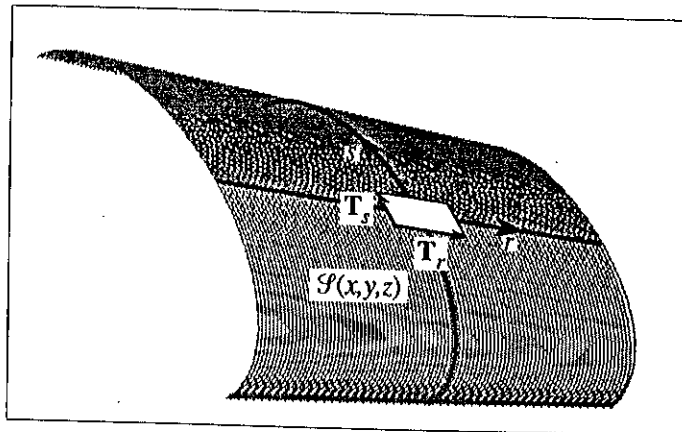


Figure A-6 Schematic representation of the tangent plane to the three-dimensional surface $\mathcal{S}(x, y, z)$.

$$\mathbf{T}_r \times \mathbf{T}_s = iJ_{yz} + jJ_{zx} + kJ_{xy} = \mathbf{N}_{rs} \quad (\text{A.13})$$

with

$$J_{pq} = \begin{vmatrix} D_r p & D_s p \\ D_r q & D_s q \end{vmatrix} = D_r p D_s q - D_r q D_s p$$

the Jacobian of the two global coordinates p and q under the map $(p, q) \Rightarrow (r, s)$.

The plane spanned by the vectors \mathbf{T}_r and \mathbf{T}_s is, by definition, tangential to the surface $\mathcal{S}(x, y, z)$ at the point P (see Figure A-6). This implies that the vector \mathbf{N}_{rs} , in Equation (A.13), will be parallel to the unit normal vector \mathbf{n} in Equation (A.7). The surface integral in Equation (A.7) can thus be expressed in the new coordinates (r, s) as

$$\mathcal{A} = \iint_{\partial\Omega} \mathbf{q}[x(r, s), y(r, s), z(r, s)] \cdot \mathbf{n}_{rs} dA' \quad (\text{A.14})$$

where dA' is given by Equation (A.12) and

$$\mathbf{n}_{rs} = \mathbf{N}_{rs} / N_{rs}$$

the unit vector normal to the plane spanned by \mathbf{T}_r and \mathbf{T}_s , with N_{rs} the magnitude of \mathbf{N}_{rs} .

The most suitable approximation to use for the boundary surface, $\mathcal{S}_e(x, y, z)$, of a three-dimensional element would thus be one that can be parameterized in a similar way as the mapping of the global coordinates \mathbf{x} to local coordinates ξ . This can be readily achieved by expanding the global coordinates as

$$\mathbf{x} = \sum_{l=1}^M \mathbf{x}_l \phi_l(\rho, \sigma)$$

where M is the total number of boundary nodes in the element, Ω_e , and $\phi_l(\rho, \sigma)$ the *two-dimensional* Lagrange interpolation polynomial associated with the node l ($= m, n$). This polynomial can be conveniently expressed, in the case of bi-linear approximation over the square $[0, 1] \otimes [0, 1]$, as

$$\phi_{mn}(\rho, \sigma) = [(1 - \rho_i) - (1 - 2\rho_i)\rho][(1 - \sigma_n) - (1 - 2\sigma_n)\sigma]$$

where $\rho_m, \sigma_n = 0$ or 1 .



REFERENCES

- Allen, M.B. (1985). Numerical modelling of multiphase flow in porous media. *Advances Water Resources*, 8, 162-187.
- Batu, V. and Van Genuchten, M.T. (1990). First and Third-Type Boundary Conditions in Two-Dimensional Solute Transport Modeling. *Water Resources Research*, 26, 2, 339-350.
- Bear, J. (1972). *Dynamics of fluids in porous media*. American Elsevier Publishing Company, Inc., New York.
- Bear, J. (1979). *Hydraulics of Groundwater*. McGraw-Hill Book Company, New York, N.Y.
- Bear, J. and Bachmat, Y. (1990). *Introduction to Modeling of Transport Phenomena in Porous Media*. Kluwer Academic Publishers, Dordrecht.
- Bear, J. and Verruijt, A. (1987). *Modeling Groundwater Flow and Pollution*. Kluwer Academic Publishers, Dordrecht.
- Boehmer, W.K. (1991). Personal communication.
- Botha, J.F. (1971). *Model-dependent Studies of Coulomb Displacement Energies in Mirror Nuclei*. Unpublished Ph.D. Thesis, University of Stellenbosch, Stellenbosch.
- Botha, J.F. (1986). *A revised model for the National Waste Disposal Site at Vaalputs*. Institute for Ground-water Studies, University of the Orange Free State, Bloemfontein.
- Botha, J.F. (1990). *Transport of Radioactive waste from the Disposal Site at Vaalputs*. Institute for Ground-water Studies, University of the Orange Free State, Bloemfontein.
- Botha, J.F. and Bakkes, G.N. (1982). The Galerkin finite element method and the groundwater flow equation: 1. Convergence of the method. *Advances Water Resources*, 5, 121-125.
- Botha, J.F. and Pinder, G.F. (1983). *Fundamental Concepts in the Numerical Solution of Differential Equations*. John Wiley and Sons, Inc., New York, N.Y.
- Botha, J.F. and Van Blerk, J.J. (1990). Unpublished Manuscript, Institute for Groundwater Studies, U.O.F.S., Bloemfontein.
- Botha, J.F., Verwey, J.P., Buys, J., Tredoux, G., Moodie, J.W. and Hodgkiss M. (1990). *Modelling Ground-water Contamination in the Atlantis Aquifer*. WRC Report No 175/1/90. Water Research Commission, Pretoria.
- Buys, J., Botha, J.F., Messerschmidt, H.J. (1992). *Triangular Irregular Meshes and their Application in the Graphical Representation of Geohydrological Data*. Vol. II of the Report: *A Comparative Study of Two- and Three-Dimensional Groundwater Models*. WRC Report 271/2/92, Water Research Commission, Pretoria.
- Case, C., Kautshy, M., Kearn, P., Goldfarb, R., Leatham, S. and Metcalf, L. (1983) *Unsaturated Flow Properties Data Catalog*, Vol. 1. Water Resources Centre, Desert Research Institute, University of Nevada System.
- Celia, M.A., Bouloutas, E.T. and Zorba, R.L. (1990). A General Mass-Conservative Numerical Solution for the Unsaturated Flow Equation. *Water Resources Research*, 26, 1483-1496.
- Cherry, J.A. (1989). Hydrogeologic contaminant behaviour in fractured and unfractured clayey deposits in Canada. *Contaminant Transport in Groundwater*. IAHR No 3, Kobus H.E. and Kinzelbach (Eds.), W., A.A. Balkema, Rotterdam.
- Cleary, R.W. and Unger, M.J. (1978). *Analytical methods for ground water pollution and hydrology*. Rep 78-WR-15, Water Resources Program, Princeton Univ., Princeton.
- Cogho, V.E., Van Niekerk, L.J., Pretorius, H.P.J., Hodgson, F.D.I. (1990). *The Development of Techniques for the evaluation and Effective Management of Surface and ground-water contamination in the Orange Free State Goldfields*. Report to the Water Research Commission, Pretoria.
- Dagan, G. (1989). *Flow and Transport in Porous Formations*. Springer-Verlag, Berlin.
- Dana, J.H. and Moltz, F.J. (1991). *Physical Measurements in Subsurface Hydrology*. U.S. National Report to International Union of Geodesy and Geophysics 1987 - 1990, American Geophysical Union.
- Darcy, H. (1856). *Les Fontaines Publiques de la Villa de Dijon*. Dalmont, Paris.
- Davis, A. and Neuman, S.P. (1983). *Documentation and User's Guide: UNSAT2 Variably Saturated Flow Model*. Division of Waste Management, Washington.
- Department of Water Affairs. (1986). *Management of the Water Resources of the Republic of South Africa*. CPT

- Book Printers, Cape Town.
- Duke, H.R. (1973). *Drainage Design Based upon Aeration*. Hydrology Paper No. 61, Colorado State University, Fort. Collins, Colorado.
- Geraghty and Miller. (1991). AQTESOLV: Design and Analysis of Aquifer Tests. *Geraghty and Miller Newsletter*, 2, 6-7.
- Hedstrom, W.E., Corey, A.T. and Duke, H.R. (1971). *Models for Subsurface Drainage*. Hydrology Paper No. 48, Colorado State University, Fort. Collins, Colorado.
- Hildebrand, F.B. (1976). *Advanced Calculus for Applications* (2nd ed.). McGraw-Hill, New York
- Hutson, J.L. (1983) Estimates of Percolation at the Buried Waste Facility, Bushmanland. *Site-Selection Program for the Disposal/Storage of Radioactive Waste in South Africa*, Progress Report No 16.
- Huyakorn, P.S. and Pinder, G.F. (1983). *Computational Methods in Subsurface Flow*. Academic Press, Inc., New York, N.Y.
- Huyakorn, P.S., Jones, B.G. and Andersen, P.F. (1986a). Finite Element Algorithms for Simulating Three-Dimensional Groundwater Flow and Solute Transport in Multilayer Systems. *Water Resources Research*, 22, 3, 361-374.
- Huyakorn, P.S., Springer, E.P., Guvanasen, V. and Wadsworth, T.D. (1986b). A Three-Dimensional Finite Element Model for Simulating Water Flow in Variably Saturated Porous Media. *Water Resources Research*, 22, 13, 1790-1808.
- Huyakorn, P.S., Thomas, S.D. and Thompson, B.M. (1984). Techniques for Making Finite Elements Competitive in Modeling Flow in Variably Saturated Porous Media. *Water Resources Research*, 20, 8, 1099-1115.
- Kauffmann, C., Kinzelbach, W. and Fried, J.J. (1990). Simultaneous Calibration of Flow and Transport Models and Optimization of Remediation Measures. *Modelcare 90: Calibration and Reliability in Groundwater Modelling* (Ed. Karel Kovar), IAHS Press, Wallingford, Oxfordshire.
- Kirchner, J.O.G., Van Tonder, G.J. and Lukas, E. (1991). *Exploitation Potential of Karoo Aquifers*. WRC Report No 170/1/91. Water Research Commission, Pretoria.
- Kruseman, G.P. and De Ridder, N.A. (1991). *Analysis and Evaluation of Pumping Test Data*. 2nd Ed. International Institute for Land Reclamation and Improvement, Wageningen, The Netherlands.
- Levin, M. (1988). *A Geohydrological appraisal of the Vaalputs Radioactive Waste Disposal Facility in Namaqualand, South Africa*. Unpublished Ph.D. Thesis. University of the Orange Free State, Bloemfontein.
- McDonald, M.G. and Harbaugh, A.W. (1983). *A Modular Three-Dimensional Finite-Difference Groundwater Flow Model*. Academic Press, Inc., New York, N.Y.
- Mercer, J.W. and Faust, C.R. (1980). Ground-Water Modeling: An Overview. *Ground Water*, 18, 108-115.
- Milly, P.C.D. (1985). A mass-conservative procedure for time-stepping in models of unsaturated flow. *Advances Water Resources*, 8(1), 32-36.
- Müller, J.L. and Botha, J.F. (1986). *A preliminary investigation of modelling the Atlantis aquifer*. Bulletin 15, Institute for Groundwater Studies, University of the Orange Free State, Bloemfontein
- Muskat, M. (1946). *The Flow of Homogeneous Fluids through Porous Media*. 2nd Ed., McGraw-Hill, New York.
- Neumann, S.P. (1975). Analysis of Pumping Test Data From Anisotropic Unconfined Aquifers Considering Delayed Aquifer Response. *Water Resources Research*, 11, 329-342.
- Pinder, G.F. (1974). *Galerkin-finite element models for aquifer simulation*. Rep Water Resources Program, Princeton University.
- Pinder, G.F. and Gray, W.G. (1977). *Finite Element Simulation in Surface and Subsurface Hydrology*. Academic Press, Inc., New York, N.Y.
- Pissanetzky, S. (1984). Automatic Three-Dimensional Finite Element Mesh Generation using the Program KUBIK. *Computer Physics Communications*, 32, 245-265.
- Princeton Water Resources Program (1984). *Groundwater contamination from hazardous wastes*. Prentice-Hall, Inc., Englewood Cliffs, New Jersey.
- Schäfer, G. and Kobus, H.E. (1989). Mass transport in an artificial heterogeneous aquifer: Experiments and numerical modelling. *Contaminant Transport in Groundwater*, IAHR No 3, Kobus H.E. and Kinzelbach, W. (Eds.) A.A. Balkema, Rotterdam.
- Scheidegger, A.E., (1974). *The Physics of Flow through Porous Media* (3rd Ed.). University of Toronto Press, Toronto.
- Spiegel, M.R. (1959). *Vector Calculus*. Schaum's Outline Series, McGraw-Hill, New York.
- Strang, G. and Fix, G. (1973). *An Analysis of the Finite Element Method*. Prentice Hall, Englewood Cliffs, N.J.
- Theis, C.V. (1935). The relation between the lowering of the piezometric surface and the rate and duration of

- discharge of a well using groundwater storage. *Trans. Amer. Geophys. Union*, 16, 519-524.
- Thompson, J.F. (1977). *Boundary-fitted curvilinear Coordinate Systems for Solution of Partial Differential Equations on Fields Containing any Number of Arbitrary Two-dimensional Bodies*. Mississippi State University, Mississippi.
- Van Genuchten, M.Th. (1980). A Closed-form Equation for predicting the Hydraulic Conductivity of Unsaturated Soils. *Soil Sci. Soc. Am. J.*, 44, 892-898.
- Van Genuchten, M.Th. and Nielsen, D.R. (1985). On Describing and Predicting the Hydraulic Properties of Unsaturated Soils. *Annales Geophysicae*, 3, 615-628.
- Van Sandwyk, L., Van Tonder, G.J., De Waal, D.J., and Botha J.F. (1992). *A comparison of spatial Bayesian estimation and classical Kriging procedures*. Vol. III of this report to the Water Research Commission, Pretoria.
- Van Tonder, G.J., Botha, J.F. and De Waal, D.J. (1990). Bayesian Estimation of Water Levels. *Modelcare 90: Calibration and Reliability in Groundwater Modelling* (Karel Kovar Ed.), IAHS Press, Wallingford, Oxfordshire.
- Voss, C.I. (1984). *SUTRA A Finite-Element Simulation Model for Saturated-Unsaturated, Fluid-Density-Dependent Ground-water Flow with Energy Transport or Chemically-Reactive Single-Species Solute Transport*. U.S. Geological Survey, Virginia.
- Walton, W.C. (1984). *Handbook of Analytical Ground Water Models*. IGWMC Short Courses in Ground Water Modeling, International Groundwater Modeling Centre, Indiana.
- Wright, A. (1991). *The Artificial Recharge of Urban Stormwater Runoff in the Atlantis Coastal Aquifer*. MSc Thesis, Rhodes University.
- Yeh, G.T. and Ward, D.S. (1981). *FEMWASTE: A Finite-element model of Waste Transport through Saturated-Unsaturated porous Media*. Environmental Sciences Division, Publication No. 1462, Oak Ridge, Tennessee.
- Zienkiewicz, O.C. (1977). *The Finite Element Method in Engineering Science*. 3rd Ed. McGraw-Hill, London.
-